DOUGLAS REPORT SM-48759

APPLICATION OF DISTRIBUTED SYSTEM CONCEPTS TO DYNAMIC ANALYSES AND CONTROL OF BENDING VIBRATIONS

AUGUST 1965

Prepared under Contract No. NAS8-11420
by Douglas Aircraft Company, Inc.
Missile and Space Systems Division
Santa Monica, California
for
National Aeronautics and Space Administration

DOUGLAS REPORT SM-48759

APPLICATION OF DISTRIBUTED SYSTEM CONCEPTS TO DYNAMIC ANALYSES AND CONTROL OF BENDING VIBRATIONS

AUGUST 1965

By D.R. VAUGHAN

Prepared under Contract No. NAS8-11420
by Douglas Aircraft Company, Inc.
Missile and Space Systems Division
Santa Monica, California
for
National Aeronautics and Space Administration

BLANK PAGE

CONTENTS

ILLUSTRATIONS

TABLES

BLANK PAGE

APPLICATIONS OF DISTRIBUTED SYSTEM CONCEPTS

TO DYNAMIC ANALYSIS AND CONTROL OF BENDING VIBRATIONS

By David R. Vaughan
Missile and Space Systems Division
Douglas Aircraft Company, Inc.

SUMMARY

As an alternate to the normal-mode approach to dynamics and controls analysis of flexible aerospace vehicles, bending vibrations are studied in terms of the distributed parameter concepts of propagation and reflection. Only thin uniform beams and cascades of them are studied. The results provide preliminary insight into bending vibrations for the design of controls for flexible vehicles.

Transverse vibrations are approached by an analogy developed between propagation and reflection in the Bernoulli-Euler and wave equations. Thus, longitudinal-traveling-wave solutions for beams are treated before transverse vibrations.

Solution of the Bernoulli-Euler equation for transverse bending of a thin semi-infinite beam shows that $e^{-\sqrt{Ts}}\cos\sqrt{Ts}$ and $e^{-\sqrt{Ts}}\sin\sqrt{Ts}$ are propagation operators, and the input (characteristic) admittance contains the operators $\sqrt{s}$ (fractional derivative) and $1/\sqrt{s}$ (fractional integral).

The Bernoulli-Euler equation for the transverse bending vibration of a thin uniform free-free beam is solved in terms of these propagation and characteristic-impedance operators. It is shown that a matrix transformation $(U = W^{-1}Y)$ carries the local state vector Y to a vector of characteristic variables (U) and permits factorization of the solution into propagation- and end-effects matrices. This matrix factorization is shown to have the same structure as that for the solution of the wave equation.

For beams with terminal dampers or controls, which can be represented as terminal-impedance matrices, the end-effects matrices are derived from those for the free-free beam by simple matrix algebra. The matrix relation between the incident and reflected characteristic variables (U) is treated as a generalization of the reflection coefficient for electrical transmission lines. In particular, this reflection matrix is shown to be identically zero, when the terminal- and the characteristic-impedance matrices are equal.

Several special terminal-impedance matrices are considered, and response to commands and load disturbances is studied in the time domain, by analog simulation, and in the frequency domain. An attempt to correlate the behavior of these systems with their reflection matrices was only partially successful. The matrix describing reflection and refraction of the characteristic variables at the interface of two cascaded uniform beams is developed and shown to contain only real elements.

BLANK PAGE

INTRODUCTION

The research reported herein was motivated by the feedback-control problem in flexible launch vehicles. As launch vehicles become larger, the ratio of the first bending frequency to the desired control frequency decreases. This frequency propinquity makes design of feedback controls much more difficult than it is when the bending and desired control frequencies are widely separated.

Dynamics and controls analysis of bending vibration in flexible vehicles has generally been in terms of the natural modes (refs 1 and 2). This report puts forth an alternate, fundamentally different approach based on propagation and transmission concepts. Although the present work is restricted to thin uniform beams and cascades of them, it affords a preliminary understanding of the dynamics and control of bending vibration in complex structures. Simplified examples are treated that should ultimately provide new insight into the intrinsic nature of bending vibration and its control.

Stress under impact conditions has been analyzed in terms of propagation. Vigness (ref 3) uses the theory of transverse wave propagation governed by the Bernoulli-Euler equation and points out that its solution for an infinitely long beam was developed by Boussinesq (ref 4). Traveling waves governed by the Timoshenko differential equation have also been used to study transverse impact effects (refs 5 and 6).

Although propagation concepts have been applied to transverse-beam-impact analysis, the analysis of vibration absorbers has been almost exclusively in terms of the natural modes of vibration (refs 7, 8, and 9). An exception is the field of acoustics. Klyukin (ref 10) and Klyukin and Sergeev (ref 11) have investigated the transmission and reflection of incident flexural waves by antivibration resonance systems. Their work is restricted to steady-state harmonic vibration, which is useful for acoustics studies, but not for transient analysis.

The central problem treated in the present work is twofold: (1) achieving a desired motion of a flexible structure rapidly and with minimum vibration or ringing, and (2) minimizing excursions from the desired motion caused by unpredictable loads. The problem is approached through an analogy to propagation and reflection of both flexural and longitudinal waves. The input-impedance matrix for transverse vibration of a semi-infinite beam is found to contain the operators $\sqrt{s}$ and $1/\sqrt{s}$. This leads to the investigation of the effectiveness of these operators in the terminal-impedance matrices of vibration dampers or active controls. The concept of a reflection matrix, which is a generalization of the reflection coefficient of electrical-transmission-line theory, is introduced and related to the terminal-impedance matrix.

Several different terminal-impedance matrices are considered in detail. For these cases, responses to commands and load disturbances are studied in the time domain by analog simulation, and in the frequency domain. An attempt to correlate the behavior of these systems with their reflection matrices is only partially successful.

Considerable attention is devoted to the longitudinal-traveling-wave solution for beams, because its treatment is so closely analogous to that of flexural wave propagation.

SYMBOLS

A	cross-section area of beam, $in.^2$ Also, parameter matrix for wave equation in state-vector form $dy/dx = Ay$, 2x2 for Bernoulli-Euler state-vector equation $dY/dx = AY$, 4x4
a	$\sqrt{\frac{EI}{\rho A}}$, $in.^2/sec$
B	matrix that carries P to P^* by the relation $P^* = BPB^{-1}$, 4x4
$C(Ts)$	$e^{-\sqrt{Ts}} \cos \sqrt{Ts}$
c	propagation velocity of longitudinal waves, in./sec
E	Young's modulus of elasticity, $lb/in.^2$
F_n	generalized force applied to n^{th} transverse-bending mode, lb
F	external longitudinal force, lb
f	$(M,Q)^T$, 2x1
$f(x,t)$	intensity of distributed external longitudinal loading, lb/in.
$G_y^\bullet, G_\theta^\bullet$	gains of terminal-impedance matrices [see eqs (102a and 102b)]
I	area moment of inertia of beam cross-section, $in.^4$
J	interface matrix [see eq (124), 4x4]
J_{ij}	matrix elements of partitioned J, 2x2
j	$\sqrt{-1}$
$K_y^\bullet, K_\theta^\bullet$	gains of terminal-impedance matrices [see eqs (102a and 102b)]
k_{21}	$\sqrt{\frac{E_1 I_1 \rho_2 A_2}{E_2 I_2 \rho_1 A_1}}$

L	left-side longitudinal end-effects matrix for beam terminated in z_a. Also, left-side lateral end-effects matrix for beam with terminal Z_a at face a, 4x4
L_{ij}	matrix elements of partitioned L, 2x2
L°	left-side longitudinal end-effects matrix for free-free beam, 2x2. Also, left-side lateral end-effects matrix for free-free beam, 4x4
ℓ	length of finite beam, in.
ℓ_{ij}	elements of L
M	external moment, in.-lb
M_n	n^{th} modal mass
m	mass of beam, lb-sec^2/in.
P	diagonal matrix of eigenvalues of A for wave equation, 2x2, and for Bernoulli-Euler equation, 4x4
P^*	matrix of real variables, diagonal in the 2x2-partitioned sense, derived from P by the relation $P^* = BPB^{-1}$, 4x4
$Q_n(t)$	generalized force applied to n^{th} longitudinal mode
Q	external transverse force, lb
$Q'(x)$	intensity of distributed external transverse loading, lb/in.
q_n	n^{th} normal coordinate
R	right-side longitudinal end-effects matrix for beam terminated in z_b, 2x2. Also, right-side lateral end-effects matrix for beam with terminal impedance Z_b at face b, 4x4.
R_{ij}	matrix elements of partitioned R, 2x2
R°	right-side longitudinal end-effects matrix for free-free beam, 2x2. Also, right-side lateral end-effects matrix for free-free beam, 4x4
r_{ij}	elements of R
$S(Ts)$	$e^{-\sqrt{Ts}} \sin \sqrt{Ts}$

s	Laplace transform operator, sec^{-1}
T	$\ell^2/(2a)$, sec
$T_{r_1 r_2}$	transmission matrix for longitudinal beam vibration with convention $y_{r_1} = T_{r_1 r_2} y_{r_2}$, 2x2
$T^*_{r_1 r_2}$	Bernoulli-Euler transmission matrix for thin-beam transverse bending with the convention $Y_{r_1} = T^*_{r_1 r_2} Y_{r_2}$, 4x4
$T(x)$	time for longitudinal wave to travel from $x = 0$ to station x, sec. Also $x^2/(2a)$, sec
t	time, sec
U	vector of characteristic variables, 4x1
u	longitudinal beam displacement, in.
u^-, u^+	characteristic variables for transverse bending vibration
v	longitudinal velocity of beam, in./sec
v^-, v^+	characteristic variables for transverse bending vibration
W	matrix of eigenvectors of A for wave equation, 2x2, and for Bernoulli-Euler equation, 4x4
W^*	WB^{-1}, 4x4
x	location coordinate along beam, in.
$\dot{x}$	$(\dot{y}, \dot{\theta})^T$, 2x1
x_r	location coordinate of station r
Y	beam lateral state vector $= (\dot{y}, \dot{\theta}, M, Q)^T$
Y_{aa}	longitudinal input admittance for station a, in./(lb-sec). Also, lateral-input-admittance matrix for station a, 2x2
Y_{ba}	longitudinal transfer admittance ($v_b = Y_{ba} F_a$), in./(lb-sec). Also, lateral-transfer-admittance matrix with convention $\dot{x}_b = Y_{ba} f_a$

Y_o	characteristic admittance for longitudinal beam waves in./(lb-sec). Also, characteristic admittance matrix for thin beam bending, 2x2
Y_{oa}	characteristic-admittance matrix for face a, 2x2
Y_{ob}	characteristic-admittance matrix for face b, 2x2
y	beam longitudinal state vector = $(v,F)^T$, 2x1. Also, transverse beam displacement, in.
$\dot{y}$	transverse beam velocity, in./sec
y_{ij}	elements of admittance matrix for thin-beam bending [see eq (94)]
Z_a	terminal-impedance matrix at face a, 2x2
Z_b	terminal-impedance matrix at face b, 2x2
Z_o	characteristic impedance for longitudinal beam waves, lb-sec/in. Also, characteristic-impedance matrix for thin-beam bending, 2x2
Z_{oa}	characteristic-impedance matrix for face a, 2x2
Z_{ob}	characteristic-impedance matrix for face b, 2x2
z	vector of characteristic variables = $(z^-,z^+)^T$
z_a	terminal impedance at face a, lb-sec/in.
z_b	terminal impedance at face b, lb-sec/in.
z^+,z^-	characteristic variables for longitudinal wave transmission
$\alpha_b,\beta_b,\gamma_b,\delta_b$	changes in elements of R_{22}^o resulting from Z_b
ε^+	$(v^+,u^+)^T$, 2x1
ε^-	$(u^-,v^-)^T$, 2x1
θ	angular rotation of beam, rad
$\dot{\theta}$	angular velocity of beam, rad/sec

ρ	density of beam material, lb-sec^2/in.^{4}
$\Lambda_{ab}, \Lambda_{ba}$	propagation matrices, 2x2 [see eqs (98a and 98b)]
$\phi_n(x)$	n^{th} normal-mode function
$\phi_n'(x)$	$d\phi(x)/dx$, in.$^{-1}$
ω_n	n^{th} modal frequency, rad/sec

Subscripts:

n	normal-mode number, integer
r	denotes value of subscripted quantity at specially designated station, such as a or b, lower-case letter
a	denotes value of subscripted quantity at face a of beam
b	denotes value of subscripted quantity at face b of beam

Superscripts:

T	denotes transpose of superscripted matrix
*	denotes external command or disturbance of superscripted quantity

Operations:

$\mathcal{L}^{-1}( )$	denotes inverse Laplace transform of quantity operated upon
$(\dot{})$	denotes $d( )/dt$
$( )'$	denotes $d( )/dt$

Matrices in block diagrams:

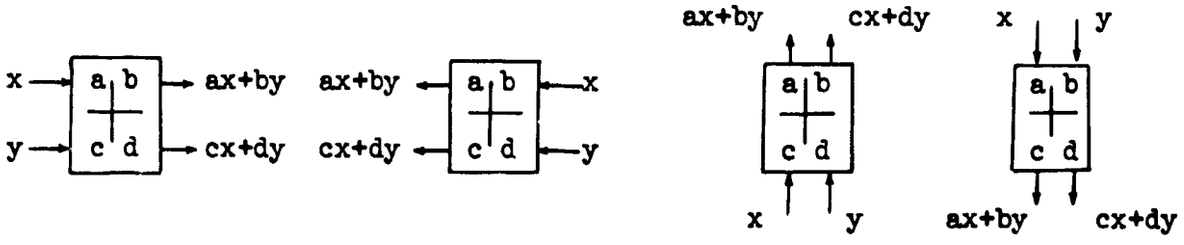

LONGITUDINAL VIBRATION IN BEAMS

The Wave Equation

General background.- Longitudinal vibration of a uniform continuous beam, characterized by a linear elastic field with distributed mass, is governed by the wave equation (ref 12). With sign conventions as shown in figure 1, if a

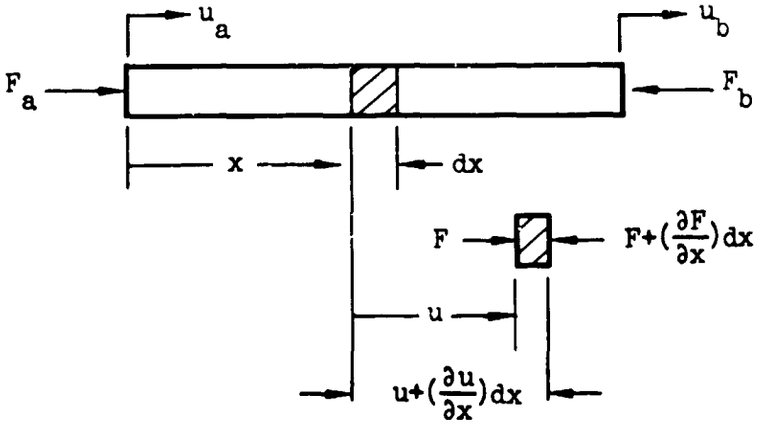

Figure 1.--Longitudinal forces and displacements for a uniform beam and micro-element.

beam is of length ℓ, cross-sectional area A, mass per unit volume ρ, and modulus of elasticity E, the displacement u of any cross-section in the direction of the location coordinate x is governed by the wave equation:

$$\frac{\partial^2 u}{\partial t^2} = c^2 \frac{\partial^2 u}{\partial x^2} \tag{1}$$

The wave velocity c is determined from the local properties E and ρ:

$$c = \sqrt{\frac{E}{\rho}} \tag{2}$$

Equation (1) is the classical wave equation found in nearly all treatments of partial differential equations. It governs the dynamics of such diverse wave phenomena as water hammer (ref 13), lossless electrical transmission lines (ref 14), and torsional vibration of rods (refs 1 and 12). Although all continuous physical systems have internal dissipation and, thus, cannot obey the

wave equation exactly, many systems have such small energy losses that solutions of equation (1) are quite useful in engineering analysis. Moreover, many features of this solution are retained for lossy systems, such as electrical transmission lines with distributed series resistance and shunt conductance.

Normal-mode solution.- In addition to the traveling-wave solution, equation (1) can be solved in terms of its natural modes of vibration (refs 1 and 12). If the beam of figure 1 is free at both ends, the natural frequencies are

$$\omega_n = \frac{n\pi}{\ell}\sqrt{\frac{E}{\rho}} \tag{3}$$

The normal functions or mode shapes are

$$\phi_n(x) = \cos\frac{n\pi x}{\ell} \tag{4}$$

The total displacement $u(x,t)$ is given by the sum of the mode displacements:

$$u(x,t) = \sum_{n=0}^{\infty} \phi_n(x)\, q_n(t) \tag{5}$$

where $q_n(t)$ are the normal coordinates.

For forced motion, the normal coordinates are governed by the transfer function

$$q_n(s) = \frac{1}{M_n s^2 + M_n \omega_n^2} Q_n(s) \tag{6}$$

where M_n is the n^{th} modal mass.

The generalized force Q_n is

$$Q_n(t) = \int_0^{\ell} f(x,t)\, \phi_n(x)\, dx + \sum_r F_r(t)\, \phi_n(x_r) \tag{7}$$

where $f(x,t)$ is the intensity of the distributed external longitudinal loading, and F_r are the concentrated forces applied at stations r.

The normal-mode station is detailed further in references 1 and 12. This diversion into the normal-mode solution of the wave equation serves to show that transfer functions derived from modal considerations consist entirely of polynomials in the Laplace operator s, as shown in equation (6). Thus,

rational algebraic functions of s (e.g., ratios of two polynomials in s) are derived from a continuous system or a partial-differential-equation problem formulation. This is most attractive for dynamic analysis and control, and is a major advantage of the normal-mode-type solution to the wave equation. This series solution exhibits the system poles most clearly; the most significant (i.e., low-frequency) poles are retained simply by dropping the higher modes from equation (5). Rational algebraic transfer functions can also be generated by replacing the continuous beam with an approximate lumped-spring-mass model. The, n, natural frequencies of such a model will not, in general, be exactly equal to the first, n, natural frequencies of the continuous beam. For complicated nonuniform structures, lumped-spring-mass models are presently the only practical means to establish transfer functions.

Semi-Infinite Beam

The traveling-wave solution is considerably simpler for a semi-infinite than for a finite beam. Moreover, it affords considerable insight into the fundamental nature of propagation.

For a semi-infinite beam (right end extending to $x = \infty$), the boundary condition at $x = \infty$ is

$$u(\infty,t) = 0 \tag{8a}$$

If an arbitrary longitudinal force F_a is applied to the left end (station a) of the beam, the second boundary condition is

$$\frac{\partial u(0,t)}{\partial x} = -\frac{F_a(t)}{EA} \tag{8b}$$

For simplicity, the beam is assumed to have no stored kinetic or elastic energy, i.e., the initial conditions are

$$\frac{\partial u(x,0)}{\partial t} = 0 \tag{9a}$$

$$u(x,0) = 0 \tag{9b}$$

Laplace transforming equation (1) with respect to t, and denoting the transform of $u(x,t)$ by $u(x,s)$, results in the following ordinary differential equation:

$$s^2 u(x,s) = c^2 \frac{d^2 u(x,s)}{dx^2} \tag{10}$$

$$\begin{bmatrix} v_b \\ z_b^- \end{bmatrix} = \overbrace{\begin{bmatrix} -Y_o & \sqrt{2} \\ -\sqrt{2}\,Y_o & 1 \end{bmatrix}}^{R^o} \begin{bmatrix} F_b \\ z_b^+ \end{bmatrix} \tag{35b}$$

Figure 4 shows the relations of equations (34) and (35a and b) in block diagram form;

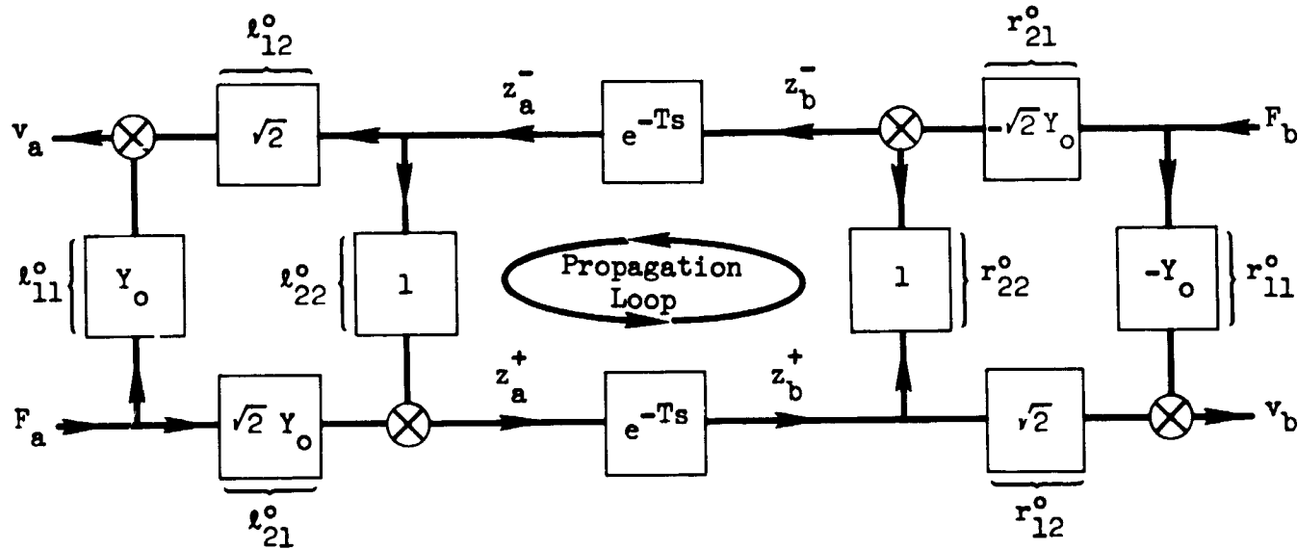

Figure 4.- Propagation and end-effects relations for longitudinal vibration of a free-free beam.

the overall relation is an admittance relation. This input-output choice at the boundaries determines the end-effects matrices L^o and R^o. Different end-effects matrices can be derived for different boundary conditions. The propagation relations described by equation (34) are not affected by boundary conditions; the propagation time, T, is of course proportional to the beam length, ℓ. The end-effects matrices are a function only of the local properties and the cross-section geometry and, hence, independent of ℓ.

The sequence of events following the application of unit impulse in F_a can be readily derived from the block diagram (fig 4). First, the velocity v_a responds instantaneously in an impulse of magnitude Y_o. After T sec, an impulse of z_b^+ emerges from the a-to-b delay simultaneously with an impulse v_b of magnitude $2Y_o$. Because $z_b^- = z_b^+$, an impulse z_a^- emerges from the b-to-a delay after 2T sec simultaneously with an impulse v_a of magnitude $2Y_o$. The general pattern of behavior is now established: the impulse

The general solution of equation (10) is

$$u(x,s) = c_1 e^{-sx/c} + c_2 e^{+sx/c} \tag{11}$$

The semi-infinite-beam boundary condition (eq 8a) requires that the coefficient c_2 be zero. The remaining coefficient c_1 can then be evaluated from the second boundary condition (eq 8b). The solution of equation (11) becomes

$$u(x,s) = \left[\frac{1}{s} Y_o \, e^{-T(x)s}\right] F_a(s) \tag{12a}$$

where

$$Y_0 \equiv \frac{1}{A\sqrt{\rho E}} \; ; \; T(x) \equiv x/c \tag{12b}$$

This report attempts to deal with impedances and admittances wherever possible. Therefore, the longitudinal velocity $v(x,t)$ is introduced:

$$v(x,t) \equiv \frac{\partial u(x,t)}{\partial t} \tag{13}$$

Because $su(x,s) = v(x,s)$, equation (12a), rewritten in terms of longitudinal velocity, becomes

$$v(x,s) = \left[Y_0 \, e^{-T(x)s}\right] F_a(s) \tag{14}$$

Propagation operator e^{-Ts}.- The operator e^{-Ts} is the propagation operator for longitudinal wave transmission. It is the pure-delay operator, as evident from the transform pair

$$f(t - T) \leftrightarrow e^{-Ts} F(s)$$

Thus, $T(x)$ is the time required for the wave to travel at a constant velocity c from station a to any station x. If a unit step is applied at station a, the velocity at station x will jump to the value Y_0, $T(x)$ sec later, as shown in figure 2a. If a sinusoidal force is applied at station a, the steady-state frequency response is

$$\frac{v(x,j\omega)}{F_a(j\omega)} = Y_0 e^{-j\omega T(x)} \tag{15}$$

The polar, or Nyquist plot of the right side of equation (15) is a circle, as shown in figure 2b.

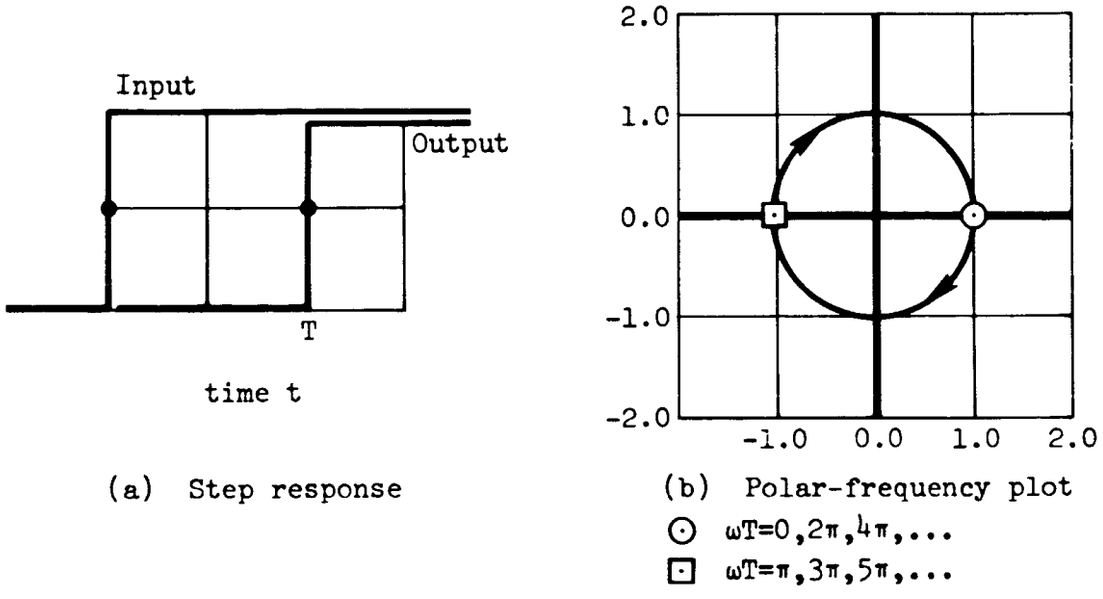

Figure 2.--The wave-equation propagation operator e^{-Ts}.

The amplitude ratio is, therefore, independent of frequency. The phase lag is $\omega T(x)$ rad and increases without limit for high frequencies.

Characteristic impedance Z_0.- If equation (14) is specialized to $x = 0$, the input admittance (Y_{aa}) of the semi-infinite beam is Y_0, and the velocity v_a is simply

$$v_a = Y_0 F_a \tag{16}$$

The quantity Y_0 is called the characteristic admittance of the beam. Note particularly that, although the transfer admittance $[Y_{xa}(s)]$ between stations x and a is a function of s and, therefore has a phase lag, the characteristic impedance Y_0^{-1} is independent of s. The reciprocal of Y_0 is called the characteristic impedance of the beam. It will be symbolized by Z_0. Thus,

$$Z_0 = A\sqrt{\rho E} \tag{17}$$

Longitudinal Vibration of a Free-Free Beam

Factored solution.- Although the traveling-wave solution for longitudinal compression waves in thin uniform beams is well-known (ref 15), the solution is derived here by a method that directly separates the processes of propagation within the beam from the process of reflection at the boundary. The method, which follows closely a treatment of wavelike transmitters by Paynter (ref 16), is developed in detail for subsequent use as a model for generalizing to the transverse-bending problem.

For a uniform thin beam of length, ℓ, which obeys the wave equation and has the initial conditions assumed in equations (9a and 9b), application of the Laplace transform with respect to t yields the same ordinary differtial equation as that for the semi-infinite beam. The energy state of the beam is determined by the longitudinal velocity $v(x,t)$ and the axial compression force $F(x,t)$. Thus, a state vector y can be defined as

$$y(x,t) = \begin{bmatrix} v(x,t) \\ F(x,t) \end{bmatrix} \tag{18}$$

The transform $y(x,s)$ of $y(x,t)$ is related to $u(x,s)$ by the following:

$$y(x,s) = \begin{bmatrix} v(x,s) \\ F(x,s) \end{bmatrix} = \begin{bmatrix} su(x,s) \\ -EA \dfrac{du(x,s)}{dx} \end{bmatrix} \tag{19}$$

Equation (19) is used to write the transformed wave equation (eq 10) in the canonical form,

$$\frac{d}{dx} \begin{bmatrix} v(x,s) \\ F(x,s) \end{bmatrix} = \overset{A}{\left[\begin{array}{c|c} 0 & -\dfrac{s}{EA} \\ \hline -\dfrac{EAs}{c^2} & 0 \end{array}\right]} \begin{bmatrix} v(x,s) \\ F(x,s) \end{bmatrix} \tag{20}$$

Equation (20) can be written compactly as

$$\frac{dy}{dx} = Ay \tag{21}$$

where A is the 2x2 matrix on the right side of equation (20). Equation (21) is the canonical form for the state-variable formulation currently so popular in the theory of automatic control (ref 17). Note that the independent variable in the present case is the spacial variable x; and the components of y are Laplace transforms of the physical variables.

The eigenvalues of λ_1 and λ_2 of the matrix A are

$$\lambda_1 = s/c; \quad \lambda_2 = -s/c \tag{22}$$

The theory for diagonalization of matrices with distinct eigenvalues (ref 18) permits matrix A to be written in the factored form $A = WPW^{-1}$ where P is a diagonal matrix of eigenvalues, and W is a matrix formed by the use of the corresponding eigenvectors as columns. If we choose P as

$$P = \begin{bmatrix} \frac{s}{c} & 0 \\ 0 & -\frac{s}{c} \end{bmatrix} \tag{23}$$

then the following W and W^{-1} satisfy the requirements:

$$W = \frac{1}{\sqrt{2}} \begin{bmatrix} 1 & 1 \\ -Z_o & Z_o \end{bmatrix} \quad ; \quad W^{-1} = \frac{1}{\sqrt{2}} \begin{bmatrix} 1 & -Y_o \\ 1 & Y_o \end{bmatrix} \tag{24}$$

where Z_0 and Y_0 are the characteristic impedance and characteristic admittance defined in equations (12a and 17). If a new state vector z is chosen, so that

$$y = Wz \tag{25}$$

then z satisfies the matrix differential equation

$$\frac{dz}{dx} = Pz \tag{26}$$

The solution of equation (26) can be written in terms of the matrix exponential (ref 18) as

$$z_b(s) = e^{\ell P} z_a(s) \tag{27}$$

where z_a and z_b are the values of z at stations a and b. For the matrix P in equation (23), the matrix $e^{\ell P}$ is

$$e^{\ell P} = \left[\begin{array}{c|c} e^{Ts} & 0 \\ \hline 0 & e^{-Ts} \end{array}\right] \tag{28}$$

Because $y = Wz$, [eq (25)] the relation between y_b and y_a is determined from equation (27) as

$$y_b = [W\, e^{\ell P}\, W^{-1}]\, y_a \tag{29}$$

Transmission matrix.- The matrix product $We^{\ell P} W^{-1}$ will be called the transmission matrix T_{ba}. If the matrix product is formed, the relation $y_b = T_{ba}\, y_a$ becomes

$$\begin{bmatrix} v_b(s) \\ F_b(s) \end{bmatrix} = \overbrace{\left[\begin{array}{c|c} \cosh Ts & -Y_0 \sinh Ts \\ \hline -Z_0 \sinh Ts & \cosh Ts \end{array}\right]}^{T_{ba}} \begin{bmatrix} v_a(s) \\ F_a(s) \end{bmatrix} \tag{30}$$

The use of transmission matrices for both lumped and distributed systems is treated in references 14, 15, and 16. The transmission matrix is particularly useful in the analysis of cascade systems, because it is simply the matrix product of the constituent matrices; e.g., if $y_b = T_{ba}\, y_a$ and $y_c = T_{cb}\, y_b$ then $y_c = T_{cb}\, T_{ba}\, y_a$. If the transmission matrix T_{ab} is defined so that $y_a = T_{ab}\, y_b$ it is then equal to T_{ba}^{-1}. Thus,

$$\begin{bmatrix} v_a(s) \\ F_a(s) \end{bmatrix} = \overbrace{\left[\begin{array}{c|c} \cosh Ts & Y_o \sinh Ts \\ \hline Z_0 \sinh Ts & \cosh Ts \end{array}\right]}^{T_{ab}} \begin{bmatrix} v_v(s) \\ F_b(s) \end{bmatrix} \tag{31}$$

Hence, matrices T_{ab} and T_{ba} are identical except for sign differences. This is a consequence of the symmetry of the beam.

Transfer matrices.- Although the transmission matrix form, which relates the variables v_a, F_a to v_b, F_b, is useful, other arrangements of the variables lead more directly to transfer functions that are input-output relations. Of these, the admittance matrix form is the most suitable for treating forced response:

$$\begin{bmatrix} v_a \\ \\ v_b \end{bmatrix} = \frac{1}{Z_o \sinh Ts} \left[\begin{array}{c|c} \cosh Ts & -1 \\ \hline 1 & -\cosh Ts \end{array}\right] \begin{bmatrix} F_a \\ \\ F_b \end{bmatrix} \tag{32}$$

This corresponds to the free-free boundary condition. The natural frequencies for this condition are given by $\sinh Ts = 0$, which yields the free-free-beam frequencies, $\omega T = 0, \pi, 2\pi$, etc. The system zeroes of the four admittance operators are different. The transfer admittances $Y_{ab} \equiv v_a/F_b$ and $Y_{ba} \equiv v_b/F_a$ have no zeroes. The input admittances $Y_{aa} = v_a/F_a$ and $Y_{bb} = v_b/F_b$ have zeroes determined by the equation $\cosh Ts = 0$, i.e., $\omega = \pi/2, 3\pi/2, 5\pi/2$, etc. Thus, the pole-zero pattern for Y_{aa} or Y_{bb} is a set of alterating poles and zeroes along the $j\omega$ axis, as shown in figure 3a. The frequency response of the admittance operators is found by substituting $s \to j\omega$. For example,

$$Y_{aa}(j\omega) = \frac{v_a(j\omega)}{F_a(j\omega)} = \frac{\cos \omega T}{jZ_o \sin T\omega} \tag{33}$$

Figure 3b shows the gain and phase of $Y_{aa}(j\omega)$. Other transfer matrix forms are useful for different boundary conditions, e.g., the impedance matrix form, when the velocities v_a and v_b are inputs.

Separation of propagation and reflection.- The transmission and transfer matrix forms, although computationally useful, do not emphasize the significance of the propagation and characteristic-impedance operators that are of prime importance for semi-infinite-beam dynamics.

Actually, equation (29) holds the key to a separation of the propagation and reflection processes. The thin-beam transmission matrix T_{ab} could have been derived more directly were it not desired to derive equation (29) and the relations preceeding it as a by-product. Note that equation (27) is a transmission matrix for the new state vector z, because it relates the state vectors at b and a. Elements of z will be denoted by z^- and z^+ and will be called the characteristic variables for the wave equation. The transmission matrix form of equation (27) can be converted into a transfer matrix form involving only the pure-delay operator e^{-Ts}. In terms of z^+ and z^-,

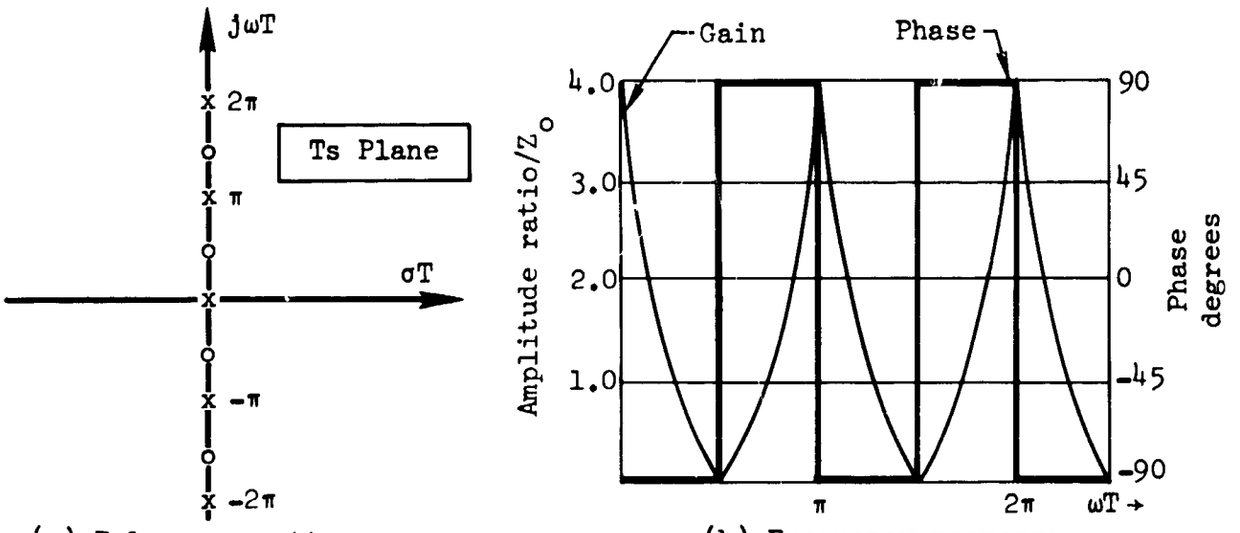

(a) Pole-zero pattern (b) Frequency response

Figure 3.- Longitudinal input admittance $Y_{aa}(s)$

this relation is

$$\begin{bmatrix} z_a^- \\ z_a^+ \end{bmatrix} = \begin{bmatrix} e^{-Ts} & 0 \\ 0 & e^{-Ts} \end{bmatrix} \begin{bmatrix} z_b^- \\ z_a^+ \end{bmatrix} \tag{34}$$

The reason for the superscripts + and - is now evident: the z^+ and z^- variables are propagated in the +x and -x direction, respectively, through the beam-propagation operator. The relations between the characteristic variables (z^+ and z^-) and the physical variables (v and F) are established by rearranging $y = Wz$ into the forms

$$\begin{bmatrix} v_a \\ z_a^+ \end{bmatrix} = \overbrace{\begin{bmatrix} Y_o & \sqrt{2} \\ \sqrt{2}\,Y_o & 1 \end{bmatrix}}^{L^o} \begin{bmatrix} F_a \\ z_a^- \end{bmatrix} \tag{35a}$$

circulates undiminished around the loop containing the two delay operators (propagation loop).

This sequence illustrates (for the free-free beam), the inherent lack of damping in terms of propagation and reflection concepts. Since an arbitrary $F_a(t)$ or $F_b(t)$ can be considered a train of impulses, an arbitrary wave will circulate undiminished around the propagation loop.

Damping and Control

Terminal constraints.- The beam behavior with terminal dampers or with active terminal controls is now considered. Terminations are appended to the block diagram of figure 4 to investigate their effects in terms of propagation and reflection.

The terminal constraints imposed at ends a and b will be written

$$F_a = z_a(v_a - v_a^*) + F_a^* \tag{36a}$$

$$F_b = z_b(v_b - v_b^*) + F_b^* \tag{36b}$$

In these relations, z_a and z_b are terminal impedances, v_a^* and v_b^* are externally applied velocity commands, and F_a^* and F_b^* are externally applied force disturbances. For passive dampers, v_a^* and v_b^* must be set to zero. For active controls, z_a and z_b need not satisfy the constraints of a passive impedance.

Appending the constraints of equations (36a and b) to the block diagram of figure 4 results in the block diagram shown in figure 5. Here, the end effects can be simplified without affecting the propagation relations and in fact, can be cast into the same form as the free-free beam. In figure 6 the new end-effects matrices are shown as L and R to distinguish them from L° and R°, the end-effects matrices for the free-free beam. The elements ℓ_{ij} and r_{ij} of L and R can be determined from the relations and parameters for figure 5

$$\ell_{11} = (1 - \ell_{11}^\circ z_a)^{-1}\ell_{11}^\circ \quad ; \quad r_{11} = (1 - r_{11}^\circ z_b)^{-1}r_{11}^\circ \tag{37a}$$

$$\ell_{21} = \ell_{21}^\circ\,(1 - z_a\ell_{11}^\circ)^{-1} \quad ; \quad r_{21} = r_{21}^\circ\,(1 - z_b r_{11}^\circ)^{-1} \tag{37b}$$

$$\ell_{12} = (1 - \ell_{11}^\circ z_a)^{-1}\ell_{12}^\circ \quad ; \quad r_{12} = (1 - r_{11}^\circ z_b)^{-1}r_{12}^\circ \tag{37c}$$

$$\ell_{22} = \ell_{22}^\circ + \ell_{21}^\circ\,(1 - z_a\ell_{11}^\circ)^{-1}z_a\ell_{12}^\circ \quad ; \quad r_{22} = r_{22}^\circ + r_{21}^\circ(1 - z_b r_{11}^\circ)^{-1}z_b r_{12}^\circ \tag{37d}$$

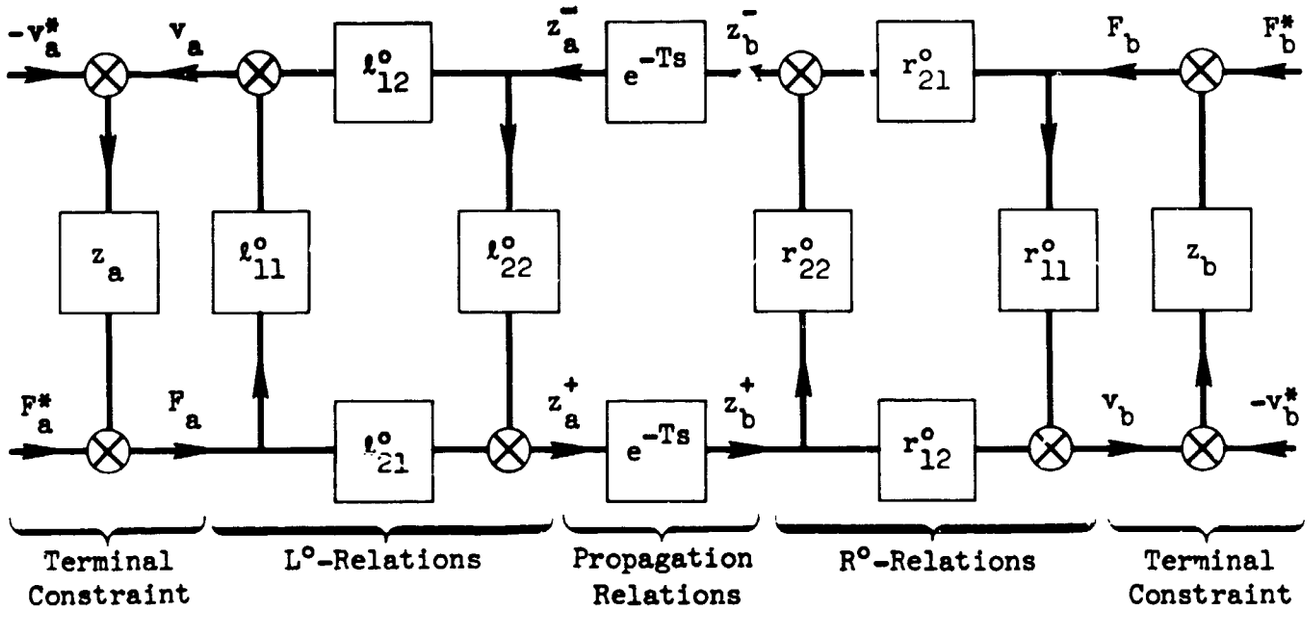

Figure 5.- Free-free beam with longitudinal terminal constraints appended.

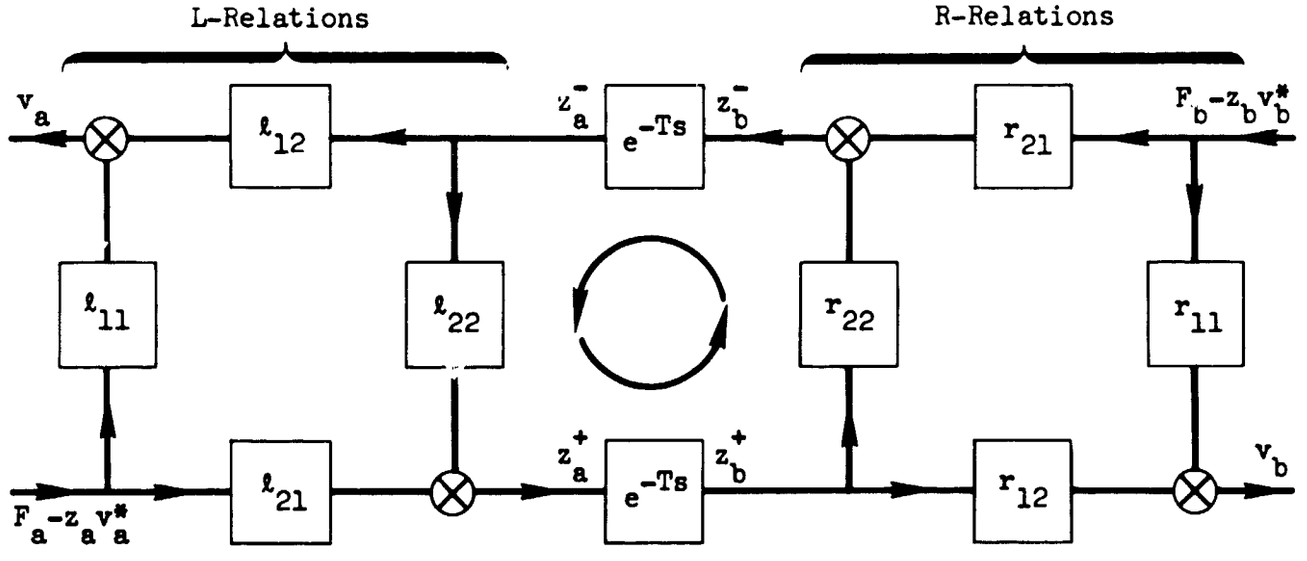

Figure 6.- Propagation and end-effects relations for beam with longitudinal terminal constraints.

The significance of these parameters is investigated by the overall transfer functions for figure 6; these relate the velocities v_a and v_b to the disturbance F_a^* and F_b^* and the velocity commands v_a^* and v_b^*:

$$v_a = [\ell_{11} + \ell_{12}(1-e^{-Ts}r_{22}e^{-Ts}\ell_{22})^{-1}\, e^{-Ts}r_{22}e^{-Ts}\ell_{21}]\,[F_a^* - z_a v_a^*]$$

$$+ [\ell_{12}(1-e^{-Ts}r_{22}e^{-Ts}\ell_{22})^{-1}\, e^{-Ts}r_{21}]\,[F_b^* - z_b v_b^*] \qquad (38a)$$

$$v_b = [r_{11} + r_{12}(1-e^{-Ts}\ell_{22}e^{-Ts}r_{22})^{-1}\, e^{-Ts}\ell_{22}e^{-Ts}r_{21}]\,[F_b^* - z_b v_b^*]$$

$$+ [r_{12}(1-e^{-Ts}\ell_{22}e^{-Ts}r_{22})^{-1}\, e^{-Ts}\ell_{21}]\,[F_a^* - z_a v_a^*] \qquad (38b)$$

These expressions are taken directly from the block diagram (fig 6) without combining terms, such as $e^{-Ts}\ell_{22}e^{-Ts}r_{22} = \ell_{22}r_{22}e^{-2Ts}$, in order to illustrate how they are derived, because the matrix form of similar relations for beam bending, which is derived subsequently, does not allow the combining of terms.

The reflection coefficients.- The coeffiecients ℓ_{22} and r_{22} play a most important role in equations (38a and b). They are known in the literature as the reflection coefficients (ref 14), because they are the ratios of the reflected-to-transmitted z variables, i.e.,

$$z_a^+ = \ell_{11}z_a^- \quad ; \quad z_b^- = r_{22}z_b^+ \qquad (39)$$

The expressions for ℓ_{22} and r_{22} [eq (37d)] can be written in the more conventional form

$$\ell_{22} = \frac{Z_o + z_a}{Z_o - z_a} \quad ; \quad r_{22} = \frac{Z_o - z_b}{Z_o + z_b} \qquad (40)$$

Clearly, ℓ_{22} and r_{22} are equal to zero, if the terminal impedances z_a and z_b match the characteristic impedance Z_o. For the free-free boundary condition, $z_a = z_b = 0$, and the reflection coefficients are plus one. This agrees with the relations between z^+ and z^- for the free-free beam (figure 4). For the fixed-fixed boundary condition, the reflection

coefficients are minus one, because z_a and $z_b \to \infty$. In general, the reflection coefficient for either end a or b is a real number with magnitude < 1 for all real positive values of the terminal impedances.

The case of no reflection is of particular interest. It can be interpreted in terms of dynamics of the semi-infinite beam, for which the free-end input admittance is Y_o, because r_{22} and z_a are zero. This is also obvious from figure 7.

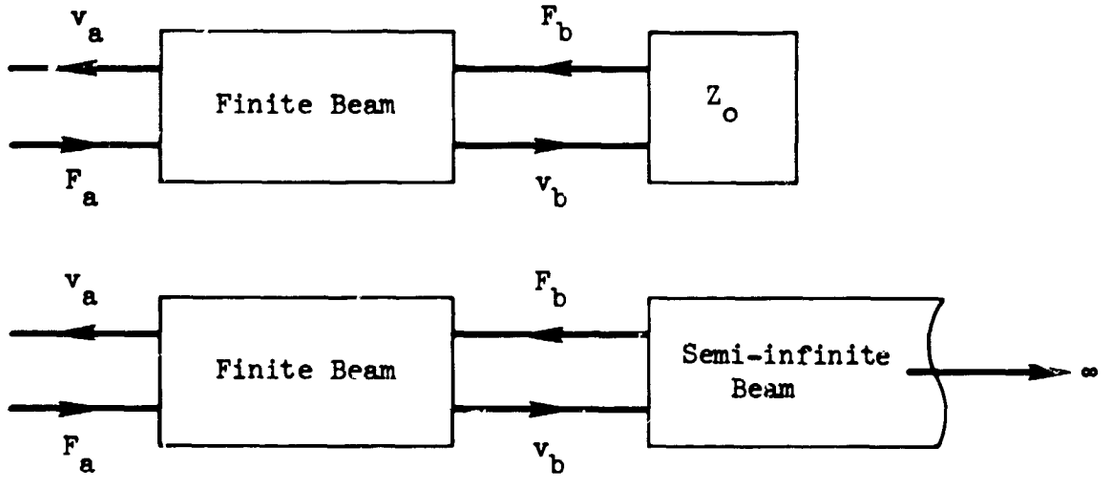

Figure 7.- Physical interpretation of Z_o termination.

When neither ℓ_{22} nor r_{22} is zero, equations (38a and b) can be used directly. More insight can be gained by writing the indicated inverses in series form:

$$(1 - e^{-Ts}\ell_{22}e^{-Ts}r_{22})^{-1} = (1 - e^{-Ts}r_{22}e^{-Ts}\ell_{22})^{-1} = 1 + \ell_{22}r_{22}e^{-2Ts}$$

$$+ (\ell_{22}r_{22})^2e^{-4Ts} + (\ell_{22}r_{22})^3e^{-6Ts} + \ldots. \qquad (41)$$

Substituting equation (41), into equation (38) results in

$$v_a = [\ell_{11} + \ell_{12}r_{22}\ell_{21}e^{-2Ts}\,(1 + \ell_{22}r_{22}e^{-2Ts} + \ell_{22}^2r_{22}^2e^{-4Ts} + \ldots)][F_a^* - z_av_a^*]$$

$$+ [\ell_{12}r_{21}e^{-Ts}\,(1 + \ell_{22}r_{22}e^{-2Ts} + \ell_{22}^2r_{22}^2e^{-4Ts} + \ldots)]\,[F_b^* - z_bv_b^*] \qquad (42)$$

A similar equation for v_b results.

The significance of the series expansion for v_a may be illustrated for the special case, where $z_a = 0$ and z_b is arbitrary. The input impedance Y_{aa} is then

$$\frac{v_a}{F_a} = Y_{aa} = Y_o[1 + 2(r_{22}e^{-2Ts} + r_{22}^2e^{-4Ts} + r_{22}^3e^{-6Ts} + \ldots)] \qquad (43)$$

The response of v_a to a unit step of F_a is shown in figure 8 for several real values of r_{22}.

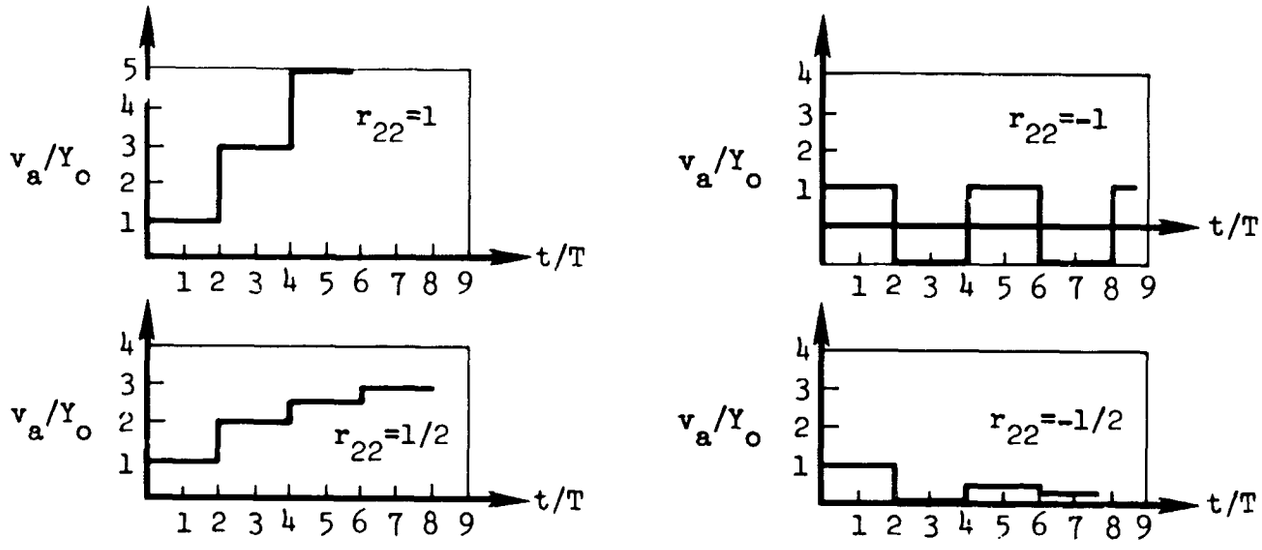

Figure 8.- Effect of the reflection coefficient r_{22} on successive waves -step response of $Y_{aa}(s)$.

The responses clearly show that the series solution (eq 43) is an expansion in terms of successive waves. Such expansions are well-known in electrical-transmission-line theory (ref 14).

Load disturbances.- One fundamental problem of automatic control is the regulator problem, i.e., holding the output constant. This is in contrast to the servomechanism problem, i.e., making the output follow the input. Load disturbances can be regulated with active or passive devices. In the present context, viscous dampers, spring-mass-damper vibration absorbers, and active controls with fixed set-points may all be considered regulators of longitudinal beam velocity.

Velocity regulators at the beam terminals, whose damping forces are a function only of the velocity at the point of application, are described by equations (38a and b), if the disturbances also occur at the terminals.

Consider the problem of reducing, by a regulator mounted at b, the velocity v_a resulting from disturbances F_a. The transfer function for this is given by equation (43). The case of no regulator corresponds to $r_{22} = 1$; if the regulator impedance is a real number (i.e., velocity feedback), the reflection coefficient r_{22} will vary monotonely from plus one to minus one as z_b varies from zero to infinity [see eq (37d)]. If the beam is disturbed by an impulse of F_a, the response is most simply calculated from equation (43) and visualized in terms of propagation and reflection. Moreover, an impulse has some merit as a test signal when the frequency spectrum of the disturbance is broad. Figure 9 shows the response of v_b to a unit impulse of F_a for several different values of r_{22}.

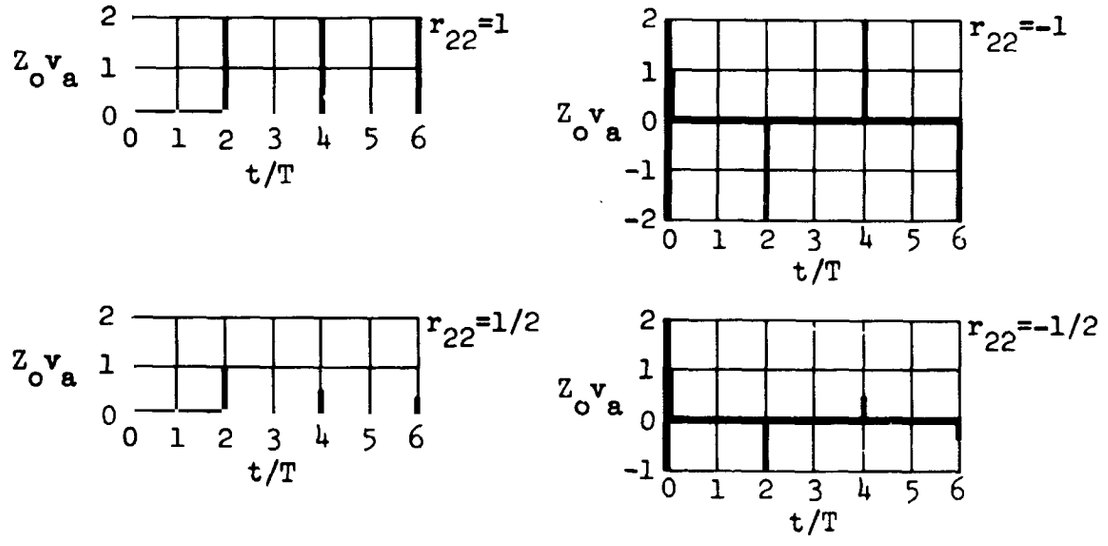

Figure 9.- Effect of the reflection coefficient r_{22} on response of v_a to a unit impulse disturbance of F_a.

It is clearly preferable to make $r_{22} = 0$; thus, the optimum setting of the regulator gain is Z_o. In addition, too much feedback is as undesirable as too little.

Application of transmission concepts to regulation problems ranges from the electrical-transmission-line voltage-regulation problem (ref 19) to pulsation damping in fluid lines (ref 20).

Velocity control.- As an example of the application of propagation and reflection concepts to velocity control, assume that an active rate feedback control is mounted at b to control v_a and v_b, and the control transfer

function z_b is a pure gain. The variation of r_{22} with z_b is the same as that in the regulator problem. Equation (38) and the series expansion of equation (41) can be used to determine the response:

$$v_a = \left[\frac{z_b Y_o}{1+z_b Y_o} + \frac{2z_b Y_o}{(1+z_b Y_o)^2}\left(e^{-2Ts} + r_{22}\, e^{-4Ts} + r_{22}^2\, e^{-6Ts} + \ldots\right)\right] v_b^* \tag{44}$$

$$v_b = \left[\frac{2z_b Y_o}{1+z_b Y_o}\left(e^{-Ts} + r_{22}\, e^{-3Ts} + r_{22}^2\, e^{-5Ts} + \ldots\right)\right] v_b^*$$

Figure 10 shows the response of v_a and v_b to a step command for several different values of controller gain.

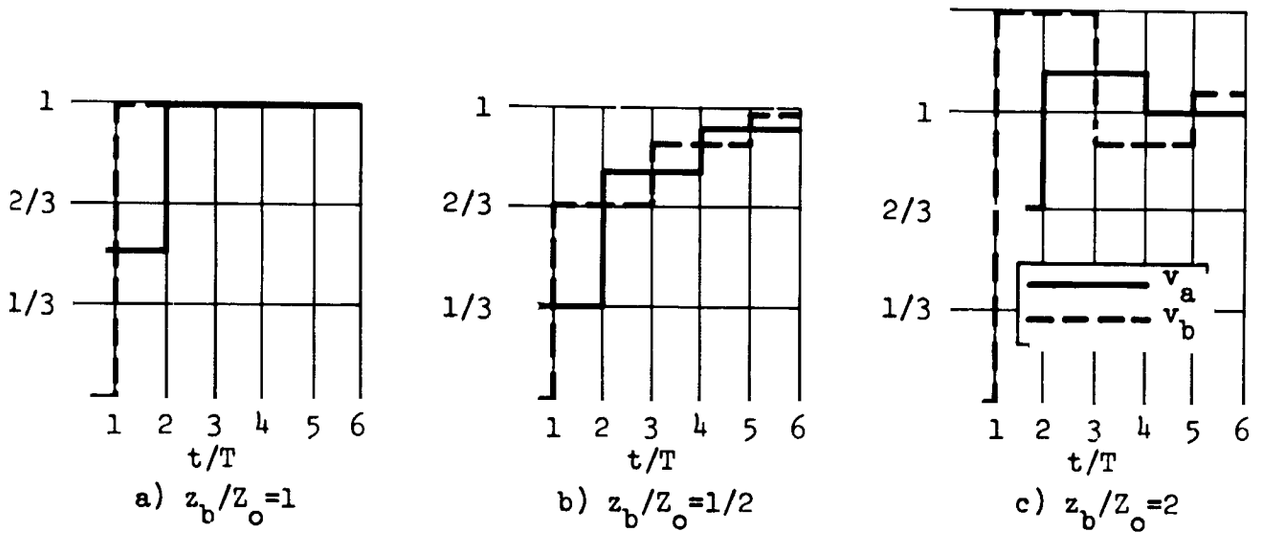

Figure 10.- Effect of z_b/Z_o on response of v_a and v_b to a unit step v_a command.

The conclusion is much the same as that for the load-disturbance problem, i.e., a control gain of $z_b = Z_o$ optimizes the response at the uncontrolled end a. Increasing the gain beyond this value produces oscillation rather than faster response.

This example is admittedly idealized, but it shows that the control loop is an impedance affecting the reflection of waves at the controlled end of the beam. Even for this idealized situation, where the controller has an infinite bandwidth actuator, the inherent propagation delay T is shown to limit the speed of response at stations physically separated from the control.

Nonuniform beams.- A nonuniform beam can be approximated by a cascade of dissimilar uniform beams having an overall transmission matrix which is simply the matrix product of the constituent transmission matrices. The subleties of minimizing the number of uniform elements, the insights gained by factored forms, and concepts of transmission and reflection are treated in an elegant fashion by Paynter (ref 16), Paynter and Ezekiel (ref 21), and Brown (ref 22). They show that a transformation of variables may greatly reduce the variability of wave forms caused by property variations. Since nonuniform structures are not considered in depth in this report, these transformations are not treated here; however, they are highly recommended for analysis of nonuniform structures.

TRANSVERSE BENDING VIBRATIONS OF THIN BEAMS

The Bernoulli-Euler Equation

The preceding treatment of the dynamics and control of longitudinal beam vibration by propagation and reflection concepts is used in this section as a model to generalize these concepts for the dynamics and controls analysis of thin-beam bending. This is a preliminary step toward understanding the flexible-vehicle control problem in terms of these concepts.

The central roles of the propagation operator, characteristic impedance, and the reflection coefficient in the dynamics and control of longitudinal vibrations suggest that generalizations of these concepts may be equally useful for bending vibrations. This is confirmed in the remainder of this report.

General background.- Unfortunately, the transverse bending dynamics of beams do not obey the wave equation. The equation for transverse bending of a thin beam is known as the Bernoulli-Euler equation. It assumes that energy is stored only in the beam's lateral translation inertia and bending compliance. The thin beam equation for transverse bending is assumed in the work that follows. The implications of this assumption are treated by Vigness (ref 3), Dengler and Goland (ref 6), and Flügge and Zajac (ref 23). According to the latter, Lamb (ref 24) showed, in 1914, that the Bernoulli-Euler equation gives instantaneous spatial propagation of effect. This result is contained in Boussinesq's theory (ref 4) for transverse impact of beams. Timoshenko proposed correcting the thin-beam behavior by two additional energy-storage mechanisms: kinetic energy in the beam's rotary inertia and potential energy in the beam's shear complicance. In 1942, Flügge demonstrated that Timoshenko's theory results in a finite spatial propagation velocity (ref 25). Many analytical studies of traveling waves in the Timoshenko beam have been published. Reference 5 (Leonard and Budiansky), and references 6, and 23 cover this subject rather completely.

Nearly all of this work was developed to predict the stress caused by sharp impact. For this purpose, the use of the Bernoulli-Euler equation can result in serious errors. On the other hand, the effects of rotary inertia and shear compliance are often ignored in the dynamics and controls analysis of flexible vehicles (which is universally performed by normal modes).

Accordingly, the deficiencies of the propagation behavior of the solution to the Bernoulli-Euler equation, which are unacceptable for impact studies, may be of little consequence in controls applications, where the extremely high-frequency behavior emphasized in the impact problem is of secondary importance. The distributed-parameter approach is well established in the treatment of heat propagation (ref 26) and of distributed RC electrical lines (ref 14), where spatial propagation velocity is infinite.

A clear derivation of the Bernoulli-Euler equation for transverse vibration of thin beams is given by Jacobsen and Ayre (ref 12). Sign conventions, nomenclature, and pertinent relations used in this report are discussed in the following paragraphs.

Figure 11 shows the nomenclature and sign conventions for shear forces, moments, and angular and transverse displacements of a thin beam and a micro-element.

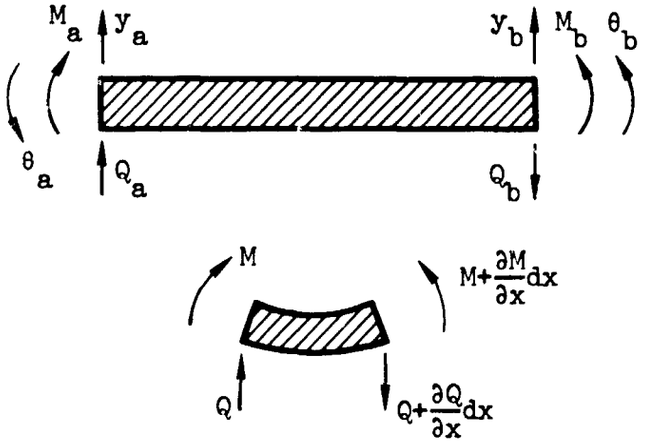

Figure 11.- Lateral forces and displacements, moments, and angular displacements for a uniform beam and a micro-element thereof.

The symbols y, θ, M, and Q denote the transverse displacement, angular rotation, moment, and shear force, respectively. The lateral location coordinate is x, and the beam length is ℓ, as in the analysis of longitudinal vibration.

Analysis of the micro-element yields the following relations:

Static Beam Flexure $$M = EI \frac{\partial^2 y}{\partial x^2} \tag{45a}$$

$$\underline{F = ma \text{ in } y \text{ direction}} \qquad \frac{\partial Q}{\partial x} = -\rho A \frac{\partial^2 y}{\partial t^2} \tag{45b}$$

$$\underline{\text{Moment Balance}} \qquad Q = \frac{\partial M}{\partial x} \tag{45c}$$

$$\underline{\text{Geometry}} \qquad \theta = \frac{\partial y}{\partial x} \tag{45d}$$

where I = the area moment of inertia of the cross-section, and E, A, and ρ are the Young's modulus, cross-sectional area, and density previously defined. Combining equations (45a, b, and c) yields the Bernoulli-Euler equation.

$$a^2 \frac{\partial^4 y}{\partial x^4} + \frac{\partial^2 y}{\partial t^2} = 0 \tag{46}$$

where

$$a^2 \equiv \frac{EI}{\rho A} \tag{47}$$

Normal-mode solution.- Normal-mode solution of the Bernoulli-Euler equation closely parallels that of the wave equation. Extensive treatments are given by Bishop and Johnson (ref 27) and in references 1 and 12. However, a distinct treatment of the rigid-body motion as an integral part of the normal-mode analysis could not be found; therefore, it is considered in the following paragraphs.

In addition to the flexible modes, two rigid-body modes exist: rigid body rotation and rigid body lateral translation. These modes will be given the subscripts -1 and 0, respectively. Thus, the total lateral deflection is

$$y(x,t) = \sum_{n=-1}^{\infty} \phi_n(x)\, q_n(t) \tag{48}$$

The normal-mode coordinates, q_n, are determined, as before from the generalized forces, F_n, by the transfer functions

$$q_n = \frac{F_n}{M_n s^2 + \omega_n^2 M_n} \tag{49}$$

But now, the generalized force F_n is

$$F_n = \int_0^\ell Q'(x)\ \phi_n(x)\ dx + \sum_r Q_r\ \phi_n(x_r) + M_r\ \phi_n'(x_r) \tag{50}$$

where $Q'(x)$ is the distributed lateral force intensity, M_r is the concentrated moment at station r, and $\phi_n' = d\phi_n/dx$ is the n^{th} mode slope.

The mode shapes and natural frequencies are determined by the boundary conditions. The rigid-body mode shapes for a free-free uniform beam, in terms of arbitrary scales C_n, are

$$\phi_{-1} = C_{-1}\left(1 - 2\,\frac{x}{\ell}\right); \quad \phi_o = C_o \tag{51}$$

The rigid-body-motion modal masses and frequencies are

$$M_{-1} = \frac{m}{3}\,\phi_{-1}^2(\ell); \quad M_o = m\,\phi_o^2(x) \tag{52}$$

$$\omega_{-1} = 0; \quad \omega_o = 0$$

The flexible mode shapes are given in references 27, 1, and 12, and are tabulated for a variety of boundary conditions by Bishop and Johnson (ref 28). The flexible free-free mode masses are given by

$$M_n = \frac{m}{4}\,\phi_n^2(\ell) \qquad n = 1,2,3, \ldots \tag{53}$$

The free-free frequencies are determined from the frequency equation

$$\cos\sqrt{\frac{\omega\ell^2}{a}}\ \cosh\sqrt{\frac{\omega\ell^2}{a}} = 1 \tag{54}$$

The normal mode solution for the Bernoulli-Euler equation has great appeal, because it retains almost all the simplicity of the normal-mode solution for the wave equation. Moreover, although the mode shapes, masses, and frequencies must be determined, equations (48), (49), and (50) retain their simplicity for nonuniforms structures. The modal solution has the same advantages for the Bernoulli-Euler equation as it has for the wave equation: (1) the transfer-function poles are evident, (2) high-frequency poles are eliminated simply by truncating equation (48), and (3) the transfer functions are rational algebraic functions of s. Moreover, these advantages are retained in the normal-mode solution for the Timoshenko beam.

However, the solution of the Bernoulli-Euler equation in terms of propagation concepts will be shown to reveal features of the beam dynamics that are well-hidden in the normal-mode solution.

Semi-Infinite Beam

The traveling-wave solution of the wave equation for a semi-infinite medium was shown to yield, in a simple manner, the concepts of the propagation operator and the characteristic impedance. Similarily, it is instructive to investigate the solution to the Bernoulli-Euler equation for a semi-infinite uniform thin beam before studying the finite beam.

The boundary conditions at $x = \infty$ are

$$y(\infty, t) = 0 \tag{55a}$$

$$\frac{\partial y}{\partial x}(\infty, t) = 0 \tag{55b}$$

If the beam is initially at rest and undeflected, the initial conditions can be written

$$\frac{\partial y}{\partial t}(x, 0) = 0 \tag{56a}$$

$$y(x, 0) = 0 \tag{56b}$$

The Laplace transform of equation (46) with respect to time yields the following ordinary differential equation:

$$s^2 y(x, s) + a^2 \frac{d^4 y(x,s)}{dx^4} = 0 \tag{57}$$

The general solution of equation (57) can be written

$$y(x,s) = c_1 e^{\lambda_1 x} + c_2 e^{\lambda_2 x} + c_3 e^{\lambda_3 x} + c_4 e^{\lambda_4 x} \tag{58}$$

where

$$\lambda_1 = \sqrt{s/a}\,(1+j)/\sqrt{2}; \quad \lambda_2 = \sqrt{s/a}\,(1-j)/\sqrt{2}$$

$$\lambda_3 = \sqrt{s/a}\,(-1+j)/\sqrt{2}; \quad \lambda_4 = \sqrt{s/a}\,(-1-j)/\sqrt{2} \tag{59}$$

or, alternately, it can be written

$$y(x,s) = c_1 e^{\sqrt{T(x)s}} \sin \sqrt{T(x)s} + c_2 e^{\sqrt{T(x)s}} \cos \sqrt{T(x)s}$$
$$+ c_3 e^{-\sqrt{T(x)s}} \sin \sqrt{T(x)s} + c_4 e^{-\sqrt{T(x)s}} \cos \sqrt{T(x)s} \tag{60}$$

where

$$T(x) \equiv \frac{x^2}{2a} \tag{61}$$

The advantage of equation (60) is that complex numbers are avoided entirely. If equation (60) is used, the boundary conditions at $x = \infty$ (eqs 55a and b) require that $c_1 = c_2 = 0$. Thus, the only operators remaining are $e^{-\sqrt{T(x)s}} \cos \sqrt{T(x)s}$ and $e^{-\sqrt{T(x)s}} \sin \sqrt{T(x)s}$. Because they occur so frequently, the following notation is introduced for convenience:

$$C(Ts) \equiv e^{-\sqrt{Ts}} \cos \sqrt{Ts} \tag{62a}$$

$$S(Ts) \equiv e^{-\sqrt{Ts}} \sin \sqrt{Ts} \tag{62b}$$

If an arbitrary transverse velocity, $\dot{y}_a(t)$, and moment, $M_a(t)$, are applied at $x = 0$, the remaining two boundary conditions are

$$sy(0,s) = \dot{y}_a(s) \tag{63a}$$

$$\frac{d^2y(0,s)}{dx^2} = \frac{M_a(s)}{EI} \tag{63b}$$

If c_3 and c_4 are evaluated by equations (63a and b), the result can be written

$$\dot{y}(x,s) = C[T(x)s]\, \dot{y}_a(s) - S[T(x)s]\, \frac{M_a(s)}{EI} \tag{64}$$

Bernoulli-Euler propagation operators.- In analogy to e^{-Ts} of the wave equation, $C(Ts)$ and $S(Ts)$ will be called the Bernoulli-Euler propagation operators. To call e^{-Ts} the wave-propagation operator is not in strict accord with standard practice, wherein the negative exponent Ts would be so termed (refs 16 and 22).

The inversion transforms of the propagation operators $C(Ts)$ and $S(Ts)$ are far more complicated than that of e^{-Ts}. The step response of $C(Ts)$ is treated by Carslaw and Jaeger (ref 29), who show, by a contour integration, that

$$\mathcal{L}^{-1}\left[\frac{1}{s}\,C(T(x)s)\right] = 1 - \frac{1}{\pi}\int_0^{\frac{x}{\sqrt{2\pi at}}}\left[\cos\frac{1}{2}\,\S^2 + \sin\frac{1}{2}\,\S^2\right]d\S \tag{65}$$

This integral can be evaluated using the Fresnel integrals tabulated by Janke and Emde (ref 30):

$$I_c(x) \equiv \int_0^x \cos\frac{\pi}{2}\,x^2\,dx$$

$$I_s(x) \equiv \int_0^x \sin\frac{\pi}{2}\,x^2\,dx \tag{66}$$

In terms of these functions, the result is

$$\mathcal{L}^{-1}\left[\frac{1}{s}\,C(T(x)s)\right] = 1 - \left[I_c\,\frac{T(x)}{\pi t} + I_s\,\frac{T(x)}{\pi t}\right] \tag{67}$$

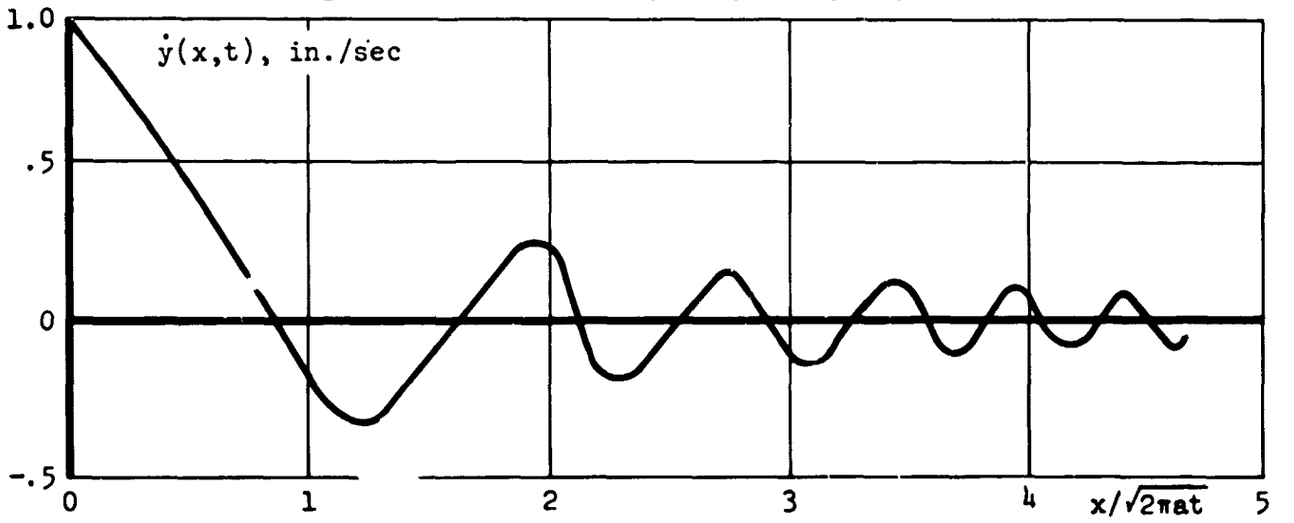

Figure 12.- Lateral semi-infinite beam velocity, $\dot{y}(x,t)$, due to a unit step of $\dot{y}$ at $x=0$; plotted as a function of $x/\sqrt{2\pi at}$.

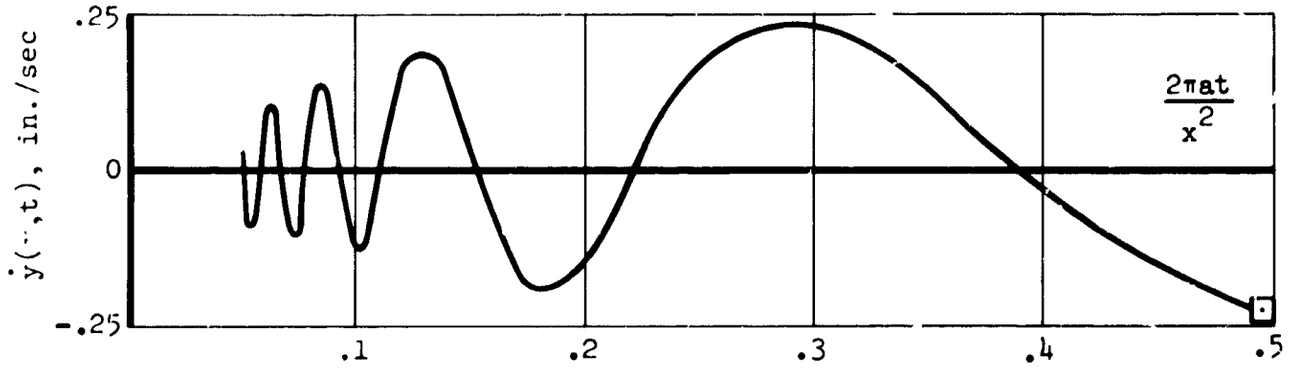

(a) $0.05 \leq \frac{2\pi at}{x^2} \leq 5$

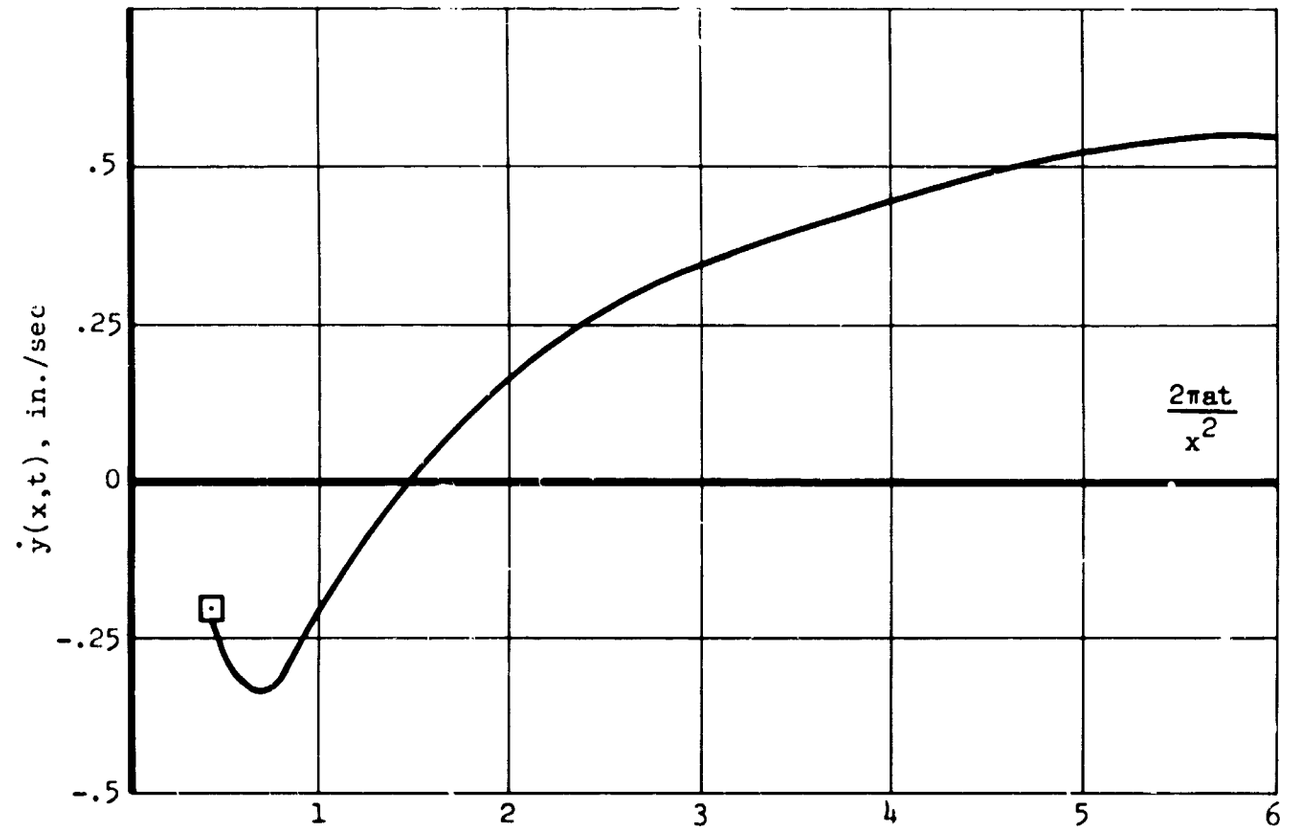

(b) $0.5 \leq \frac{2\pi at}{x^2} \leq 6$

Figure 13.- Lateral semi-infinite beam velocity, $\dot{y}(x,t)$ due to a unit step of $\dot{y}$ at x=0; plotted as a function of $2\pi at/(x^2)$.

Because $C(Ts)$ is the transfer function from $\dot{y}_a(s)$ to $\dot{y}(x,s)$, the right side of equation (67) must be the response of $\dot{y}(x,t)$ to a unit step of $\dot{y}_a$. This is plotted as a function of $x/\sqrt{2\pi at}$ in figure 12. The time response of $\dot{y}(x,t)$ is shown in figure 13 as a function of $\pi t/[[T(x)]$. The behavior for small values of $\pi t/[T(x)]$ cannot be plotted because of high-frequency ringing, a manifestation of the deficiencies of the Bernoulli-Euler equation. The integral of the velocity response shown in figure 13 is the lateral displacement $y(x,t)$ which results from a step-velocity input at a. The high-frequency ringing is heavily filtered by the integration process. Thus, the position response appears more like a delay for small t.

The frequency responses of $C(Ts)$ and $S(Ts)$ are

$$C(j\omega T) = [e^{-\sqrt{2\omega t}} + e^{-j\sqrt{2\omega T}}]/2 \tag{68a}$$

$$S(j\omega T) = [e^{-\sqrt{2\omega T}} - e^{-j\sqrt{2\omega T}}]/(2j) \tag{68b}$$

These are shown in figure 14.

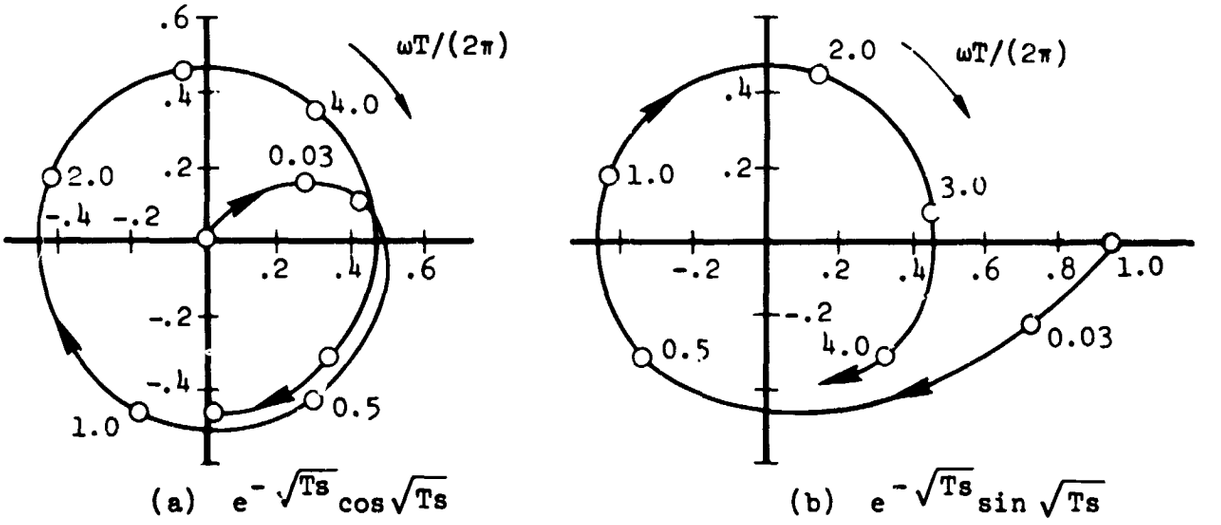

Figure 14.--Polar-frequency plots for the Bernoulli-Euler propagation operators

The low-frequency approximations are

$$C(Ts) \to e^{-\sqrt{Ts}} \quad ; \quad S(Ts) \to \sqrt{Ts} \tag{69}$$

Thus, at low frequencies, $C(Ts)$ approaches the distributed lag $e^{-\sqrt{Ts}}$, and $S(Ts)$ approaches the fractional-derivative operator. At high frequencies, the magnitude of both operators approaches 0.5, the phase lag is proportional to $\sqrt{\omega T}$, and $S(j\omega T)$ leads $C(j\omega T)$ by 90°. These frequency plots can be interpreted as the amplitude and phase of $\dot{y}$ at station x which result from inputs of $\dot{y}$ or M at station a [see eq (64)].

Characteristic-impedance matrix.- If an arbitrary transverse force Q_a and moment M_a are applied at $x = 0$, the remaining two boundary conditions are determined from equations (45a and c) as

$$\frac{d^2y(x,s)}{dx^2} = \frac{M_a(s)}{EI} \tag{70a}$$

$$\frac{d^3y(x,s)}{dx^3} = \frac{Q_a(s)}{EI} \tag{70b}$$

The coefficients c_3 and c_4 can be evaluated, and the transverse and angular velocities $\dot{y}$ and $\dot{\theta}$ can be determined in terms of M_a and Q_a as

$$\begin{bmatrix} \dot{y}(x,s) \\ \dot{\theta}(x,s) \end{bmatrix} = \frac{a}{EI} \left[\begin{array}{c|c} C[T(x)s] - S[T(x)s] & \sqrt{\frac{2a}{s}}\, C[T(x)s] \\ \hline -\sqrt{\frac{2s}{a}}\, C[T(x)s] & -\{C[T(x)s] + S[T(x)s]\} \end{array}\right] \begin{bmatrix} M_a(s) \\ Q_a(s) \end{bmatrix} \tag{71}$$

If this equation is specialized for the case $x = 0$, the result

$$\begin{bmatrix} \dot{y}_a \\ -\dot{\theta}_a \end{bmatrix} = \overbrace{\left[\begin{array}{c|c} \frac{a}{EI} & \frac{a}{EI}\sqrt{\frac{2a}{s}} \\ \hline \frac{a}{EI}\sqrt{\frac{2s}{a}} & \frac{a}{EI} \end{array}\right]}^{Y_o} \begin{bmatrix} M_a \\ Q_a \end{bmatrix} \tag{72}$$

The matrix designated Y_o in equation (72) will be called the characteristic-admittance matrix for thin-beam bending. The need for a matrix of characteristic admittance elements arises from the duplexity both of velocity variables $(\dot{y},\dot{\theta})$ and force variables (M,Q).

The sign conventions of figure 11 reveal that the signs of the motions predicted by equation (72) are consistent with physical intuition, which would have the end a of the semi-infinite beam move in the plus $\dot{y}_a$ and minus $\dot{\theta}_a$ directions in response to either M_a or Q_a. The minus is appended to $\dot{\theta}_a$ because of the sign convention chosen. No sign convention compatible with the transmission-matrix concept (i.e., fitting together in cascade with compatible sign convention) can obviate minus signs in the characteristic admittance relation both for left and right extending semi-infinite beams. For the sign convention shown, if station b is considered the terminal face of a left extending semi-infinite beam, the characteristic-admittance relation is

$$\begin{bmatrix} \dot{y}_b \\ \dot{\theta}_b \end{bmatrix} = \begin{bmatrix} \\ Y_o \\ \\ \end{bmatrix} \begin{bmatrix} M_b \\ -Q_b \end{bmatrix} \tag{73}$$

In this case, the minus must be appended to Q_b.

A discussion of the operators $\sqrt{s}$ and $1/\sqrt{s}$ is now in order. Their step responses can be found in most extensive tables of transform pairs (e.g., table 7.1 of ref 14):

$$\mathcal{L}^{-1}\left(\frac{1}{s\sqrt{s}}\right) = \frac{2}{\sqrt{\pi}}\sqrt{t} \quad ; \quad \mathcal{L}^{-1}\left(\frac{1}{\sqrt{s}}\right) = \frac{1}{\sqrt{\pi}}\sqrt{\frac{1}{t}} \tag{74}$$

Thus, the step response of the Y_o matrix has the form shown in figure 15. The infinite response of $\dot{\theta}_a$ to a step of M_a at $t = 0^+$ does not appear, of course, if the step is replaced by an input with no jump function at $t = 0$.

The frequency response of the Y_o matrix has the form shown in figure 16, because $\sqrt{j\omega}$ has a phase of 45° and gain-frequency slope of 10 dB/decade, whereas $1/\sqrt{j\omega}$ has a phase of -45° and gain-frequency slope of -10 dB/decade.

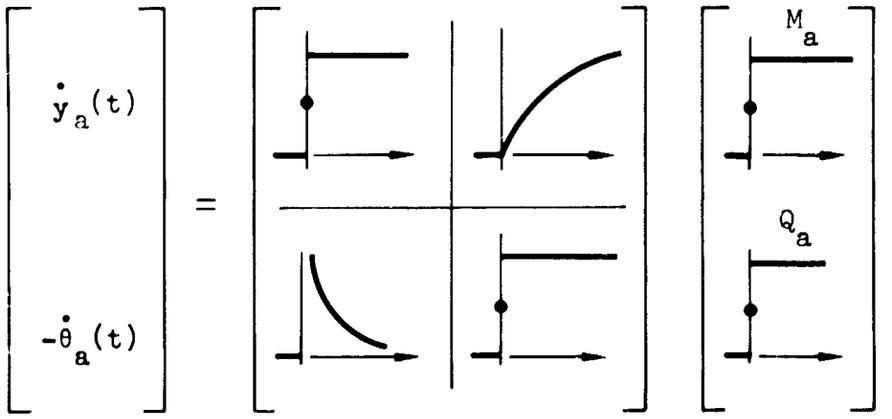

Figure 15.--Matrix pictograph of step responses of the characteristic-impedance matrix.

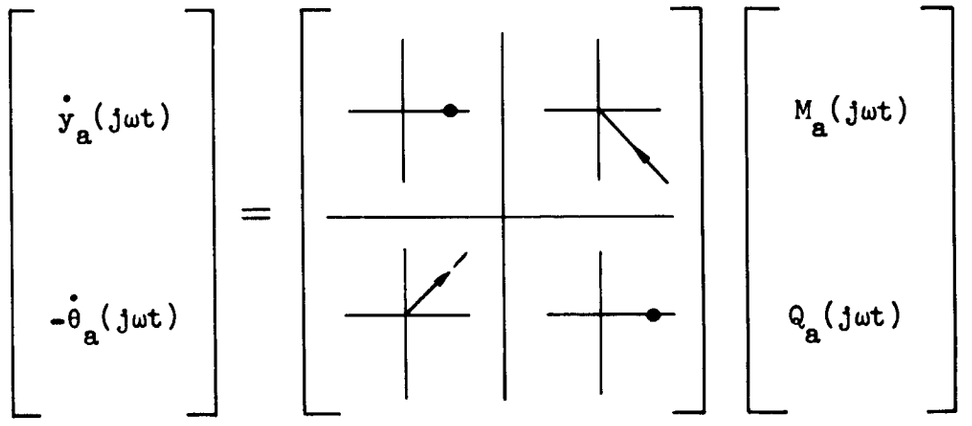

Figure 16.--Matrix pictograph of frequency responses of the characteristic-admittance matrix

The inverse of the characteristic-admittance relation [eq (72)] is

$$\begin{bmatrix} -M_a \\ Q_a \end{bmatrix} = \overbrace{\left[\begin{array}{c|c} \frac{EI}{a} & \frac{EI}{a}\sqrt{\frac{2s}{a}} \\ \hline \frac{EI}{a}\sqrt{\frac{2a}{s}} & \frac{EI}{a} \end{array}\right]}^{Z_o} \begin{bmatrix} \dot{y}_a \\ \dot{\theta}_a \end{bmatrix} \tag{75}$$

The 2x2 matrix Z_o in equation (75) will be called the characteristic-impedance matrix. This relation shows the forces M_a and Q_a that would act on the face of a semi-infinite beam in terms of the input motions $\dot{y}_a$ and $\dot{\theta}_a$. The characteristic-impedance relation for face b can be written

$$\begin{bmatrix} M_b \\ Q_b \end{bmatrix} = \begin{bmatrix} Z_o \end{bmatrix} \begin{bmatrix} -\dot{y}_b \\ \dot{\theta}_b \end{bmatrix} \tag{76}$$

The characteristic-impedance relation has the same meaning for face b as equation (75) has for face a; i.e., M_b and Q_b are the forces that would act on face b of a semi-infinite beam in terms of the input motions $\dot{y}_b$ and $\dot{\theta}_b$.

The minus sign appended to one term of each of the equations (72, 73, 75, and 76) must be treated carefully. The meaning of the signs in the characteristic-impedance relations [eqs (75 and 76)] is particularly difficult to visualize. A better intuitive picture can be achieved by visualizing the relations at a cut in an infinite beam as shown in figure 17. The forces exerted on face b by face a are given by the characteristic-impedance relation for face a. Thus, the impedance relation seen by face b, when it is connected to a semi-infinite beam, is

$$\begin{bmatrix} -M_b \\ Q_b \end{bmatrix} = \begin{bmatrix} Z_o \end{bmatrix} \begin{bmatrix} \dot{y}_b \\ \dot{\theta}_b \end{bmatrix} \tag{77}$$

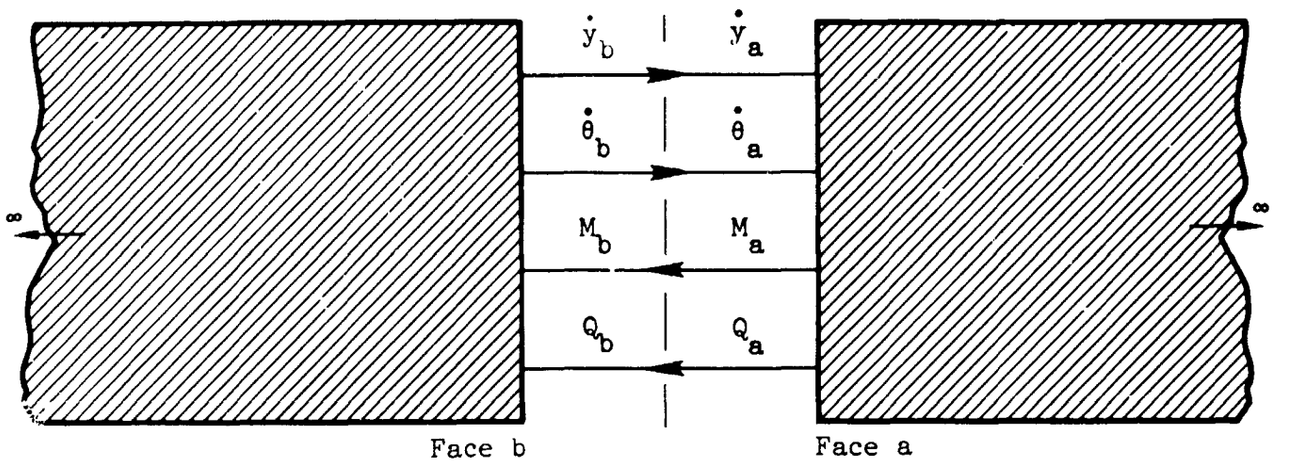

Figure 17.--The impedance matrix seen by face b of a semi-infinite beam is the characteristic impedance of face a.

The sign conventions of figure 11 confirm that all forces exerted on face b are restoring forces. The distinction between equations (76) and (77) is that equation (76) is the input impedance of face b, and equation (77) is the impedance seen by face b, when it is connected to a semi-infinite beam. These distinctions are much simpler for the scalar characteristic impedance in longitudinal vibration, and very little care is required to keep the sign relations in order for that case.

Note that Y_o and Z_o have been defined so that all elements are positive. With this definition, $Y_o \neq Z_o^{-1}$. If the minus signs are moved within the 2x2 matrices in equations (72, 73, 75, and 76), and the resultant 2x2 matrices named Y_{oa}, Y_{ob}, Z_{oa}, and Z_{ob}, respectively, then $Y_{oa} = Z_{oa}^{-1}$, and $Y_{ob} = Z_{ob}^{-1}$; however, $Y_{oa} \neq Z_{ob}^{-1}$ and $Y_{ob} \neq Z_{oa}^{-1}$. Thus, a definition with the desired inverse relation requires two Y_o and two Z_o matrices, and even then the desired inverse relation does not apply to all pairs of Y_o and Z_o matrices.

The characteristic-impedance matrix concept for thin-beam bending has not been treated in the literature, as far as can be determined. Considerable work, however, has been done on the characteristic impedance for flexure waves in plates (for example, refs 31, 32, 33, and 34).

Factored solution. - Now that the nature of the propagation operators and characteristic-impedance matrix for the Bernoulli-Euler equation has been established through analysis of the semi-infinite-beam solution, the transverse vibration of a free-free beam can be investigated. The solution is analogous to the treatment of longitudinal vibrations; it is developed by a method that directly separates the process of propagation within the beam from the process of reflection at the boundaries. The development is a generalization of the methods used to factor the solution of the wave equation.

The Laplace transform with respect to t, applied to a uniform thin beam of length ℓ, which obeys the Bernoulli-Euler equation and has no initial stored energy [eqs (56a and b)], yields the same ordinary differential equation as that for the semi-infinite beam [eq (57)].

A vector Y defining the state of the beam can be defined as the column vector $(\dot{y}, \dot{\theta}, M, Q)^T$. It is related to $y(x, s)$ by the following:

$$Y(x,s) \begin{bmatrix} \dot{y}(x,s) \\ \dot{\theta}(x,s) \\ M(x,s) \\ Q(x,s) \end{bmatrix} = \begin{bmatrix} sy(x,s) \\ sy'(x,s) \\ \frac{1}{EI}\dot{y}''(x,s) \\ \frac{1}{EI}\dot{y}'''(x,s) \end{bmatrix} \tag{78}$$

Equation (78) can be used to reduce the transformed Bernoulli-Euler equation [eq (57)] to in canonical form as four first-order differential equations:

$$\frac{d}{dx} \begin{bmatrix} \dot{y} \\ \dot{\theta} \\ M \\ Q \end{bmatrix} = \left[\begin{array}{c|c|c|c} 0 & 1 & 0 & 0 \\ \hline 0 & 0 & \frac{s}{EI} & 0 \\ \hline 0 & 0 & 0 & 1 \\ \hline \frac{-EIs}{a^2} & 0 & 0 & 0 \end{array}\right] \begin{bmatrix} \dot{y} \\ \dot{\theta} \\ M \\ Q \end{bmatrix} \tag{79}$$

Equation (79) can be written compactly in the state vector form

$$\frac{dY}{dx} = AY \tag{80}$$

where A is the $4x4$ matrix in equation (79). Note that Y here represents the Laplace transform of the states. The eigenvalues of the A matrix, λ_1, λ_2, λ_3, and λ_4 are simply the roots of $\lambda^4 + s^2/a^2 = 0$ given in equation (59). The A matrix can be factored as in the wave equation to $A = WPW^{-1}$, where P, W, and W^{-1} are

$$P = \begin{bmatrix} \lambda_1 & 0 & 0 & 0 \\ 0 & \lambda_2 & 0 & 0 \\ 0 & 0 & \lambda_3 & 0 \\ 0 & 0 & 0 & \lambda_4 \end{bmatrix} \tag{81a}$$

$$W = \frac{1}{2}\begin{bmatrix} s & s & s & s \\ s\lambda_1 & s\lambda_2 & s\lambda_3 & s\lambda_4 \\ EI\lambda_1^2 & EI\lambda_2^2 & EI\lambda_3^2 & EI\lambda_4^2 \\ EI\lambda_1^3 & EI\lambda_2^3 & EI\lambda_3^3 & EI\lambda_4^3 \end{bmatrix} ; \quad W^{-1} = \frac{1}{2}\begin{bmatrix} \frac{1}{s} & \frac{1}{s\lambda_1} & \frac{1}{EI\lambda_1^2} & \frac{1}{EI\lambda_1^3} \\ \frac{1}{s} & \frac{1}{s\lambda_2} & \frac{i}{EI\lambda_2^2} & \frac{1}{EI\lambda_2^3} \\ \frac{1}{s} & \frac{1}{s\lambda_3} & \frac{1}{EI\lambda_3^2} & \frac{1}{EI\lambda_3^3} \\ \frac{1}{s} & \frac{1}{s\lambda_4} & \frac{1}{EI\lambda_4^2} & \frac{1}{EI\lambda_4^3} \end{bmatrix} \tag{81b}$$

Because λ_1, λ_2, λ_3, and λ_4 are complex, the elements of W and W^{-1} are, in general, also complex. This is the spatial analog of the solution for a damped-spring-mass system in terms of its complex roots, which, although possible, is generally awkward: manipulation of real variables is usually more convenient.

A transformation is required that carries the eigenvalue matrix of a complex conjugate pair $(\lambda_r + j\,\lambda_j, \lambda_r - j\,\lambda_j)$

$$\begin{bmatrix} \lambda_r + j\,\lambda_j & 0 \\ 0 & \lambda_r - j\,\lambda_j \end{bmatrix}$$

to the related conical form matrix (ref 35):

$$\begin{bmatrix} \lambda_r & \lambda_j \\ -\lambda_j & \lambda_r \end{bmatrix}$$

The required transformation is

$$\begin{bmatrix} \lambda_r & \lambda_j \\ -\lambda_j & \lambda_r \end{bmatrix} = \frac{1}{2} \begin{bmatrix} 1 & 1 \\ j & -j \end{bmatrix} \begin{bmatrix} \lambda_r + j\lambda_j & 0 \\ 0 & \lambda_r - j\lambda_j \end{bmatrix} \begin{bmatrix} 1 & -j \\ 1 & j \end{bmatrix} \tag{82}$$

Applying this transformation to both pairs of conjugate eigenvalues in the P matrix yields

$$P^* = \frac{s}{2a} \begin{bmatrix} 1 & 1 & & \\ -1 & 1 & 0 & \\ & & -1 & 1 \\ 0 & & -1 & -1 \end{bmatrix} = \frac{1}{\sqrt{2}} \begin{bmatrix} 1 & 1 & & \\ j & -j & 0 & \\ & & 1 & 1 \\ 0 & & j & -j \end{bmatrix} \begin{bmatrix} \lambda_1 & 0 & & \\ 0 & \lambda_2 & 0 & \\ & & \lambda_3 & 0 \\ 0 & & 0 & \lambda_4 \end{bmatrix} \begin{bmatrix} 1 & j & & \\ 1 & j & 0 & \\ & & 1 & j \\ 0 & & 1 & -j \end{bmatrix} \frac{1}{\sqrt{2}} \tag{83}$$

Hence, transformation BPB^{-1} carries P to the matrix P*, which is diagonal in the 2x2-partitioned sense and has only real elements. Using the factorization of A into $A = WPW^{-1}$ and the transformation of equation (83) ($P^* = BPB^{-1}$) gives

$$A = WB^{-1} P^* BW^{-1} = W^* P^* W^{*-1} \tag{84}$$

where

$$W^* \equiv WB^{-1} \tag{85}$$

Thus, W* provides a transformation between the A matrix and the quasidiagonal P* matrix. The matrices W* and W^{*-1} are

$$W^* = \frac{1}{2}\left[\begin{array}{c|c|c|c} \sqrt{2}\,s & 0 & \sqrt{2}\,s & 0 \\ \hline \frac{s^{3/2}}{a^{1/2}} & \frac{s^{3/2}}{a^{1/2}} & -\frac{s^{3/2}}{a^{1/2}} & \frac{s^{3/2}}{a^{1/2}} \\ \hline 0 & \sqrt{2}\,\frac{EIs}{a} & 0 & -\sqrt{2}\,\frac{EIs}{a} \\ \hline -\frac{EIs^{3/2}}{a^{3/2}} & \frac{EIs^{3/2}}{a^{3/2}} & \frac{EIs^{3/2}}{a^{3/2}} & \frac{EIs^{3/2}}{a^{3/2}} \end{array}\right] \tag{86a}$$

$$W^{*-1} = \frac{1}{2}\left[\begin{array}{c|c|c|c} \frac{\sqrt{2}}{s} & \frac{a^{1/2}}{s^{3/2}} & 0 & \frac{-a^{3/2}}{EIs^{3/2}} \\ \hline 0 & \frac{a^{1/2}}{s^{3/2}} & \frac{\sqrt{2}\,a}{EIs} & \frac{a^{3/2}}{EIs^{3/2}} \\ \hline \frac{\sqrt{2}}{s} & \frac{-a^{1/2}}{s^{3/2}} & 0 & \frac{a^{3/2}}{EIs^{3/2}} \\ \hline 0 & \frac{a^{1/2}}{s^{3/2}} & \frac{-\sqrt{2}\,a}{EIs} & \frac{a^{3/2}}{EIs^{3/2}} \end{array}\right] \tag{86b}$$

A new state vector U is defined, analogous to equation (25), by

$$Y = W^* U \tag{87}$$

and, analogous to equation (26), U satisfies the matrix differential equation

$$\frac{dU}{dx} = P^* U \tag{88}$$

The solution of equation (88) in terms of the matrix exponential is

$$U_b(s) = e^{\ell P^*} U_a(s) \tag{89}$$

where U_a and U_b are the values of the U vector at stations a and b. For the matrix P^* in equation (83), the matrix $e^{\ell P^*}$ is

$$e^{\ell P^*} = \left[\begin{array}{cc|cc} e^{\sqrt{Ts}}\cos\sqrt{Ts} & e^{\sqrt{Ts}}\sin\sqrt{Ts} & \multicolumn{2}{c}{\multirow{2}{*}{0}} \\ -e^{\sqrt{Ts}}\sin\sqrt{Ts} & e^{\sqrt{Ts}}\cos\sqrt{Ts} & & \\ \hline \multicolumn{2}{c|}{\multirow{2}{*}{0}} & e^{-\sqrt{Ts}}\cos\sqrt{Ts} & e^{-\sqrt{Ts}}\sin\sqrt{Ts} \\ & & -e^{-\sqrt{Ts}}\sin\sqrt{Ts} & e^{-\sqrt{Ts}}\cos\sqrt{Ts} \end{array}\right] \tag{90}$$

The relation between Y_b and Y_a can be determined from equations (87) and (89):

$$Y_b = [W^* \, e^{\ell P^*} \, W^{*-1}] \, Y_a \tag{91}$$

Bernoulli-Euler equation transmission matrix.- The matrix $W^* \, e^{\ell P^*} \, W^{*-1}$ is thus the thin-beam bending or Bernoulli-Euler-equation transmission matrix. It will be denoted T^*_{ba}. If the matrix product is formed, $Y_b = T^*_{ba} \, Y_a$ becomes

$$\left[\begin{array}{c} \dot{y}_b \\ \dot{\theta}_b \\ M_b \\ Q_b \end{array}\right] = \left[\begin{array}{c|c|c|c} \alpha & \sqrt{\frac{a}{2s}}\,\beta & \frac{a}{EI}\,\gamma & \frac{a}{EI}\sqrt{\frac{a}{2s}}\,\delta \\ \hline -\sqrt{\frac{s}{2a}}\,\delta & \alpha & \frac{a}{EI}\sqrt{\frac{s}{2a}}\,\beta & \frac{a}{EI}\,\gamma \\ \hline -\frac{EI}{a}\,\gamma & -\frac{EI}{a}\sqrt{\frac{a}{2s}}\,\delta & \alpha & \sqrt{\frac{a}{2s}}\,\beta \\ \hline -\frac{EI}{a}\sqrt{\frac{s}{2a}}\,\beta & -\frac{EI}{a}\,\gamma & -\sqrt{\frac{s}{2a}}\,\delta & \alpha \end{array}\right] \left[\begin{array}{c} \dot{y}_a \\ \dot{\theta}_a \\ M_a \\ Q_a \end{array}\right] \tag{92}$$

where α, β, γ, and δ are defined as

$$\alpha \equiv \cos\sqrt{Ts}\,\cosh\sqrt{Ts} \tag{93a}$$

$$\beta \equiv -[\sin\sqrt{Ts}\,\cosh\sqrt{Ts} + \cos\sqrt{Ts}\,\sinh\sqrt{Ts}] \tag{93b}$$

$$\gamma \equiv \sin\sqrt{Ts}\,\sinh\sqrt{Ts} \tag{93c}$$

$$\delta \equiv \sin\sqrt{Ts}\,\cosh\sqrt{Ts} - \cos\sqrt{Ts}\,\sinh\sqrt{Ts} \tag{93d}$$

The 4x4 transmission matrix in equation (92) is a generalization of the 2x2 wave-equation transmission matrix in equation (30). It retains the useful property that, for a cascade of systems where $Y_b = T^*_{ba}\, Y_a$ and $Y_c = T^*_{cb}\, Y_b$, the overall transmission relation is $Y_c = T^*_{cb}\, T^*_{ba}\, Y_a$. The inverse relation to equation (92) is $Y_a = T^{*-1}_{ba}\, Y_b$, which will be symbolized $Y_a = T^*_{ab}\, Y_b$. It is not used in this report and will not be reproduced here. The elements of T^*_{ab} differ from those of T^*_{ba}, at most, by an algebraic sign, in analogy to the relations between T_{ba} and T_{ab} for the wave equation.

Transfer matrices for the Bernoulli-Euler equation.- For the reasons advanced in the section on transfer matrices for the wave equation, the admittance matrix form of the relation between the variables of Y_a and Y_b is most suitable for treating forced transverse response of the beam. Because the beam is symmetrical, the elements of the lower half of the admittance matrix may be defined in terms of those of the upper half. Thus,

$$\begin{bmatrix} \dot{y}_a \\ \dot{\theta}_a \\ \dot{y}_b \\ \dot{\theta}_b \end{bmatrix} = \left[\begin{array}{cc|cc} y_{11} & y_{12} & y_{13} & y_{14} \\ y_{21} & y_{22} & y_{33} & y_{44} \\ \hline -y_{13} & y_{14} & -y_{11} & y_{12} \\ y_{23} & -y_{24} & y_{21} & -y_{22} \end{array}\right] \begin{bmatrix} Q_a \\ M_a \\ Q_b \\ M_b \end{bmatrix} \tag{94}$$

The elements y_{ij} can be found in terms of the elements of the transmission matrix T^*_{ba}, but details will not be developed here. However, the natural frequencies of the admittance elements are easily shown to be determined by the zeroes of the determinant

$$\left[\begin{array}{c|c} \frac{EI}{a}\,\gamma & \frac{-EI}{a}\sqrt{\frac{a}{2s}}\,\delta \\ \hline \frac{-EI}{a}\sqrt{\frac{s}{2a}}\,\beta & \frac{-EI}{a}\,\gamma \end{array}\right] = 0 \tag{95}$$

Substitution of the expressions for β, γ, and δ into equation (95), plus considerable algebraic manipulation, reduces this condition to

$$\sinh^2 \sqrt{Ts} \quad \sin^2 \sqrt{Ts} = 0 \tag{96}$$

The roots of equation (96) can be shown to be $s = \pm j\omega$, where ω is given by the frequency equation

$$\cos \sqrt{\frac{\omega \ell^2}{a}} \cosh \sqrt{\frac{\omega \ell^2}{a}} = 1 \tag{97}$$

This is identical to equation (54) for the modal bending frequencies of a free-free beam. Thus, the closed-form transfer functions of the admittance matrix do indeed contain all the modal bending frequencies of the free-free beam; this confirms the consistency of the modal and transmission forms of the solution.

The frequency responses of the elements of the admittance matrix can be found by substituting $s = j\omega$. This generates transcendental functions of $\sqrt{\omega T}$, which are computationally inconvenient and result from expressing the T^*_{ba} matrix in real functions of s. A form of the transmission matrix which yields real functions of ω is given by Brown (ref 22). Alternately, Pestel and Leckie (ref 36) and Bishop and Johnson (ref 27) assume harmonic motion at the outset of analysis and derive a frequency-dependent transmission matrix equivalent to that of Brown.

The formulation in this report gives real functions of s both in the transmission matrix and admittance matrices; no single formulation can yield real functions of both s and ω.

Separation of propagation and reflection.- The transmission and transfer matrices for the Bernoulli-Euler equation do not lend themselves to a clear visualization of the processes of propagation and reflection of energy in a thin beam. Factorization of the T^*_{ba} matrix in equation (91) is the starting point, analogous to the wave-equation treatment presented earlier, for a separation of the propagation and reflection processes.

The transmission matrix relation between U_b and U_a (eq 89) can be converted into a transfer function involving only the propagation operators $C(Ts) = e^{-\sqrt{Ts}} \cos \sqrt{Ts}$ and $S(Ts) = e^{-\sqrt{Ts}} \sin \sqrt{Ts}$. If the four components of U are denoted u^-, v^-, v^+, and u^+, this relation is

$$\begin{matrix}\varepsilon_a^- \\ \\ \\ \varepsilon_b^+\end{matrix}\left\{\begin{bmatrix} u_a^- \\ v_a^- \\ v_b^+ \\ u_b^+ \end{bmatrix}\right. = \overbrace{\left[\begin{array}{cc|cc} C(Ts) & -S(Ts) & 0 & 0 \\ S(Ts) & C(Ts) & 0 & 0 \\ \hline 0 & 0 & C(Ts) & S(Ts) \\ 0 & 0 & -S(Ts) & C(Ts) \end{array}\right]}^{\Lambda_{ab}} \underbrace{\left[\begin{array}{c} u_b^- \\ v_b^- \\ v_a^+ \\ u_a^+ \end{array}\right]}_{\begin{matrix}\varepsilon_b^- \\ \varepsilon_b^+\end{matrix}} \qquad (98a)$$

Λ_{ba}

The symbols ε_a^-, ε_b^-, ε_b^+, ε_a^+, Λ_{ab}, and Λ_{ba} in equation (98a) can be used to write that equation in partitioned form:

$$\begin{bmatrix} \varepsilon_a^- \\ \varepsilon_b^+ \end{bmatrix} = \left[\begin{array}{c|c} \Lambda_{ab} & 0 \\ \hline 0 & \Lambda_{ba} \end{array}\right] \begin{bmatrix} \varepsilon_b^- \\ \varepsilon_a^+ \end{bmatrix} \qquad (98b)$$

This, the transfer-function relation between the states of u is diagonalized in the 2x2-partitioned sense. The variables are named so that the propagation relation between u^- and v^- is the same as that between u^+ and v^+, i.e.,

$$\begin{bmatrix} u_a^- \\ v_a^- \end{bmatrix} = \left[\begin{array}{c|c} C & -S \\ \hline S & C \end{array}\right] \begin{bmatrix} u_b^- \\ v_b^- \end{bmatrix} ; \begin{bmatrix} u_b^+ \\ v_b^+ \end{bmatrix} \left[\begin{array}{c|c} C & -S \\ \hline S & C \end{array}\right] \begin{bmatrix} v_a^+ \\ u_a^+ \end{bmatrix} \qquad (99)$$

This fact is not particularly evident when it is written in the order shown in equation (98a), which, nevertheless, is retained, because it arises naturally from the matrix transformations. The propagation of the u and v variables is illustrated in the matrix block diagram of figure 18.

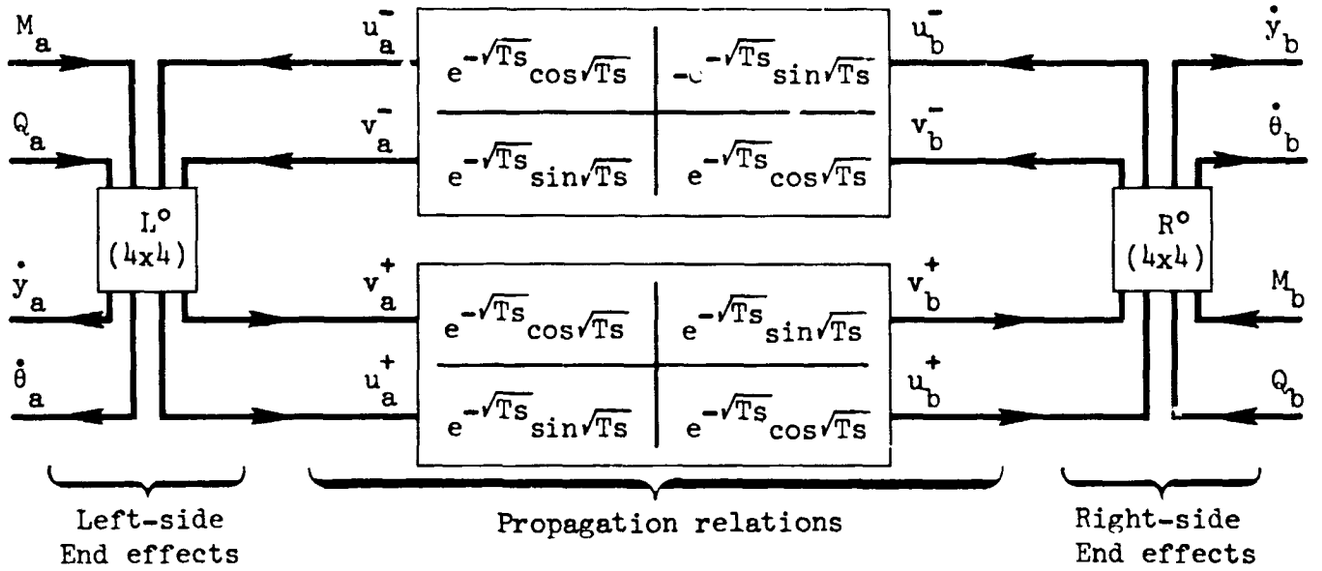

Figure 18.- Propagation and end-effects relations for lateral vibration of free-free beam.

The matrices L^o and R^o, relating the physical variables $\dot{y}$, $\dot{\theta}$, M, and Q and the transformed variables u^-, v^-, v^+, and u^+, are rearrangements of $y = W^*U$. The left-side end-effects matrix (L^o) is given by

$$\begin{Bmatrix} \dot{x}_a \\ \varepsilon_a^+ \end{Bmatrix} = \begin{bmatrix} L_{11}^o & L_{12}^o \\ L_{21}^o & L_{22}^o \end{bmatrix} \begin{Bmatrix} f_a \\ \varepsilon_a^- \end{Bmatrix} \qquad (100a)$$

$$\begin{Bmatrix} \dot{y}_a \\ \dot{\theta}_a \\ v_a^+ \\ u_a^+ \end{Bmatrix} = \begin{bmatrix} \frac{a}{EI} & \frac{a}{EI} & \frac{\sqrt{2a}}{s} & \sqrt{2}s & -\sqrt{2}s \\ \frac{-a}{EI} & \frac{\sqrt{2}s}{a} & \frac{-a}{EI} & 0 & 2s\ \frac{\sqrt{s}}{a} \\ \frac{a}{EI} & \frac{\sqrt{2}}{s} & \frac{2a}{EIs} & \frac{\sqrt{a}}{s} & 1 \quad -2 \\ \frac{-a}{EI} & \frac{\sqrt{2}}{s} & 0 & 0 & 1 \end{bmatrix} \begin{Bmatrix} M_a \\ Q_a \\ u_a^- \\ v_a^- \end{Bmatrix}$$

or, in terms of the variables $\dot{x}_a$, f_a, ε_a^+, ε_a^-, L_{11}^o, L_{12}^o, L_{21}^o, and L_{22}^o, it is

$$\begin{bmatrix} \dot{x}_a \\ \varepsilon_a^+ \end{bmatrix} = \left[\begin{array}{c|c} L_{11}^o & L_{12}^o \\ \hline L_{21}^o & L_{22}^o \end{array}\right] \begin{bmatrix} f_a \\ \varepsilon_a^- \end{bmatrix} \tag{100b}$$

The right-side end-effects matrix (R^o) is given by

$$\dot{x}_b \begin{Bmatrix} \dot{y}_b \\ \dot{\theta}_b \end{Bmatrix} = \left[\begin{array}{cc|cc} \overbrace{\frac{a}{EI} & \frac{-a}{EI}\sqrt{\frac{2a}{s}}}^{R_{11}^o} & \overbrace{\sqrt{2s} & \sqrt{2s}}^{R_{12}^o} \\ \frac{a}{EI}\sqrt{\frac{2s}{a}} & \frac{-a}{EI} & 0 & 2s\sqrt{\frac{s}{a}} \\ \hline \underbrace{\frac{a}{EI}\frac{\sqrt{2}}{s} & \frac{-2a}{EIs}\sqrt{\frac{a}{s}}}_{R_{21}^o} & \underbrace{1 & 2}_{R_{22}^o} \\ \frac{a}{EI}\frac{\sqrt{2}}{s} & 0 & 0 & 1 \end{array}\right] \begin{Bmatrix} M_b \\ Q_b \end{Bmatrix} f_b \quad \varepsilon_b^- \begin{Bmatrix} u_b^- \\ v_b^- \end{Bmatrix} \begin{Bmatrix} v_b^+ \\ u_b^+ \end{Bmatrix} \varepsilon_b^+ \tag{101a}$$

or, in terms of the variables $\dot{x}_b$, f_b, ε_b^-, ε_b^+, R_{11}^o, R_{12}^o, R_{21}^o, and R_{22}^o, it is

$$\begin{bmatrix} \dot{x}_b \\ \varepsilon_b^- \end{bmatrix} = \left[\begin{array}{c|c} R_{12}^o & R_{12}^o \\ \hline R_{21}^o & R_{22}^o \end{array}\right] \begin{bmatrix} f_b \\ \varepsilon_b^+ \end{bmatrix} \tag{101b}$$

The block diagram in figure 18 is an admittance relation. The end-effects matrices L^o and R^o would change for different boundary conditions, which, of course, do not effect propagation relations. Different end-effects matrices can be derived by rearranging $y = W^* U$ into appropriate forms; they are, of course, dependent only on the local beam properties. The propagation time constant T of the Bernoulli-Euler equation is proportional to ℓ^2 in contrast to that of the wave equation, which is proportional to ℓ.

Damping and Control of Bending Vibrations

Terminal constraints.- The behavior of the Bernoulli-Euler beam with terminal dampers and/or active terminal controls is now considered in terms of propagation and reflection. The terminal constraints assumed are:

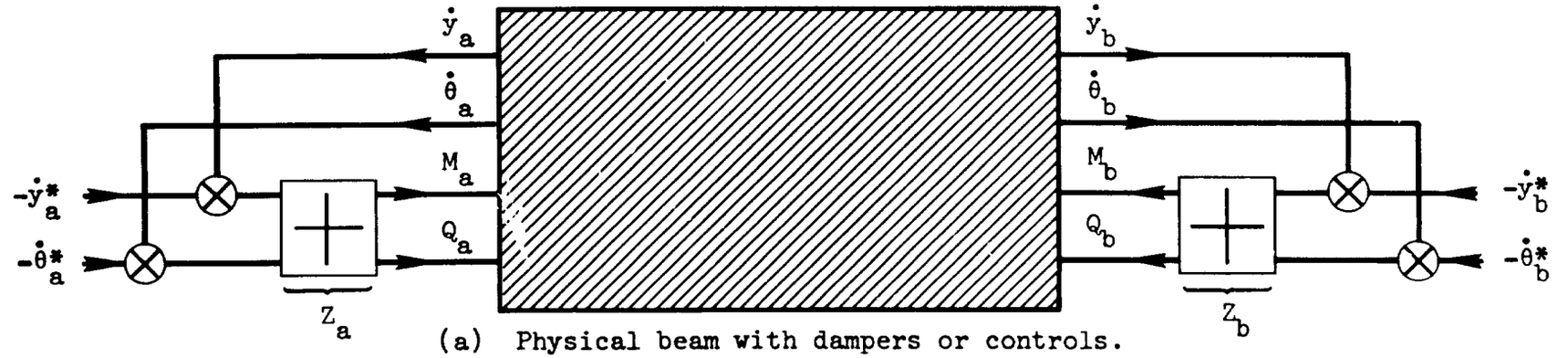

(a) Physical beam with dampers or controls.

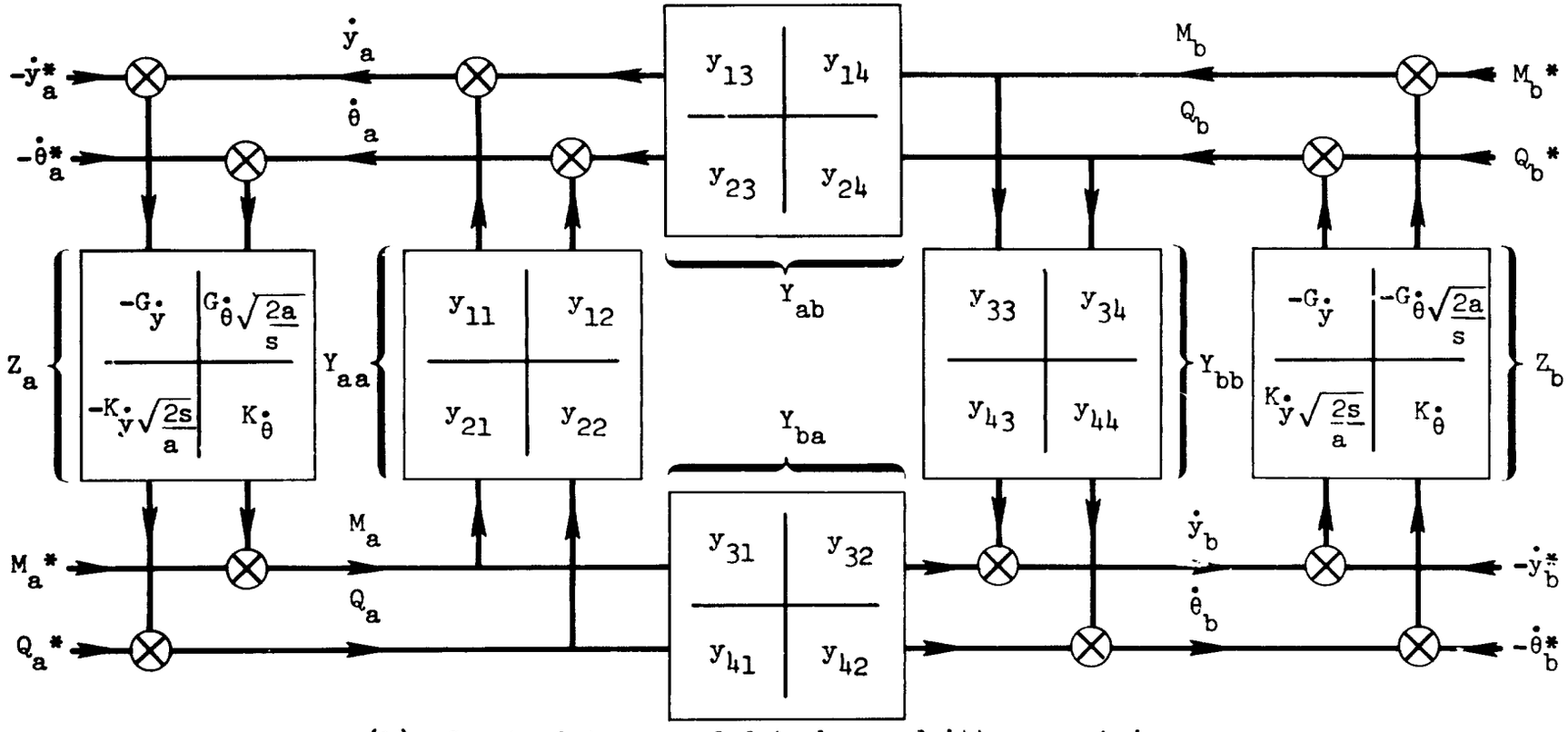

(b) Constraints appended to beam-admittance matrix.

Figure 19.--Free-free beam with lateral terminal constraints appended.

$$\underbrace{\begin{bmatrix} M_a \\ Q_a \end{bmatrix}}_{f_a} = \underbrace{\left[\begin{array}{c|c} -G_{\dot{y}} & G_{\dot{\theta}}\sqrt{\frac{2a}{s}} \\ \hline -K_{\dot{y}}\sqrt{\frac{2s}{a}} & K_{\dot{\theta}} \end{array}\right]}_{Z_a} \underbrace{\begin{bmatrix} \dot{y}_a - y^*_a \\ \dot{\theta}_a - \theta^*_a \end{bmatrix}}_{\dot{x}_a - \dot{x}^*_a} + \underbrace{\begin{bmatrix} M^*_a \\ Q^*_a \end{bmatrix}}_{f^*_a} \quad \text{or} \quad f_a = Z_a\,(\dot{x}_a - \dot{x}^*_a) + f^*_a \qquad (102a)$$

$$\underbrace{\begin{bmatrix} M_b \\ Q_b \end{bmatrix}}_{f_b} = \underbrace{\left[\begin{array}{c|c} -G_{\dot{y}} & -G_{\dot{\theta}}\sqrt{\frac{2a}{s}} \\ \hline K_{\dot{y}}\sqrt{\frac{2s}{a}} & K_{\dot{\theta}} \end{array}\right]}_{Z_b} \underbrace{\begin{bmatrix} \dot{y}_b - \dot{y}^*_b \\ \theta_b - \theta^*_b \end{bmatrix}}_{\dot{x}_b - \dot{x}^*_b} + \underbrace{\begin{bmatrix} M^*_b \\ Q^*_b \end{bmatrix}}_{f^*_a} \quad \text{or} \quad f_b = Z_b\,(\dot{x}_b - \dot{x}^*_b) + F^*_b \qquad (102b)$$

There are generalizations of the longitudinal-beam constraints of equations (36a and b). The signs are placed so that any motion produces restoring forces and moments. Figure 19a shows the terminal controls appended to the beam terminals, and figure 19b, shows this in block-diagram form, in terms of the admittance of the free-free beam. Because this study is in terms of propagation and reflection, appending the terminal constraints to the beam as shown in figure 18 is preferable.

Now, the terminal constraints of equations (102a and b) appended to the block diagram of figure 18 are shown in the matrix block diagram in figure 20.

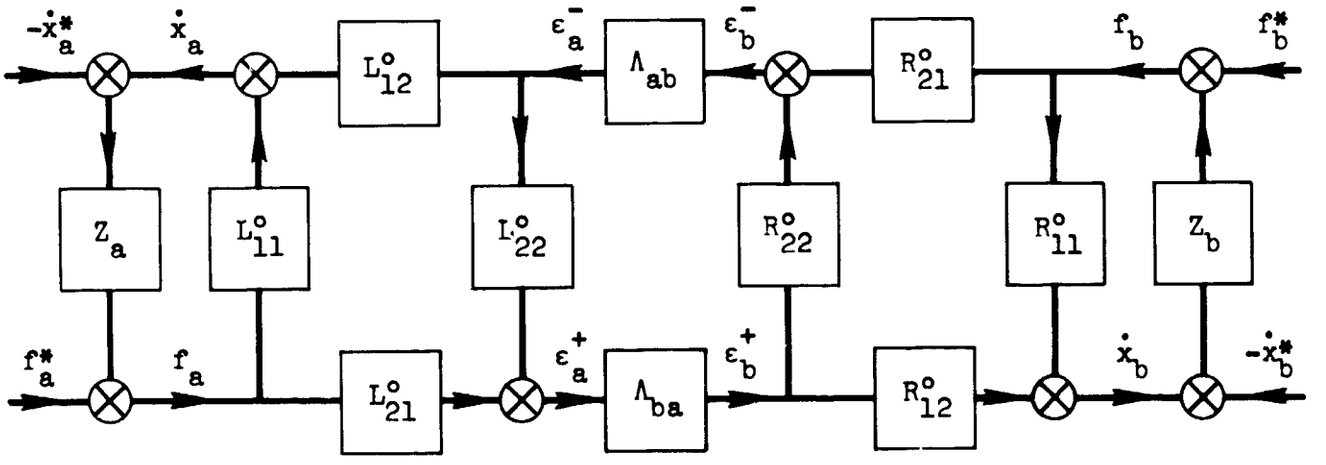

Figure 20. Free-free beam propagation and end effects relations with lateral constraints appended.

The end effects shown are simplified in figure 21 without affecting the propagation relations.

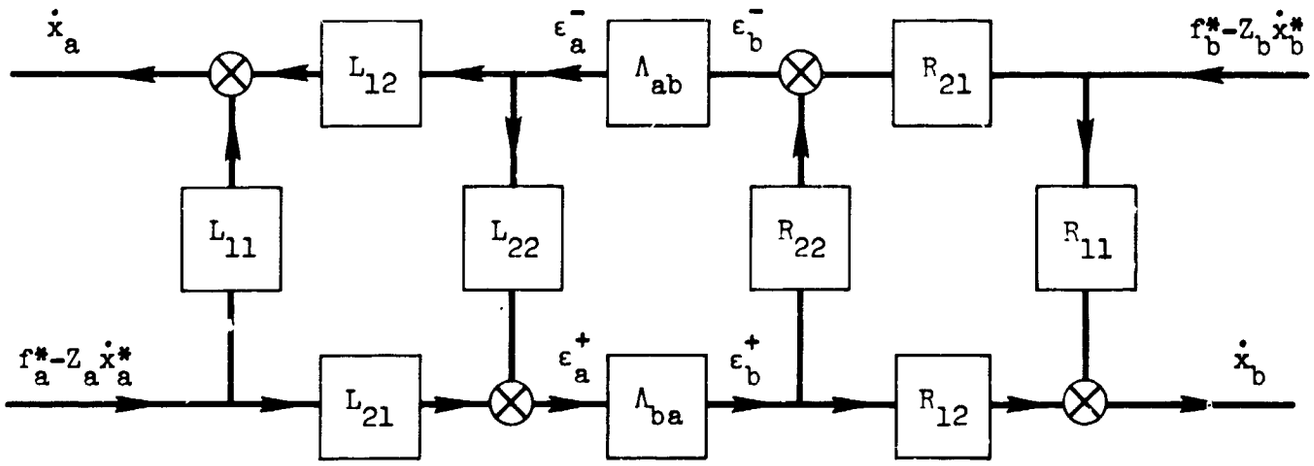

Figure 21. Propagation and end-effects relations for beam with lateral terminal constraints.

The matrices in figure 21 can be determined from those in figure 20 as:

$$L_{11} = [(I - L_{11}^{\circ} Z_a)^{-1} L_{11}^{\circ}]; \quad R_{11} = [(I - R_{11}^{\circ} Z_b)^{-1} R_{11}^{\circ}] \tag{103a}$$

$$L_{21} = [L_{21}^{\circ}(I - Z_a L_{11}^{\circ})^{-1}]; \quad R_{21} = [R_{21}^{\circ}(I - Z_b R_{11}^{\circ})^{-1}] \tag{103b}$$

$$L_{12} = [(I - L_{11}^{\circ} Z_a)^{-1} L_{12}^{\circ}]; \quad R_{12} = [(I - R_{11}^{\circ} Z_b)^{-1} R_{12}^{\circ}] \tag{103c}$$

$$L_{22} = L_{22}^{\circ} + [L_{21}^{\circ}(I - Z_a L_{11}^{\circ})^{-1} Z_a L_{12}^{\circ}]; \quad R_{22} = R_{22}^{\circ} + [R_{22}^{\circ} + [R_{21}^{\circ}(I - Z_b R_{11}^{\circ})^{-1} Z_b R_{12}] \tag{103d}$$

As in the wave equation, where the parameters of equation (37) were used in the overall input-output relations for figure 5, the matrices of equations (103a, b, c, and d) can be used to express the overall input-output relations for figure 19 as

$$\dot{x}_a = [L_{11} + L_{12}\,(I - \Lambda_{ab}R_{22}\Lambda_{ba}L_{22})^{-1}\Lambda_{ab}R_{22}\Lambda_{ba}L_{21}](f_a^* - Z_a\,\dot{x}_a^*)$$

$$+ [L_{12}(I - \Lambda_{ab}R_{22}\Lambda_{ba}L_{22})^{-1}\Lambda_{ab}R_{21}](f_b^* - Z_b\,\dot{x}_b^*) \qquad (104a)$$

$$\dot{x}_b = [R_{11} + R_{12}(I - \Lambda_{ba}L_{22}\Lambda_{ba}R_{22})^{-1}\Lambda_{ba}L_{22}\Lambda_{ab}R_{21}]\,(f_b^* - Z_b\,\dot{x}_b^*)$$

$$+[R_{12}(I - \Lambda_{ba}L_{11}\Lambda_{ab}R_{22})^{-1}\Lambda_{ba}L_{21}](f_a^* - Z_a\,\dot{x}_a) \qquad (104b)$$

The matrix equation (104a) relates the transverse and angular velocities $\dot{y}_a$ and $\dot{\theta}_a$ to the load disturbances M_a^*, Q_a^*, M_b^*, Q_b^* and to the transverse- and angular-velocity commands, $\dot{y}_a^*$, $\dot{\theta}_a^*$, $\dot{y}_b^*$, $\dot{\theta}_b^*$. This relation is in terms of the propagation matrices Λ_{ab}, etc., the end-effects matrices L_{11}°, R_{11}° etc., and the terminal impedances Z_a and Z_b.

The Bernoulli-Euler reflection matrices. - The 2x2 matrices L_{22} and R_{22} will be called the Bernoulli-Euler reflection matrices, in analogy to the reflection coefficient for the wave equation. In terms of the reflection matrices, the relations between scalar components of ε_a^-, ε_a^+, ε_b^+, and ε_b^- are

$$\varepsilon_a^+ = L_{22}\,\varepsilon_a^- \quad \text{or} \quad \begin{bmatrix} v_a^+ \\ u_a^+ \end{bmatrix} = L_{22} \begin{bmatrix} u_a^- \\ v_a^- \end{bmatrix} \qquad (105a)$$

$$\varepsilon_b^- = R_{22}\,\varepsilon_b^+ \quad \text{or} \quad \begin{bmatrix} u_b^- \\ v_b^- \end{bmatrix} = R_{22} \begin{bmatrix} v_b^+ \\ u_b^+ \end{bmatrix} \qquad (105b)$$

The behavior of the right-side reflection matrix R_{22} in terms of the right-side terminal impedance matrix Z_b is examined in detail to illustrate the dependence of the reflection matrix on the terminal impedance. Equation (103b) clearly shows that, for a free end ($Z_b = 0$), the reflection matrix is equal to R_{22}°. Thus, in terms of the elements of R_{22} [eq (101)],

$$Z_b = 0 \rightarrow \Gamma_b = \left[\begin{array}{c|c} 1 & 2 \\ \hline 0 & 1 \end{array}\right] = R_{22} \tag{106}$$

where $A \rightarrow B$ is read if A then B.

The expression for R_{22}, in general, can be written in terms of its deviation from its value for $Z_b = 0$.

$$R_{22} = \left[\begin{array}{c|c} 1 + \alpha_b & 2 + \beta_b \\ \hline \gamma_b & 1 + \delta_b \end{array}\right] \tag{107}$$

Then, from equations (103d), (106), and (107),

$$\left[\begin{array}{c|c} \alpha_b & \beta_b \\ \hline \gamma_b & \sigma_b \end{array}\right] = R^o_{21}(I - Z_b R^o_{11})^{-1} Z_b R^o_{12} \tag{108}$$

If the right side of equation (108) is expanded in terms of the elements of Z_b, R^o_{11}, R^o_{12}, and R^o_{22}, the expressions for α_b, β_b, γ_b, and δ_b are

$$\alpha_b = [2(\tfrac{a}{EI})^2 G_{\dot{y}} K_{\dot{\theta}} - 2(\tfrac{a}{EI}) G_{\dot{y}} - 4(\tfrac{a}{EI})^2 K_{\dot{y}} G_{\dot{\theta}} - 4(\tfrac{a}{EI}) K_{\dot{y}}]/D \tag{109a}$$

$$\beta_b = [2(\tfrac{a}{EI})^2 G_{\dot{y}} K_{\dot{\theta}} - 2(\tfrac{a}{EI}) G_{\dot{y}} - 4(\tfrac{a}{EI})^2 K_{\dot{y}} G_{\dot{\theta}} - 4(\tfrac{a}{EI}) K_{\dot{y}} - 4(\tfrac{a}{EI}) G_{\dot{\theta}} - 4(\tfrac{a}{EI}) K_{\dot{\theta}}]/D \tag{109b}$$

$$\gamma_b = [-2(\tfrac{a}{EI})^2 G_{\dot{y}} K_{\dot{\theta}} + 4(\tfrac{a}{EI})^2 K_{\dot{y}} G_{\dot{\theta}} - 2(\tfrac{a}{EI}) G_{\dot{y}}]/D \tag{109c}$$

$$\delta_b = [2(\tfrac{a}{EI})^2 G_{\dot{y}} K_{\dot{\theta}} - 2(\tfrac{a}{EI}) G_{\dot{y}} - 4(\tfrac{a}{EI})^2 K_{\dot{y}} G_{\dot{\theta}} - 4(\tfrac{a}{EI}) G_{\dot{\theta}}]/D \tag{109d}$$

where

$$D = [1 + 2(\tfrac{a}{EI}) K_{\dot{y}} + (\tfrac{a}{EI}) K_{\dot{\theta}} + (\tfrac{a}{EI}) G_{\dot{y}} \; 2(\tfrac{a}{EI}) G_{\dot{\theta}} + 2(\tfrac{a}{EI})^2 G_{\dot{\theta}} K_{\dot{y}}] \tag{109e}$$

Equations (109a, b, c, d, and e) indicate that the reflection matrix remains independent of s, if $G_{\dot{y}}$, $G_{\dot{\theta}}$, $K_{\dot{y}}$, and $K_{\dot{\theta}}$ are independent of s. In other words, if the elements of the terminal-control matrix Z_a are made to have the same functional form as those of the characteristic-impedance matrix Z_b, then the elements of the reflection matrix R_{22} have the same functional form as those of the matrix R^o_{22}, i.e., constants independent of s.

Several special cases of Z_b are considered and named, because they are treated extensively in the remainder of this report. The "Z_o" termination is the general case, where no element of Z_b is zero. The "$K_{\dot{\theta}} + K_{\dot{y}}$" termination has $G_{\dot{y}} = G_{\dot{\theta}} = 0$. The "$K_{\dot{\theta}}$" termination has $G_{\dot{y}} = G_{\dot{\theta}} = K_{\dot{y}} = 0$. The "free" termination has $Z_b = 0$. The equations for these different cases and their special relations are summarized in table I.

The "Z_o" termination can affect all elements of R_{22}. In particular, if $G_{\dot{y}} = G_{\dot{\theta}} = K_{\dot{y}} = K_{\dot{\theta}} = EI/a$, all elements of the reflection matrix are zero. This is the case of $Z_b = Z_{oa}$ and corresponds to terminating face b of the beam with face a of a semi-infinite beam. Thus, the reflection matrix, like the reflection coefficient, is nulled when the beam is terminated in its characteristic impedance. For the Bernoulli-Euler case, distinction between Z_{oa} and Z_{ob} must be made. Physical reasoning requires that $Z_b = Z_{oa}$, not $Z_b = Z_{ob}$. Figure 17 helps to clarify this point.

The "$K_{\dot{\theta}} + K_{\dot{y}}$" termination can affect only the terms α_b and β_b of equation (107). In particular, if $K_{\dot{y}} = K_{\dot{y}} = K_{\dot{\theta}} = EI/a$, then $\alpha_b = -1$ and $\beta_b = -2$. Thus, all elements of R_{22}, which can be modified, are nulled, if $K_{\dot{y}}$ and $K_{\dot{\theta}}$ are adjusted so that the nonzero elements of Z_b match the corresponding elements of Z_{oa}.

The "$K_{\dot{\theta}}$" termination can affect only β_b in equation (107). In particular, if $K_{\dot{\theta}} = EI/a$, then $\beta_b = -2$. Thus, the only element of R_{22}, which is affected by $K_{\dot{\theta}}$, is nulled, if $K_{\dot{\theta}}$ is adjusted so that the nonzero element of Z_b matches the corresponding element of Z_{oa}.

The behavior of the reflection matrix in these special cases is considered significant, although it is not yet fully understood. The case of $R_{22} = 0$ is particularly interesting in view of the benefits for damping and control by setting the reflection coefficient to zero in the longitudinal-wave problem.

TABLE I

REFLECTION MATRIX FOR SPECIAL CASES OF TERMINAL-IMPEDANCE MATRIX

Termination	Equation	Special Relations
Z_o	$Z_b = \left[\begin{array}{c\|c} -G_y^\bullet & G_\theta^\bullet\sqrt{\frac{2a}{s}} \\ \hline -K_y^\bullet\sqrt{\frac{2s}{a}} & K_\theta^\bullet \end{array}\right]$	$Z_b = \left[\begin{array}{c\|c} \frac{-EI}{a} & \frac{EI}{a}\sqrt{\frac{2a}{s}} \\ \hline \frac{-EI}{a}\sqrt{\frac{2s}{a}} & \frac{EI}{a} \end{array}\right] \rightarrow R_{22} = \left[\begin{array}{c\|c} 0 & 0 \\ \hline 0 & 0 \end{array}\right]$
$K_\theta^\bullet + K_y^\bullet$	$Z_b = \left[\begin{array}{c\|c} 0 & 0 \\ \hline -K_y^\bullet\sqrt{\frac{2s}{a}} & K_\theta^\bullet \end{array}\right]$	$Z_b = \left[\begin{array}{c\|c} 0 & 0 \\ \hline \frac{-EI}{a}\sqrt{\frac{2s}{a}} & \frac{EI}{a} \end{array}\right] \rightarrow R_{22} = \left[\begin{array}{c\|c} 0 & 0 \\ \hline 0 & 1 \end{array}\right]$
$K_\theta^\bullet$	$Z_b = \left[\begin{array}{c\|c} 0 & 0 \\ \hline 0 & K_\theta^\bullet \end{array}\right]$	$Z_b = \left[\begin{array}{c\|c} 0 & 0 \\ \hline 0 & \frac{EI}{a} \end{array}\right] \rightarrow R_{22} = \left[\begin{array}{c\|c} 1 & 0 \\ \hline 0 & 1 \end{array}\right]$
Free	$Z_b = \left[\begin{array}{c\|c} 0 & 0 \\ \hline 0 & 0 \end{array}\right]$	$R_{22} = \left[\begin{array}{c\|c} 1 & 2 \\ \hline 0 & 1 \end{array}\right] = R_{22}^o$

When $Z_b = Z_{oa}$ so that $R_{22} = 0$, the input admittance at terminal a (for $Z_a = 0$) can be derived from equations (104a) and (103a) as $\dot{x}_a = L^{\circ}_{11} f_a$. Equations (72), (73), and (100a) reveal that $L^{\circ}_{11} = Y_{oa}$ and $R_{11} = Y_{ob}$; thus,

$$\dot{x}_a = Y_{oa} f_a \tag{110}$$

Therefore, the input and characteristic admittances of a finite uniform beam, terminated in its characteristic impedance, are equal. This is evident from figure 20, because $R_{22} = 0$, and ϵ^{+}_b is not reflected; thus, for $Z_a = 0$, the relation between $\dot{x}_a$ and f_a is simply $\dot{x}_a = L_{11} f_a$. These relations can be visualized better by comparing figures 18, 19, 20, and 21.

When neither of the reflection matrices L_{22} and R_{22} is zero, equation (104a) may be expanded by the matrix series for the inverse:

$$(I - \Lambda_{ab} R_{22} \Lambda_{ba} L_{22})^{-1} = I + \Lambda_{ab} R_{22} \Lambda_{ba} L_{22} + (\Lambda_{ab} R_{22} \Lambda_{ba} L_{22})^2 + \ldots \tag{111}$$

Equation (104b) can be expanded in a similar form. The expanded form of equation (104a) is

$$\dot{x}_a = \{L_{11} + L_{12} [I + (\Lambda_{ab} R_{22} \Lambda_{ba} L_{22}) + (\Lambda_{ab} R_{22} \Lambda_{ba} L_{22})^2 + \ldots][\Lambda_{ab} R_{22} \Lambda_{ba} L_{21}]\}$$

$$\{f^*_a - Z_a \dot{x}_a\} + \{[L_{12}(I + (\Lambda_{ab} R_{22} \Lambda_{ba} L_{22}) + (\Lambda_{ab} R_{22} \Lambda_{ba} L_{22})^2 + \ldots]$$

$$[\Lambda_{ab} R_{21}]\} \{f^*_b - Z^*_b \dot{x}^*_b\} \tag{112}$$

This equation for transverse vibrations has a form similar to that for the successive wave expansion for the longitudinal-vibration problem [eq (42)]. Thus, equation (112) is a matrix generalization (for the Bernoulli-Euler equation) of the successive wave expansion for the wave equation. A word of caution is due here; the Bernoulli-Euler propagation operators have no pure-delay effect, and the equation (112) cannot be strictly interpreted as a successive wave expansion. For any $t > 0$, the response of every term of the series will be nonzero. The expansion may prove useful for computations in both the time and frequency domain for situations in which the series converge. Inasmuch as the Bernoulli-Euler propagation operators only approximate the Timoshenko-beam propagation operators (which do have a pure-delay effect), truncating the series might be expected to result in an approximation of the physical behavior of a beam, even when not permitted by the mathematics of the Bernoulli-Euler solution.

Another situation in which the propagation operator has no pure-delay effect is the one-dimensional diffusion equation. In this case, series expansions in the propagation operator $e^{-\sqrt{Ts}}$ and the diffusion reflection coefficients have the form

$$1 + \nu_a \nu_b \, e^{-2\sqrt{Ts}} + \nu_a^2 \nu_b^2 \, e^{-4\sqrt{Ts}} + \ldots$$

Weber (ref 14) describes such a series for a transmis ion line with distributed capacitance and resistance but negligible inductance, and he warns against its interpretation as a successive wave expansion.

The following paragraphs show that the early part of transient response is indeed similar to that predicted from the first term of equation (112).

Transverse load disturbances.- The problem of regulating or holding constant the transverse velocities ($\dot{y}$ and $\dot{\theta}$) of a beam subjected to transverse loading (M,Q) at the ends is now considered in terms of the Bernoulli-Euler propagation operators and reflection matrices.

Restrictions: Results are restricted to uniform beams with active or passive dampers that fit the terminal constraints of equations (102a and b). This means that all damping forces and moments are a function only of the motion at the terminals where they are applied. Moreover, the force and moment disturbances are assumed to be applied at the terminals only.

These are severe restrictions, yet a tail-controlled flexible vehicle, with sensors mounted near the tail, subjected to a gust disturbance near the nose, is not too far removed from this situation. Some terms in equations (102a and b) are more applicable to this situation than others. Lateral force disturbances seem more likely than moment disturbances, for instance. Also, the terms $G_{\dot{y}}$ and $G_{\dot{\theta}}$ imply devices that can apply damping moments. A practical scheme to apply independent damping moments and forces might be conceived, if the benefits were great. The "$K_{\dot{\theta}}$" and the "$K_{\dot{\theta}} + K_{\dot{y}}$" terminations are chosen, because the former corresponds to the conventional angular-rate feedback, and the latter is the closest possible approximation to the "Z_o" termination with $G_{\dot{y}}$ and $G_{\dot{\theta}}$ set equal to zero.

The "Z_o" termination is also treated, implementation problems notwithstanding, for several reasons: (1) because it was shown to null the reflection matrix, it has particularly simple relations and represents a limit case; (2) for the insight it might afford; and (3) for technological spin-off value, e.g., application to damping of transverse vibration in other systems. Moment disturbances are also treated for the latter two reasons.

Somewhat arbitrary but specific beam parameters, rather than nondimensional variables, were selected for study. The dimensions and parameters chosen are presented in table II. The chosen beam weighs 56 lb; the first mode frequency is 32 rad/sec; and the value of EI/a is 41.5 (in./lb)/(in./sec).

Simulation and computation: System behavior was studied both in the time domain, by an analog simulation, and frequency domain.

Analog simulation of the terminal relations requires analog models of the operators $\sqrt{s}$ and $1/\sqrt{s}$. This was achieved by operational amplifiers with lattice-network feedbacks. Theoretically, the rational algebraic driving-point impedances of the feedbacks fit the function $1/\sqrt{s}$ within approximately $\pm$ 0.5 db and $\pm$ 2° over the frequency range $10 \leq \omega \leq 1000$ rad/sec. The method of simulating $\sqrt{s}$, and $1/\sqrt{s}$, and the affect of the low-frequency asymptotic order of these approximations are described in Appendix A. The frequency-domain studies utilized, in place of $1/\sqrt{s}$, the rational algebraic approximation

$$\frac{1}{\sqrt{s}} \approx \left\{ \frac{1 + 28\left(\frac{s}{100}\right) + 70\left(\frac{s}{100}\right)^2 + 28\left(\frac{s}{100}\right)^3 + \left(\frac{s}{100}\right)^4}{10\left[8\left(\frac{s}{100}\right) + 56\left(\frac{s}{100}\right)^2 + 56\left(\frac{s}{100}\right)^3 + 8\left(\frac{s}{100}\right)^4\right]} \right\} \qquad (113)$$

This allowed the use of standard frequency-response programs. This function approximates $1/\sqrt{s}$ within the tolerances mentioned.

Analog simulation of the beam in terms of propagation operators and end-effects matrices involves approximation of the transcendental functions of $\sqrt{s}$ ratios of polynomials in s (perhaps by lattice networks as operational amplifier feedbacks). Effective approximations for the Bernoulli-Euler operator have not yet been found.

Thus, the free-free beam was simulated in terms of the first five normal modes (see table I). The normal-mode rational algebraic approximations to the admittance operators were chosen for the frequency-response calculations to permit the use of standard frequency response programs and to ensure that the frequency responses of the beam used in these calculations were consistent with those of the analog simulation of the beam. The latter had to be in terms of the normal modes. Although not required for stability, a damping ratio of 0.02 was added to the normal-mode transfer functions in the frequency-response calculations to keep the magnitudes of the bending resonances finite and of reasonable value for plotting. The normal-mode damping ratios in the analog simulations were set as close to zero as possible.

Although the factorization of the beam transfer function was not used in simulation of the beam, it served to identify the role of operators $\sqrt{s}$ and $1/\sqrt{s}$ in beam dynamics and led to an investigation of their use as control functions. The method of simulating the beam dynamics is irrelevant (as long as it is correct) in the comparison of various control schemes.

TABLE II

SPECIFIC BEAM PARAMETERS

Physical Characteristics

Length (ℓ) . . . . . 200 in.

Cross-section Area (A) . . . . . 1.0 $in.^2$

Young's modulus (E) . . . . . $30 \times 10^6 \frac{lb}{in.^2}$

Density (ρ) . . . . . $0.725 \times 10^{-3} \frac{lb\text{-}sec^2}{in.^4}$

Derived Parameters

Area moment of inertia (I) . . . . . 0.0796 $in.^4$

$a = \sqrt{EI/(\rho A)}$ . . . . . $57.5 \times 10^3 \frac{in.^2}{sec}$

EI/a . . . . . $41.5 \frac{in\text{-}lb}{(in/sec)}$

Rigid-Body and Bending-Mode Data

MODE	ω	M	$\phi(0)$	$\phi(\ell)$	$\phi'(0)$	$\phi'(\ell)$
-1	0	0.227	2.0	-2.0	-0.0200	-0.0200
0	0	0.145	1.0	1	0	0
1	32	0.145	2.0	2.0	-0.0464	0.0464
2	89	0.145	2.0	-2.0	-0.0778	-0.0778
3	174	0.145	2.0	2.0	-0.110	0.110
4	288	0.145	2.0	-2.0	-0.141	-0.141
5	433	0.145	2.0	2.0	-0.173	0.173

Frequency response: When controls are only at b ($Z_a = 0$) and disturbances only at a, figure 19 can be reduced to the block diagram shown in figure 22.

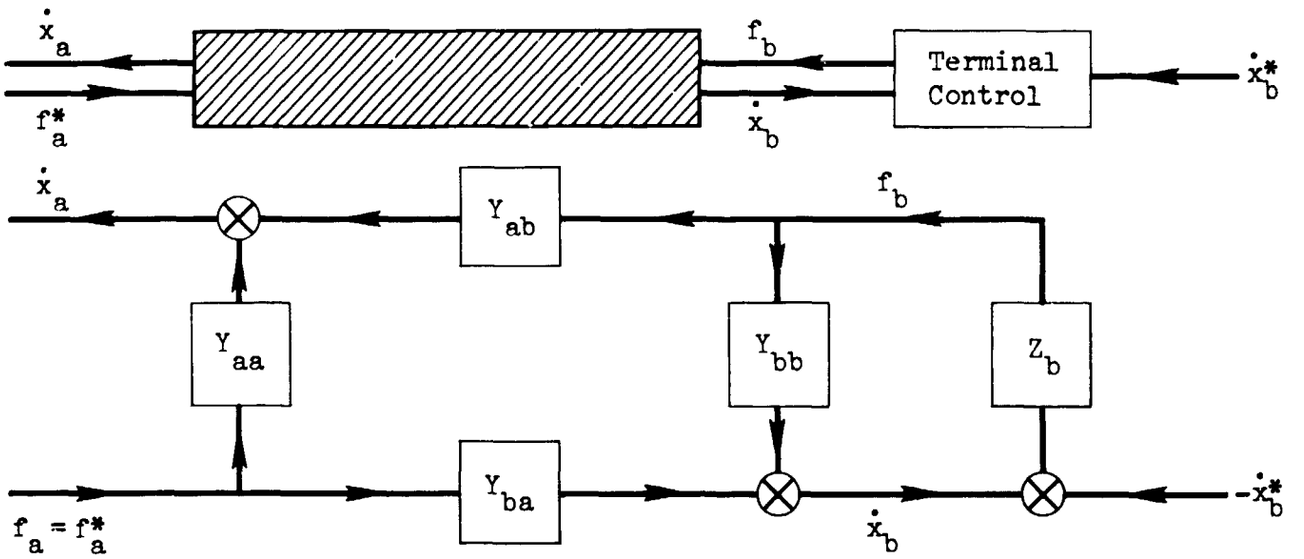

Figure 22. Beam with control at b only ($Z_a = 0$) and disturbance at a only ($f_b^* = 0$).

The frequency response can be computed from the relations

$$\dot{x}_a = [Y_{aa} + Y_{ab}(I - Z_b Y_{bb})^{-1} Z_b Y_{ba}]\, f_a^* \qquad (114a)$$

$$\dot{x}_b = [(I - Y_{bb} Z_b)^{-1} Y_{ba}]\, f_a^* \qquad (114b)$$

The four frequency responses determined from equation (114b) are shown in figures 23a,b,c, and d. They are computed from rational algebraic functions of s for the elements of Z_b, Y_{aa}, etc. For figures 23b and d, which are the responses of $\dot{y}_b$ and $\dot{\theta}_b$ to Q_a, the following four terminations were studied:

Case A	"free" termination
Case B	"$K_{\dot{\theta}}$" termination ($K_{\dot{\theta}} = EI/a$)
Case C	"$K_{\dot{\theta}} + K_{\dot{y}}$" termination ($K_{\dot{\theta}} = K_{\dot{y}} = EI/a$)
Case D	"Z_o" termination ($K_{\dot{\theta}} = K_{\dot{y}} = G_{\dot{\theta}} = G_{\dot{y}} = EI/a$)

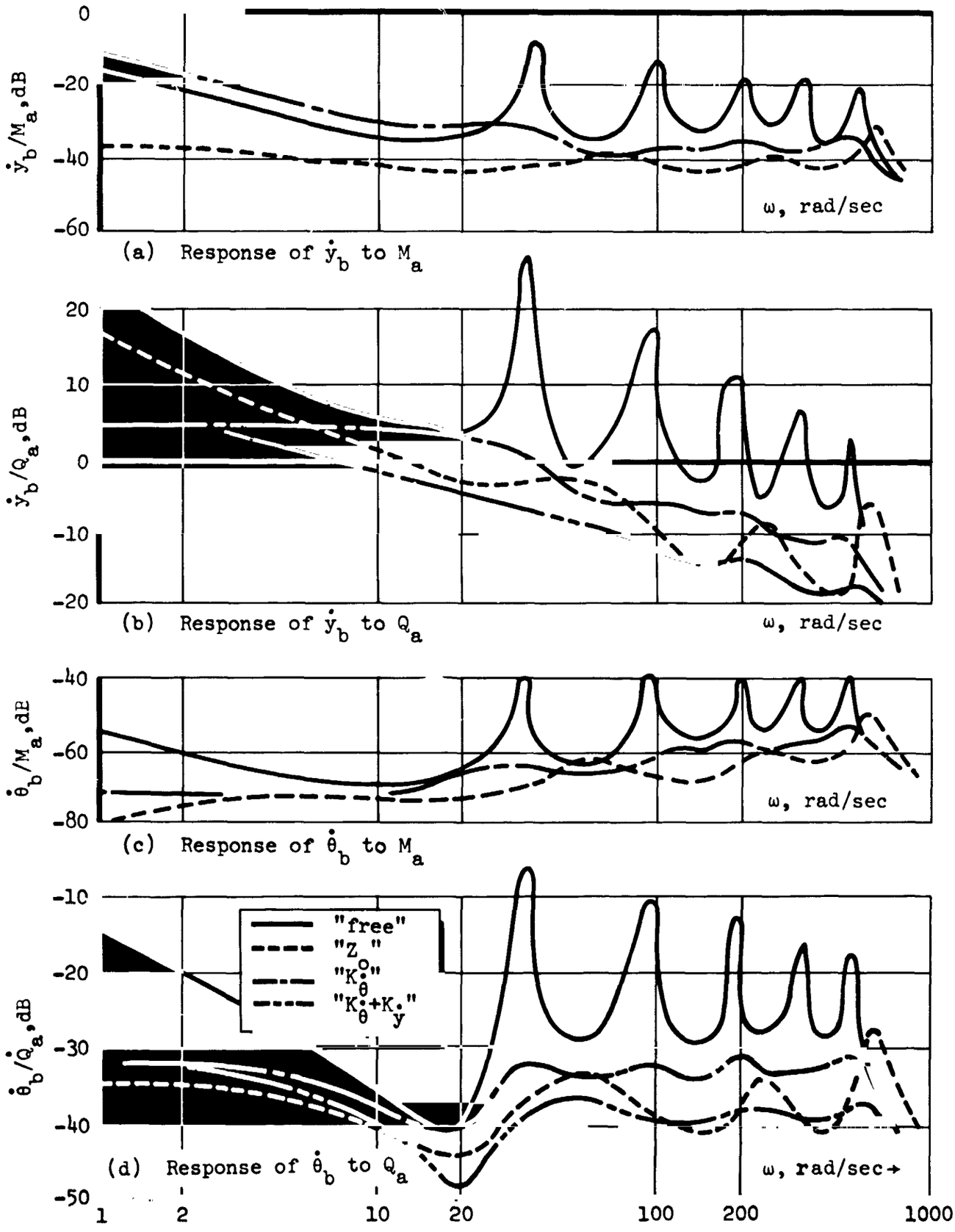

Figure 23. Effect of termination Z_b on frequency response for load disturbances (polynomial approx.).

Table I shows that, for cases A, B, C, and D, the number of nulled elements of the reflection matrix is 1, 2, 3, and 4, respectively. The supposition that damping effectiveness would increase with the number of nulled elements is not fully supported by the results shown in figures 23b and 23d. The "$K_{\dot{\theta}} + K_{\dot{y}}$" termination is most effective, as measured by the dB reduction from the case of no control, which is easily visualized for each termination. The frequency band of approximately 10 to 100 rad/sec is probably the most important. The response at lower frequencies can most likely be shaped by design of the low-frequency part of the $\sqrt{s}$ approximations. The high-frequency part cannot be shaped by the designer because of actuator bandwidth limitations; moreover, the energy spectrum of plausible loads generally drops off rapidly at high frequencies.

Figures 23a and 23c, show the responses of $\dot{y}_b$ and $\dot{\theta}_b$ to M_a; only cases B and D were studied. Here, again, the "Z_o" termination is slightly more effective than the "$K_{\dot{\theta}}$" termination. Thus, in these special circumstances, terminations of the type C and D appear a few dB more effective than conventional angular-rate damping.

For the "Z_o" termination, the reflection matrix R_{22} is, of course, zero. In this case, equation (104b) can be reduced to

$$\begin{bmatrix} \dot{y}_b \\ \dot{\theta}_b \end{bmatrix} = \frac{a}{EI} e^{-\sqrt{Ts}} \left[\begin{array}{c|c} \cos\sqrt{Ts} - \sin\sqrt{Ts} & \sqrt{\frac{2a}{s}} \cos\sqrt{Ts} \\ \hline -\sqrt{\frac{2s}{a}} \cos\sqrt{Ts} & -(\cos\sqrt{Ts} + \sin\sqrt{Ts}) \end{array}\right] \begin{bmatrix} M_a \\ Q_a \end{bmatrix} \quad (115)$$

which is identical to equation (71) for the semi-infinite beam for the special case of $x = \ell$. Because no reflections exist, this indeed must be the case.

Equation (115) describes and figure 24 shows the exact frequency response for the "Z_o" case. The behavior can be visualized from the frequency response of the Bernoulli-Euler propagation operators (see fig 13). In particular, operators C(Ts) and S(Ts) are both of magnitude 0.5, and 90° out of phase at high frequency. Thus, at high frequency, $\dot{y}_b/M_a$ and $\dot{\theta}/Q_a$ should be 3 dB below their dc gain. The other two terms of equation (115), $\dot{y}_b/Q_a$ and $\dot{\theta}_b/M_a$, should be 6 dB below their low-frequency asymptotes. Comparison of the results in figure 23 with these exact results shows that the rational algebraic approximations to Z_b, Y_{bb}, and Y_{ba} introduce a significant ripple in the frequency responses.

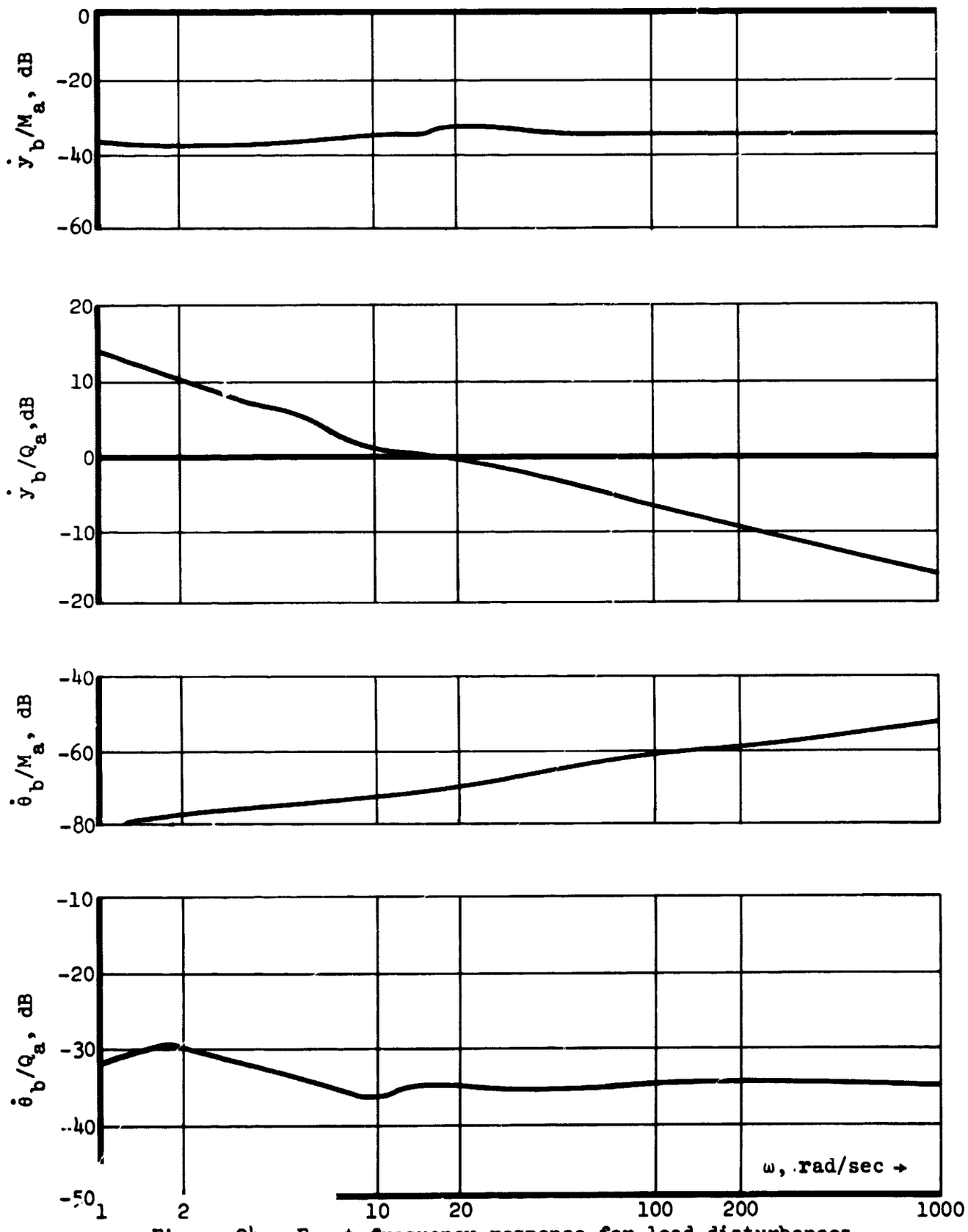

Figure 24.--Exact frequency response for load disturbances $Z_b = Z_o$

Transient response: These four cases were also studied by analog simulation described earlier. Step disturbances of M_a and Q_a were applied, and the resultant motions at both ends of the beam were recorded.

The motions at end a and end b are shown in figures 25 a, b, c, and d and in figures 26 a, b, c, and d, respectively. In the responses, the "Z_o" termination generally seems to minimize the maximum excursions of $\dot{y}$ and $\dot{\theta}$ from zero best, if the responses after, say, $t = 0.20$ are ignored. The response for large t is considered irrelevant, because a position control loop could be used to null the dc error component.

The damping forces and moments applied to the beam by the Z_o termination were also recorded for steps of M_a and Q_a to determine the force magnitude and frequency requirements of an active damper in such a situation. Results are shown in figure 27; note that quantity ℓQ, rather than Q, is plotted. In terms of the quantities ℓQ and M, results are independent of ℓ.

In general, the force must be given by $Z_{oa}\,\dot{x}_b$. Thus, from equations (115) and (102b),

$$\begin{bmatrix} M_b \\ Q_b \end{bmatrix} = \left[\begin{array}{c|c} -\frac{EI}{a} & -\frac{EI}{a}\sqrt{\frac{2a}{s}} \\ \hline \frac{EI}{a}\sqrt{\frac{2s}{a}} & \frac{EI}{a} \end{array}\right] \frac{a}{EI} \left[\begin{array}{c|c} C(Ts) - S(Ts) & \sqrt{\frac{2a}{s}}\,C(Ts) \\ \hline -\sqrt{\frac{2s}{a}}\,C(Ts) & -[C(Ts) + S(Ts)] \end{array}\right] \begin{bmatrix} M_a \\ Q_a \end{bmatrix} \tag{116}$$

If the matrix product in equation (116) is formed, the steady-state relation can be found by evaluating the limit as $s \to 0$. This result can be written

$$\lim_{s \to 0} \begin{bmatrix} M_b \\ \ell Q_b \end{bmatrix} = \left[\begin{array}{c|c} 1 & 1 \\ \hline 0 & 1 \end{array}\right] \begin{bmatrix} M_a \\ \ell Q_a \end{bmatrix} \tag{117}$$

This is simply a statement of static equilibrium for the beam. The simulation results do satisfy this equilibrium check. Morever, all transient peaks are less than 1.0 with the exception of $\ell Q_b/M_a$, which is less than 6.0. Thus, the "Z_o" termination appears to require transient control effort of the same order of magnitude as that for equilibrium.

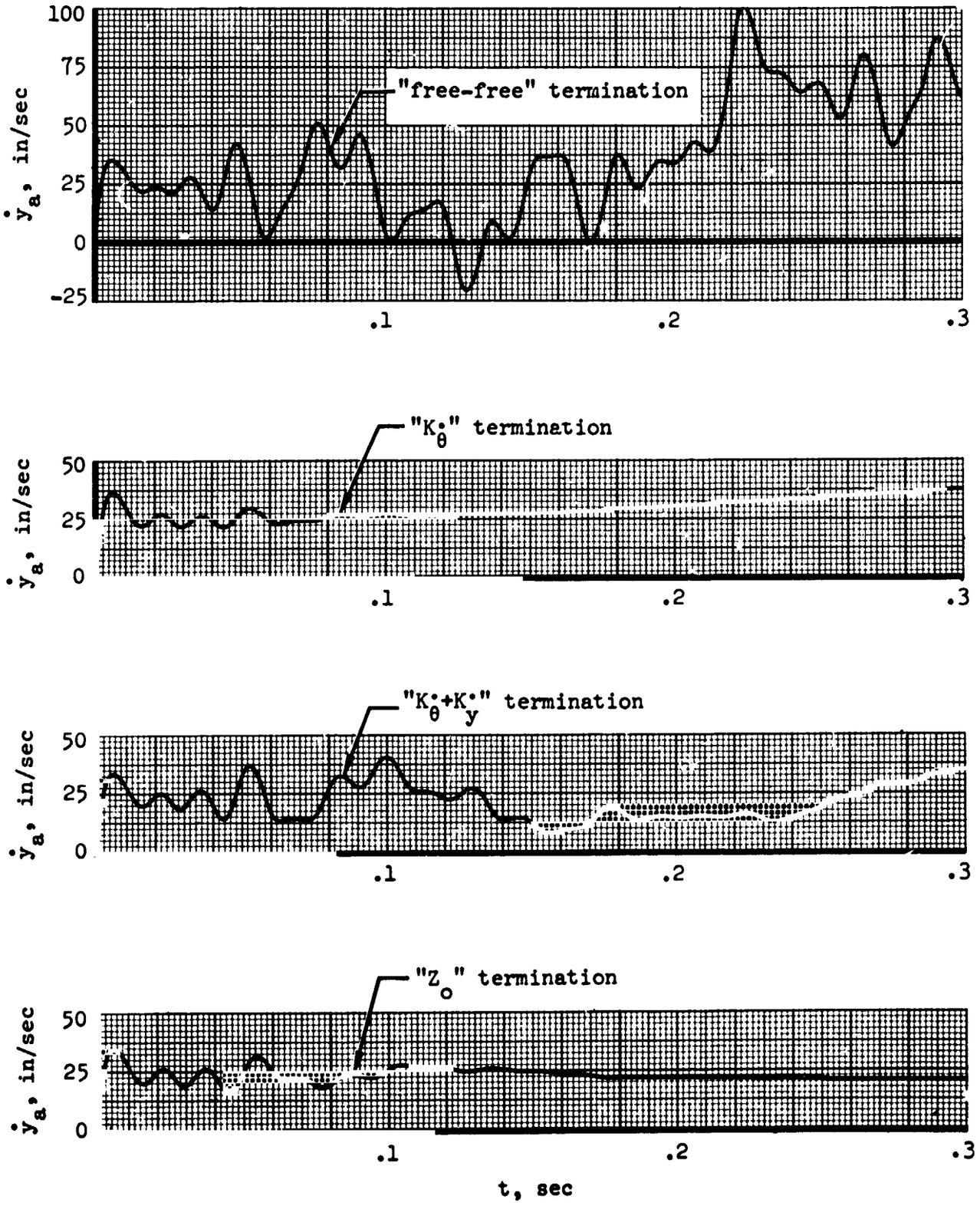

Figure 25a.- Effect of terminal impedance Z_b on the response of y_a to a 1000 in-lb step of M_a

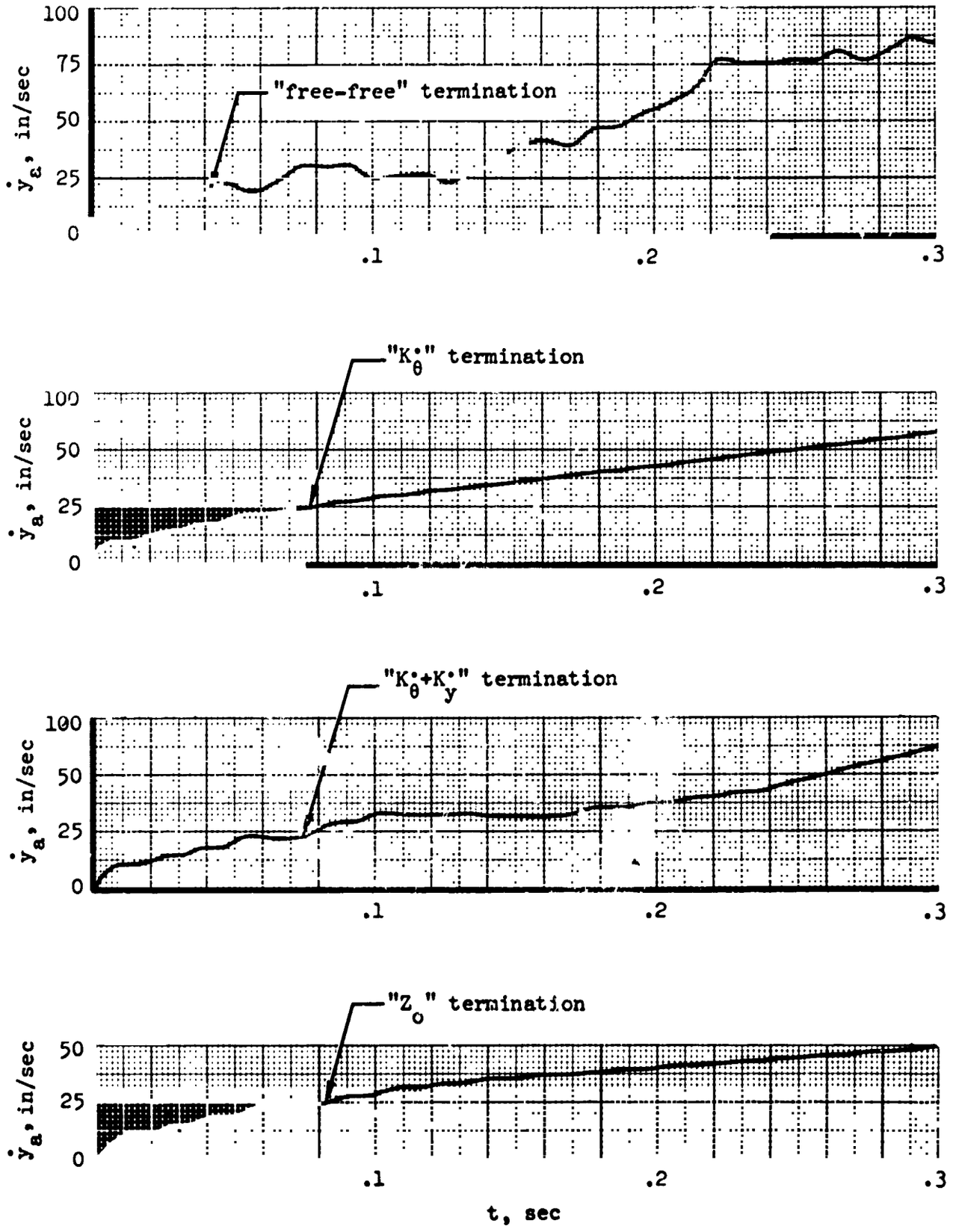

Figure 25b.- Effect of terminal impedance Z_b on the response of $\dot{y}_a$ to a 10 lb step of Q_a

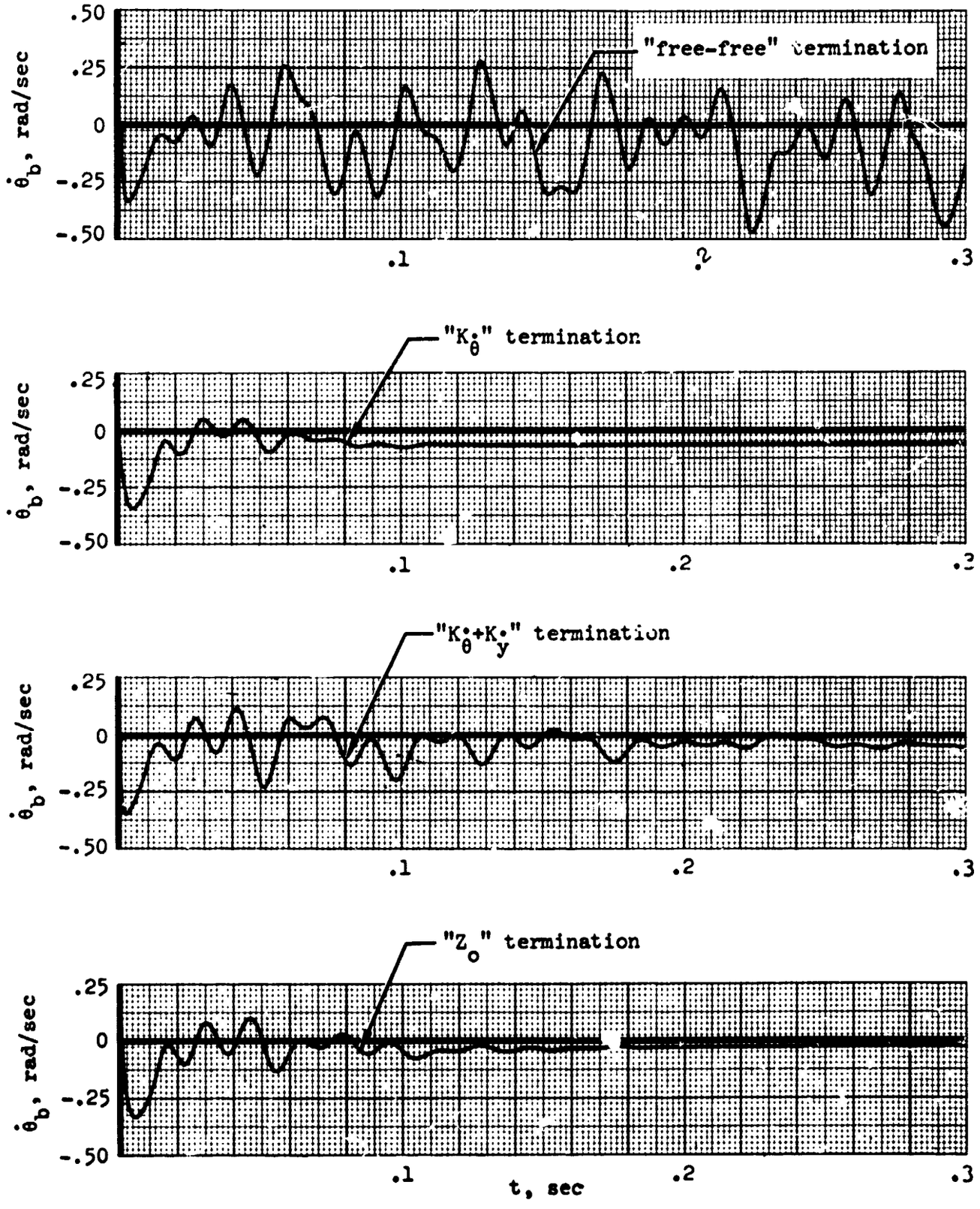

Figure 25c.- Effect of terminal impedance Z_b on the response of $\dot{\theta}_a$ to a 1000 in-lb step of M_a

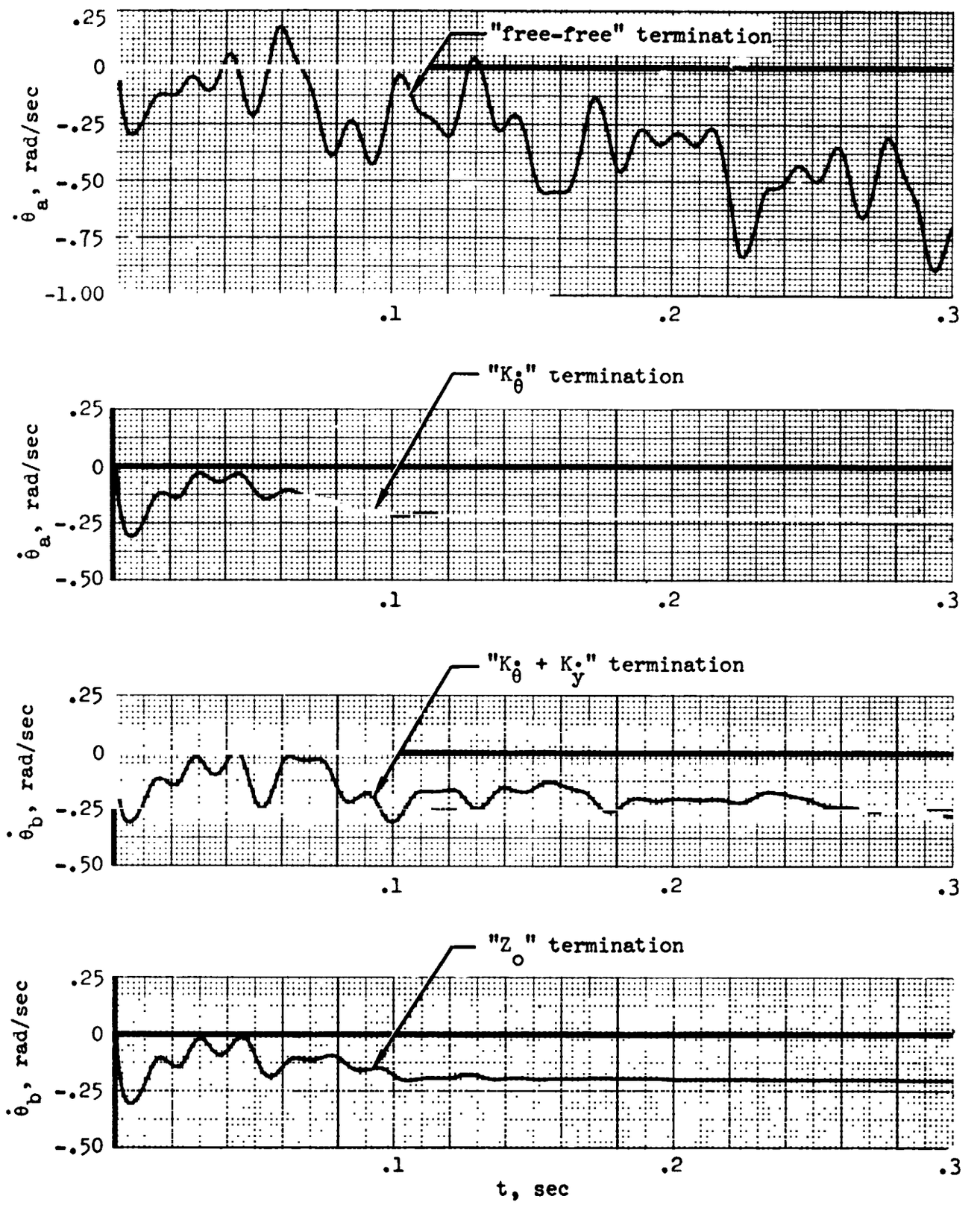

Figure 25d.- Effect of terminal impedance Z_b on the response of $\dot{\theta}_a$ to a 10 lb step of Q_a

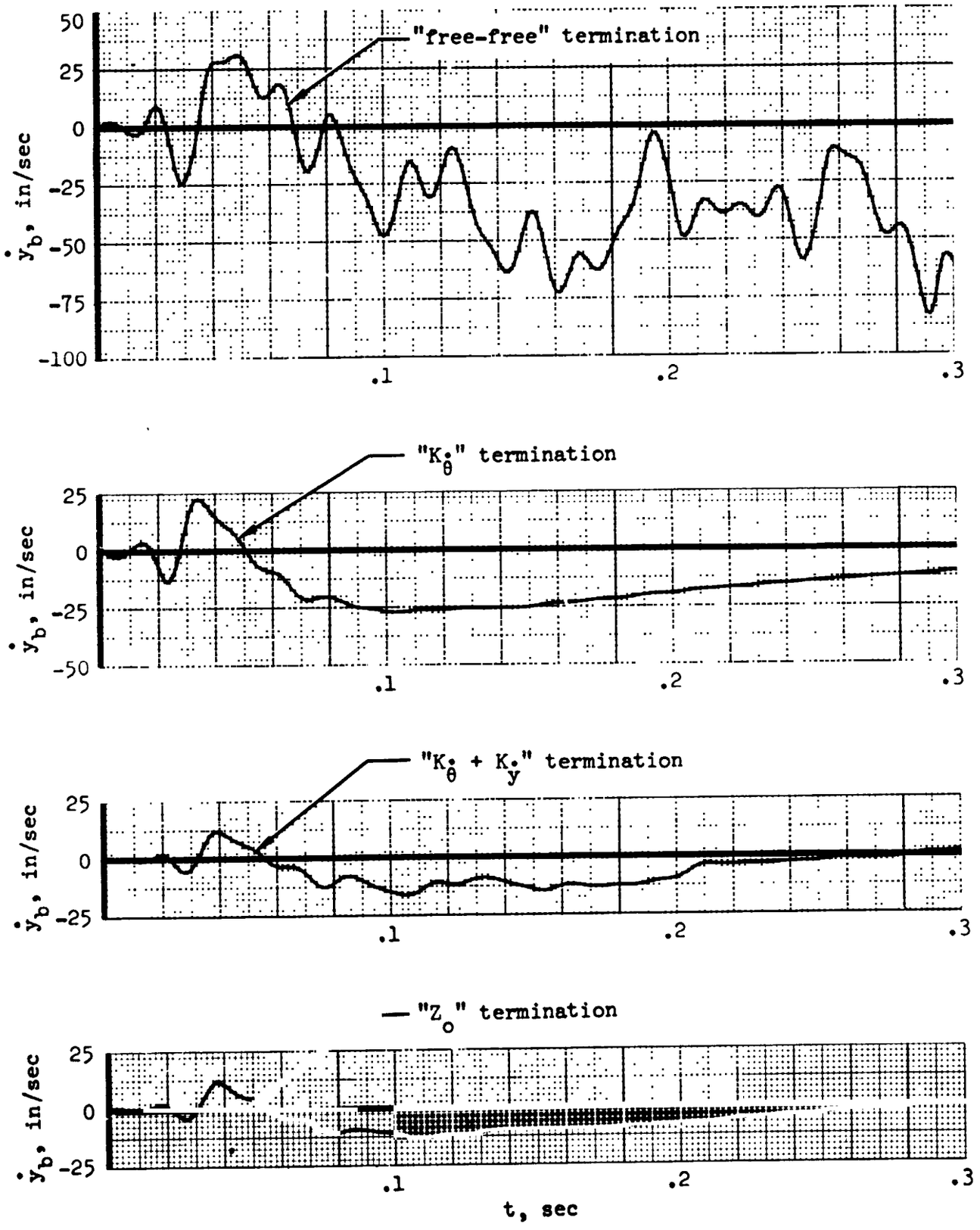

Figure 26a.- Effect of terminal impedance Z_b on the response of $\dot{y}_b$ to a 1000 in-lb step of M_a

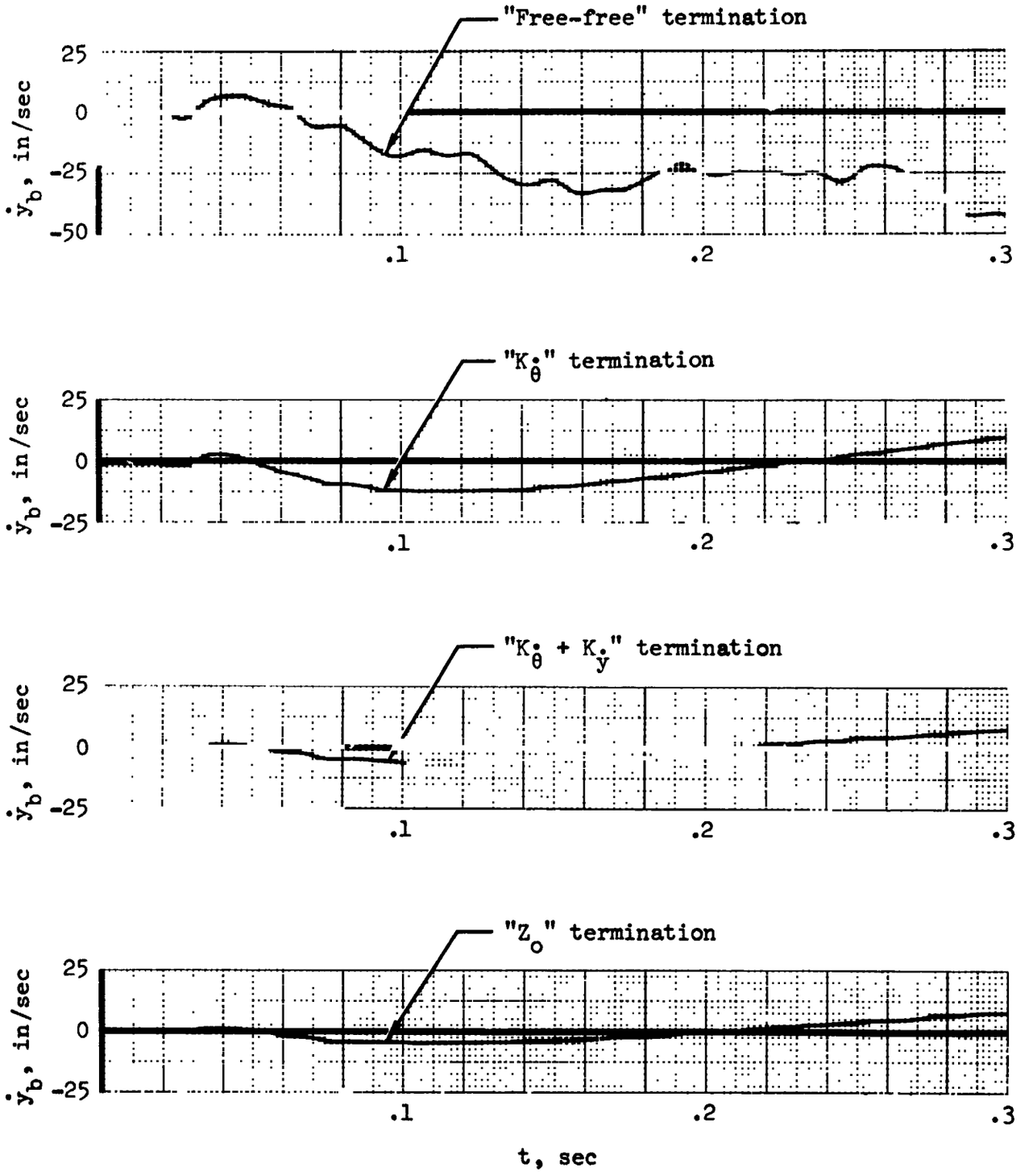

Figure 26b.- Effect of terminal impedance Z_b on the response of $\dot{y}_b$ to a 10 lb step of Q_a

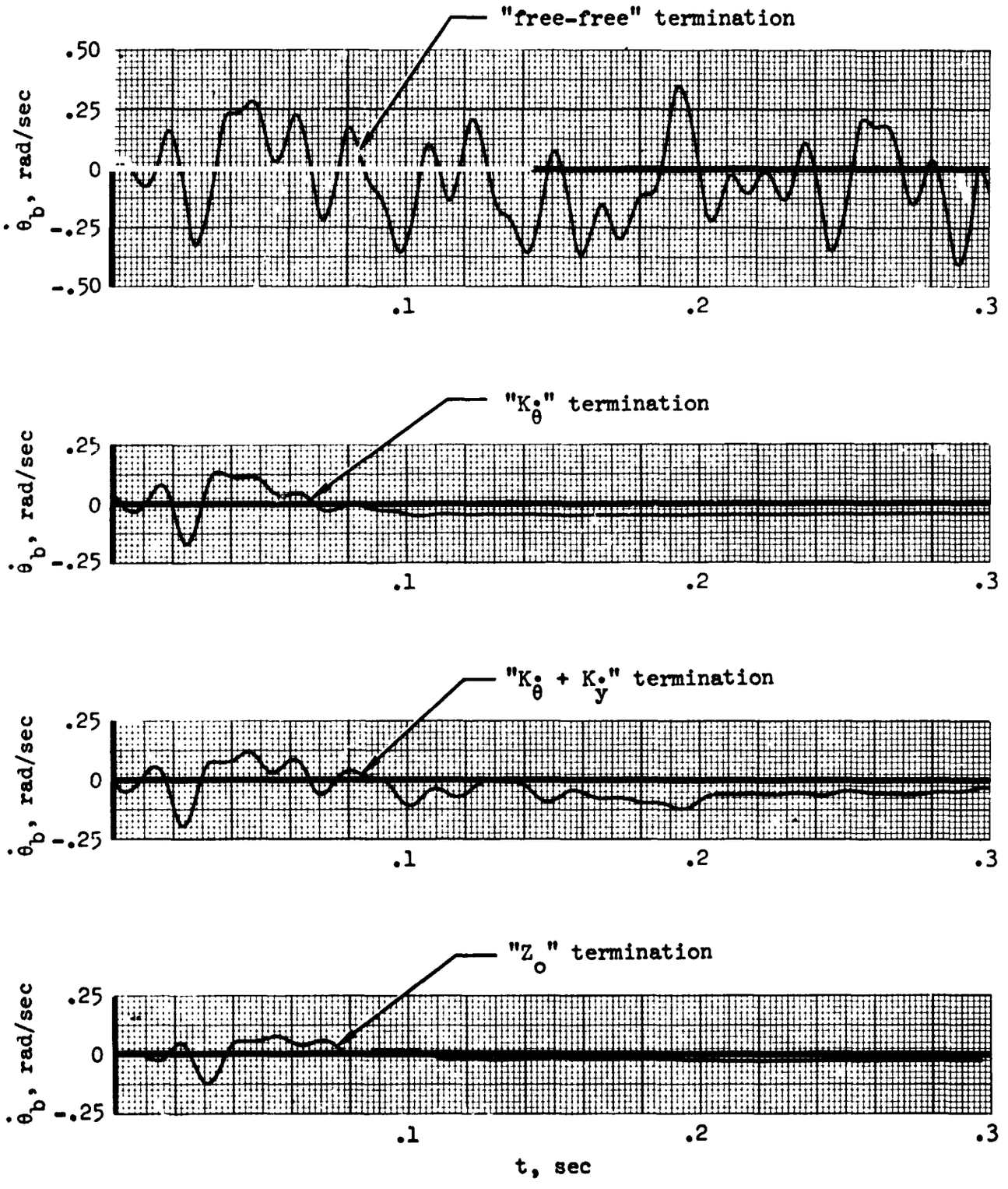

Figure 26c.- Effect of terminal impedance Z_b on the response of $\dot{\theta}_b$ to a 1000 in-lb step of M_a

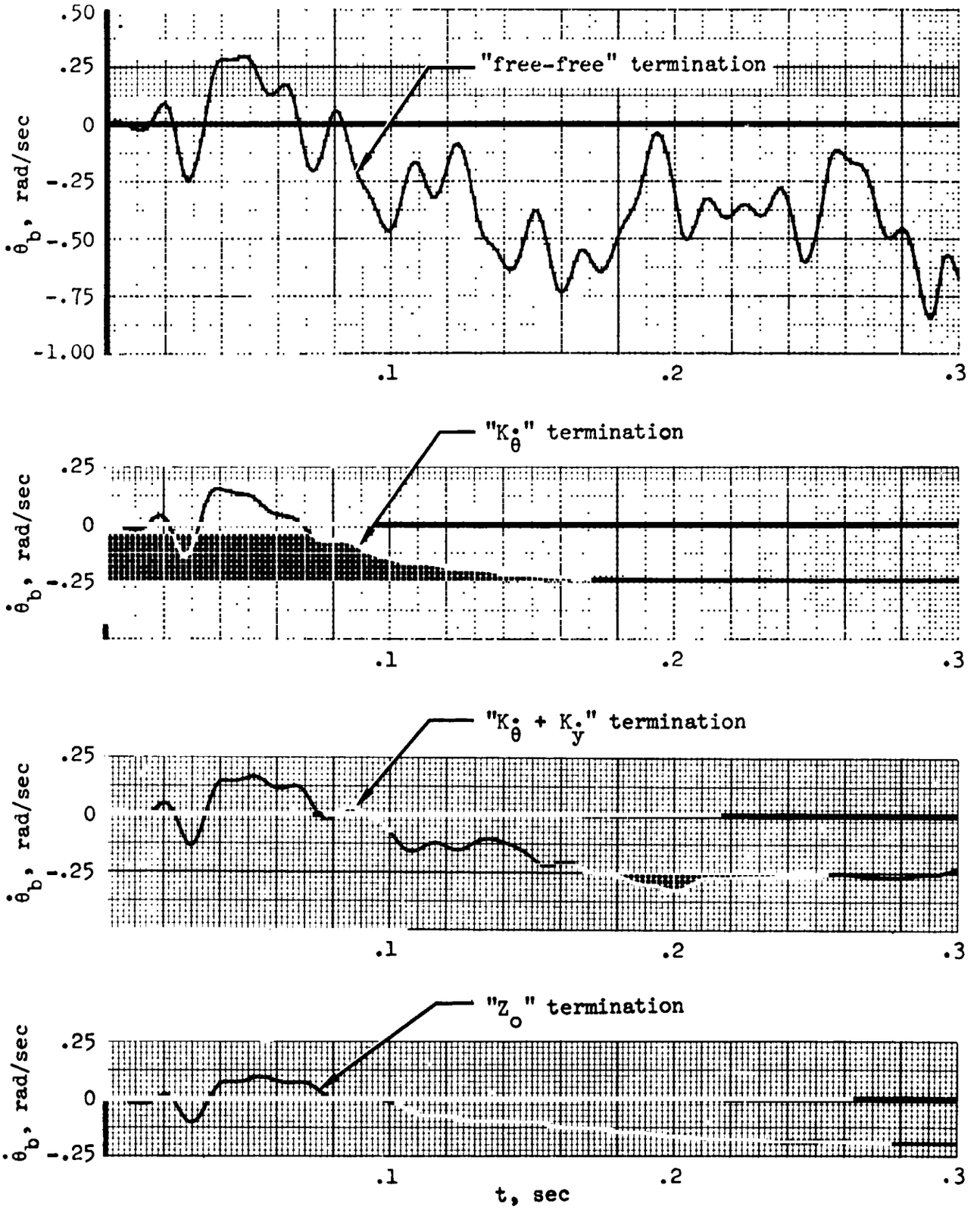

Figure 26d.- Effect of terminal impedance Z_b on the response of $\dot{\theta}_b$ to a 10 lb step of Q_a

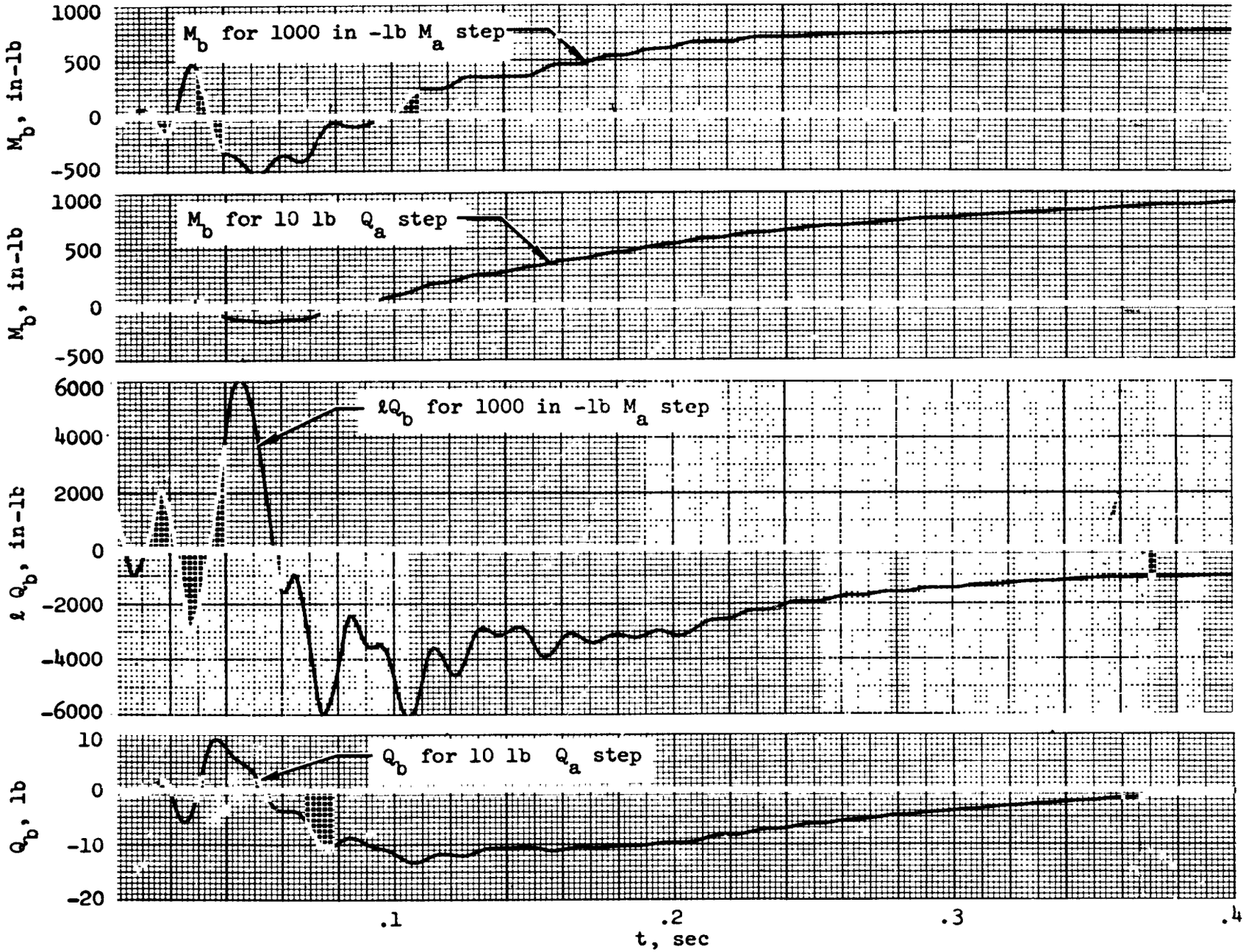

Figure 27.- Damping forces and moments applied by Z_o control in response to steps of M_a and Q_a

Lateral and angular velocity control.- The problem of tracking lateral and angular velocity commands is now treated. When commands and control are restricted to terminal b, as shown in figure 22, the frequency response can be computed from the Z_b, and the admittance elements, by the relations

$$\dot{x}_a = [Y_{ab}(I - Z_b Y_{bb})^{-1} Z_b]\, \dot{x}_b^* \tag{118a}$$

$$\dot{x}_b = [(I - Y_{bb} Z_b)^{-1} Y_{bb} Z_b]\, \dot{x}_b^* \tag{118b}$$

Because $R_{22} = 0$ for the "Z_o" termination, the response can also be simply computed in terms of the propagation operators. Using equations (104a and b) and setting $Z_a = 0$ and $Z_b = Z_{oa}$ yield

$$\begin{bmatrix} \dot{y}_a \\ \dot{\theta}_a \end{bmatrix} = \left[\begin{array}{c|c} e^{-\sqrt{Ts}}\,(1 - \sin\sqrt{Ts}) & \sqrt{\frac{2a}{s}}\, e^{-\sqrt{Ts}} \sin\sqrt{Ts} \\ \hline \sqrt{\frac{2s}{a}}\, e^{-\sqrt{Ts}} \sin\sqrt{Ts} & e^{-\sqrt{Ts}}\,(\cos\sqrt{Ts} + \sin\sqrt{Ts}) \end{array}\right] \begin{bmatrix} \dot{y}_b^* \\ \dot{\theta}_b^* \end{bmatrix} \tag{119a}$$

$$\begin{bmatrix} \dot{y}_b \\ \dot{\theta}_b \end{bmatrix} = \left[\begin{array}{c|c} \frac{1}{2} & \frac{1}{4}\sqrt{\frac{2a}{s}} \\ \hline -\frac{1}{4}\sqrt{\frac{2s}{a}} & \frac{1}{2} \end{array}\right] + e^{-2\sqrt{Ts}} \left[\begin{array}{c|c} \frac{1}{2}\,(1 - \sin 2\sqrt{Ts}) & -\frac{1}{4}\sqrt{\frac{2a}{s}}\,(\cos 2\sqrt{Ts} - \sin 2\sqrt{Ts}) \\ \hline -\frac{1}{4}\sqrt{\frac{2s}{a}}\,(2 - \cos 2\sqrt{Ts} - \sin 2\sqrt{Ts}) & \frac{1}{2}\,(\cos 2\sqrt{Ts} + \sin 2\sqrt{Ts}) \end{array}\right] \begin{bmatrix} \dot{y}_b^* \\ \dot{\theta}_b^* \end{bmatrix} \tag{119b}$$

The steady states of equations (119a and b) are

$$\lim_{s \to 0} \begin{bmatrix} \dot{y}_a \\ \dot{\theta}_a \end{bmatrix} = \left[\begin{array}{c|c} 1 & -\ell \\ \hline 0 & 1 \end{array}\right] \begin{bmatrix} \dot{y}_b^* \\ \dot{\theta}_b^* \end{bmatrix} \tag{120a}$$

$$\lim_{s \to 0} \begin{bmatrix} \dot{y}_b \\ \dot{\theta}_b \end{bmatrix} = \left[\begin{array}{c|c} 1 & 0 \\ \hline 0 & 1 \end{array}\right] \begin{bmatrix} \dot{y}_b^* \\ \dot{\theta}_b^* \end{bmatrix} \tag{120b}$$

Equation (120b) indicates that end b has no tracking error in the steady state. Equation (120a) relates the rigid-body motion of the two ends. The equations (119a and b) are useful in determining the differences between the exact solutions and those determined from equations (118a and b), using rational algebraic approximations for Y_{ab}, Y_{bb}, and Z_b.

Transient response: The responses to steps $\dot{y}_b^*$ and $\dot{\theta}_b^*$ were studied by analog simulation. The first system studied was the "Z_o" control, i.e., $Z_b = Z_{oa}$; it did not track commands. This contradicts the behavior predicted by equations (120a and b). The difficulty was traced to the low frequency of the analog approximations to $\sqrt{s}$ and $1/\sqrt{s}$, which were first used in the simulation. This was corrected and is treated in Appendix A. The "Z_o" control then responded to commands, as shown in figures 28a and b. These responses are disappointingly slow, considering that the period of the first bending mode is approximately 0.2 sec. Later, a command of $\dot{y}_b^*$ alone was observed to correspond to pure translation, whereas a command of $\dot{\theta}_b^*$ alone corresponds to rotation about the point b. These motions are clearly unnatural for the beam that rotates about its center of gravity when stimulated by a moment M_b and about the center of percussion (station $x = \ell/3$) when stimulated by a force Q_b.

This difficulty was circumvented by using simultaneous commands to $\dot{\theta}_b^*$ and $\dot{y}_b^*$ with a ratio corresponding to rotation about the center of percussion, which is two-thirds the beam length from b. The simultaneous commands were constrained by the relation:

$$\dot{y}_b^* = \frac{2\,\ell}{3}\,\dot{\theta}_b^* \tag{121}$$

The response to these simultaneous or dual commands is vastly superior to the response to single commands. The step responses at ends a and b are shown in figure 29. Also shown is the response of the first term of equation (119b); this term can be thought of, loosely, as the response caused by the initial impact. The early part of the $\dot{y}_b$ and $\dot{\theta}_b$ transients agrees quite well with this high-frequency approximation, considering that the analog simulation uses rational algebraic approximations for both Y_{bb} and Z_b. The second term of equation (119b) can be loosely considered the wave reflected from end a (the $e^{-2\sqrt{Ts}}$ factor is due to the wave's round trip through two $e^{-\sqrt{Ts}}$ operators). Because $R_{22} = 0$, no wave is reflected from end b. If this loose thinking is carried one stage further, and the trigonometric terms of the second matrix of equation (119b) are replaced by their low-frequency equivalents, the following approximation results:

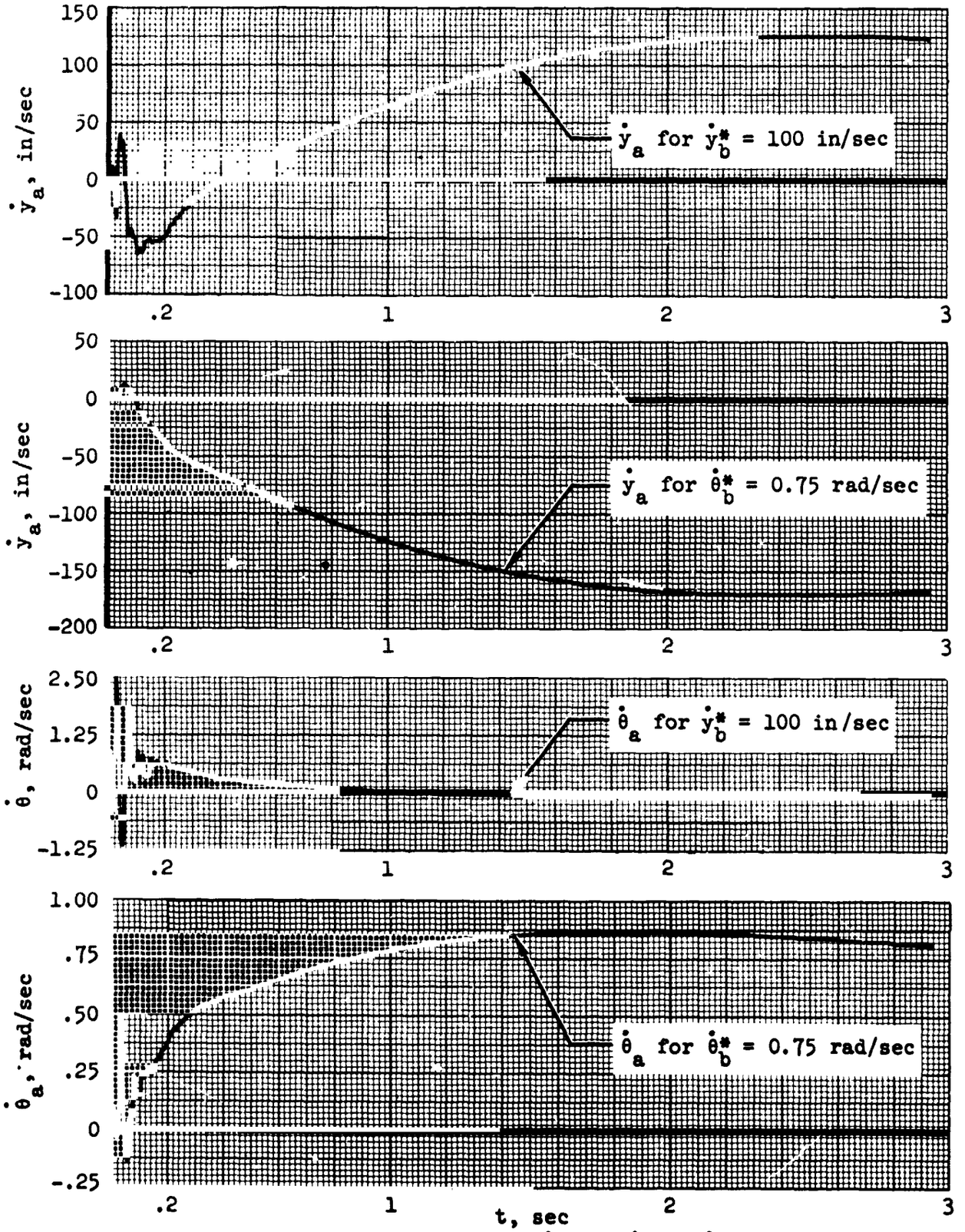

Figure 28(a).- Response of $\dot{y}_a$ and $\dot{\theta}_a$ to $\dot{y}_b$ and $\dot{\theta}_b$ commands (Z_o control)

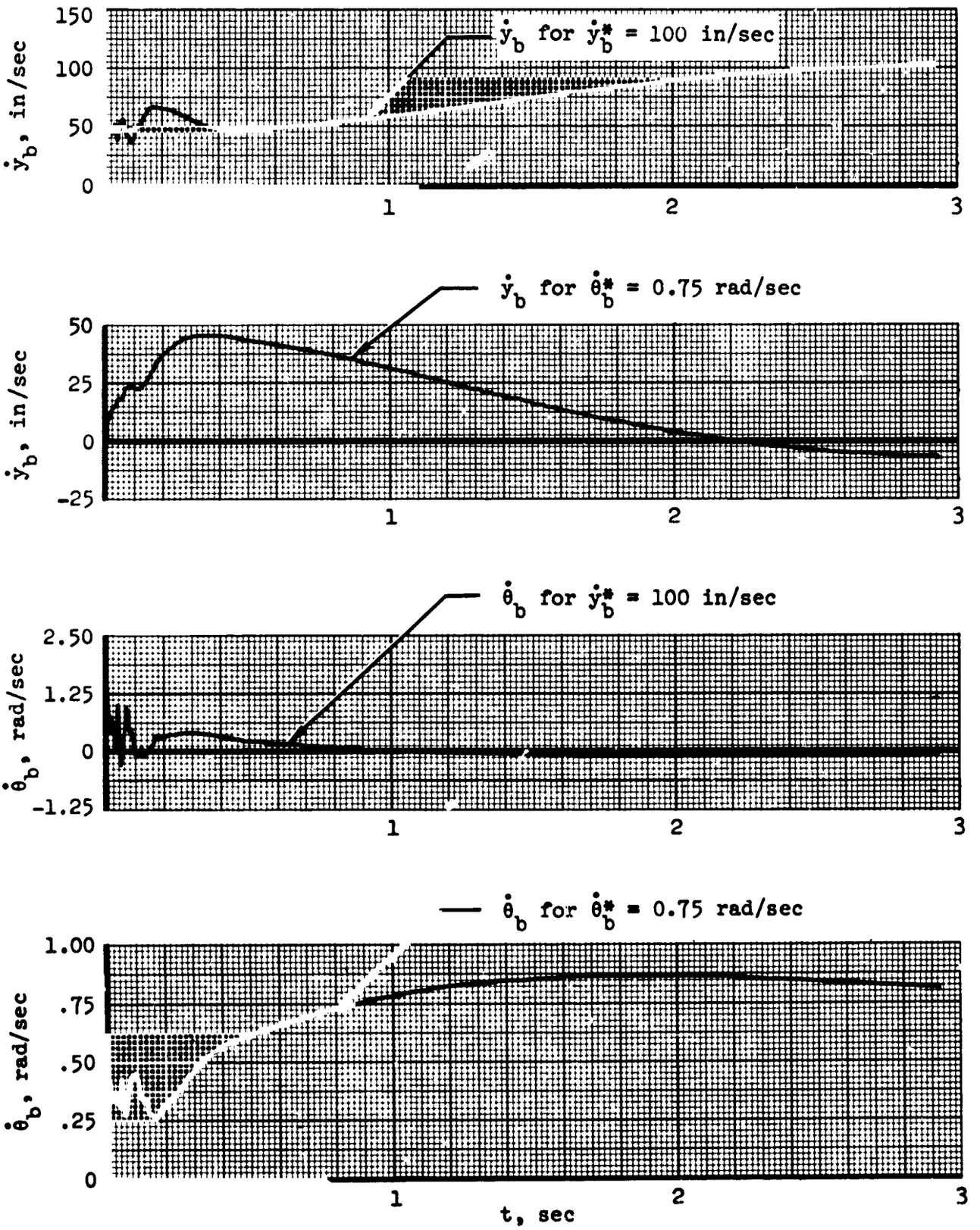

Figure 28b.- Response of $\dot{v}_b$ and $\dot{\theta}_b$ to $\dot{y}_b$ and $\dot{\theta}_b$ commands (Z_o control)

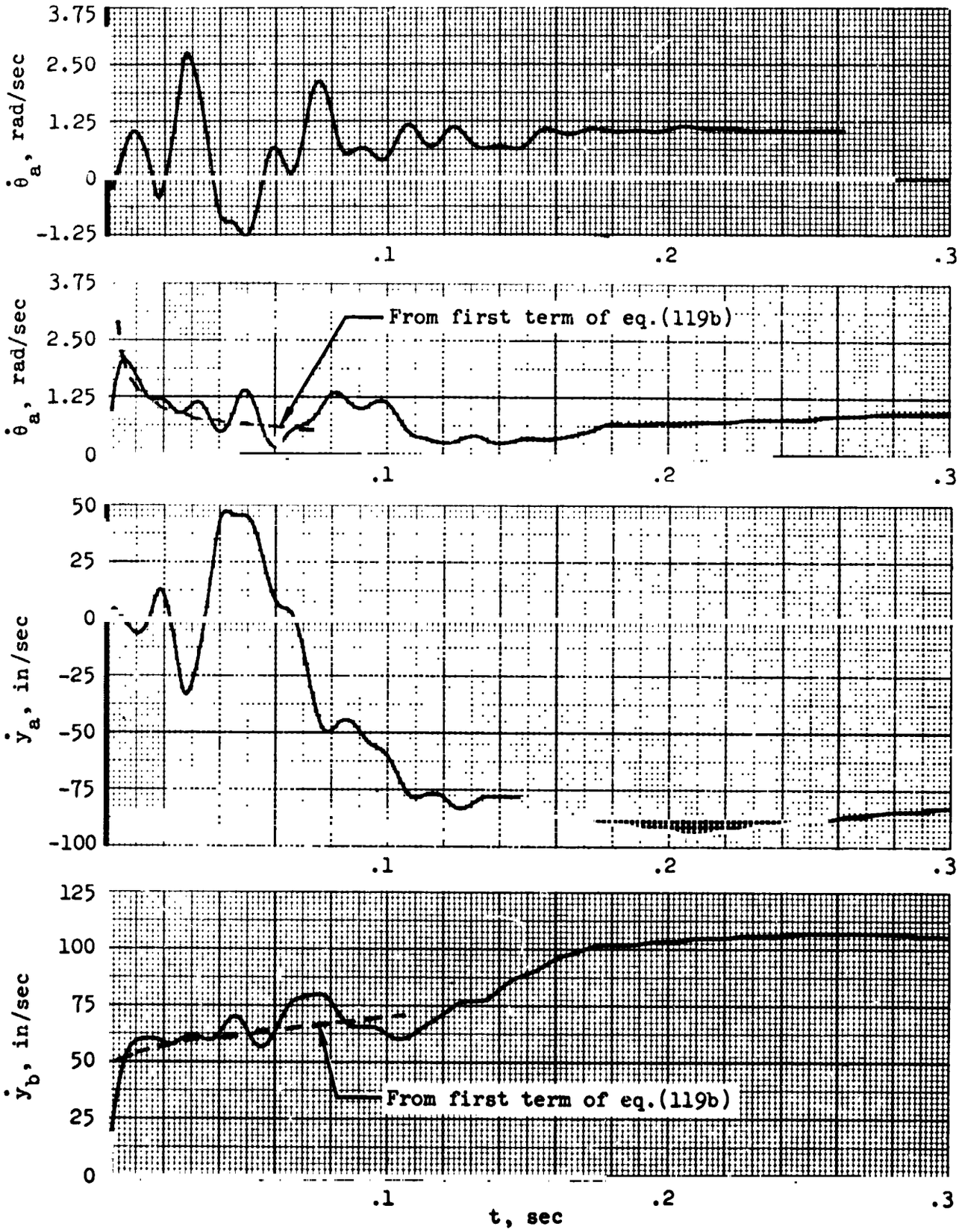

Figure 29.- Response of Z_o controller with dual commands ($\dot{y}_b^* = 100$ in/sec and $\dot{\theta}_b^* = 0.75$ rad/sec)

$$\begin{bmatrix} \dot{y}_b \\ \dot{\theta}_b \end{bmatrix} \underset{\sim}{} \left\{ \left[\begin{array}{c|c} \frac{1}{2} & \frac{1}{4}\sqrt{\frac{2a}{s}} \\ \hline \frac{1}{4}\sqrt{\frac{2s}{a}} & \frac{1}{2} \end{array}\right] + e^{-2\sqrt{Ts}} \left[\begin{array}{c|c} \frac{1}{2} & \frac{-1}{4}\sqrt{\frac{2a}{s}} \\ \hline \frac{-1}{4}\sqrt{\frac{2s}{a}} & \frac{1}{2} \end{array}\right] \right\} \begin{bmatrix} \dot{y}_b^* \\ \dot{\theta}_b^* \end{bmatrix} \quad (122)$$

Comparison of this relation to that between v_b and v_b^* for longitudinal control is interesting. In the latter [setting $z_t = Y_o$ and $r_{22} = 0$ in equation (44)], $v_b = (1/2 + 1/2\ e^{-2Ts})\ v_b^*$. The similarity is striking, although admittedly contrived by suppression of the $\cos\sqrt{Ts}$ and $\sin\sqrt{Ts}$ terms.

The constraint between the dual commands was varied somewhat from the ratio $2\ell/3$. The step responses appear to degrade, if the ratio is much greater than $2\ell/3$ or much less than $\ell/2$. Frequency-response sensitivity to the dual-command ratio was also studied and is discussed subsequently.

The "$K_{\dot{\theta}}$" and "$K_{\dot{\theta}} + K_{\dot{y}}$" terminations were also simulated. Dual step commands with $\dot{y}_b^* = (2\ell/3)\ \dot{\theta}_b^*$ were used for the "$K_{\dot{\theta}} + K_{\dot{y}}$" control. For the "$K_{\dot{\theta}}$" control, the $\dot{y}_b^*$ command is irrelevant, because both $G_{\dot{y}}$ and $K_{\dot{y}}$ are zero. The responses at ends a and b for the "$K_{\dot{\theta}} + K_{\dot{y}}$" and "$K_{\dot{\theta}}$" terminations are shown in figures 30 and 31, respectively. The performance of the "$K_{\dot{\theta}} + K_{\dot{y}}$" termination is clearly inferior to that of the "Z_o" termination. If fast rise time with little overshoot is a goal, the "$K_{\dot{\theta}}$" control is certainly the best, but not overwhelmingly so. Study of the sensitivity of the "$K_{\dot{\theta}}$" control to variations in the gain $K_{\dot{\theta}}$ from its matched value of EI/a indicates that $K_{\dot{\theta}} = EI/a$ is a practical optimum. The degrading effects of increasing or decreasing $K_{\dot{\theta}}$ significantly from this value are also shown in figure 31.

Thus, the "$K_{\dot{\theta}}$" control, whose reflection matrix is the identify matrix, appears highly desirable; that the value $K_{\dot{\theta}} = EI/a$, suggested from the reflection matrix concept, is indeed an optimum is considered significant. Note that the rigid-body transfer function for this optimized "$K_{\dot{\theta}}$" control is

$$\dot{\theta}_b = \left[\frac{K_{\dot{\theta}} \times \frac{6}{29}}{s + K_{\dot{\theta}} \times \frac{6}{29}}\right] \dot{\theta}_b^* \quad (123)$$

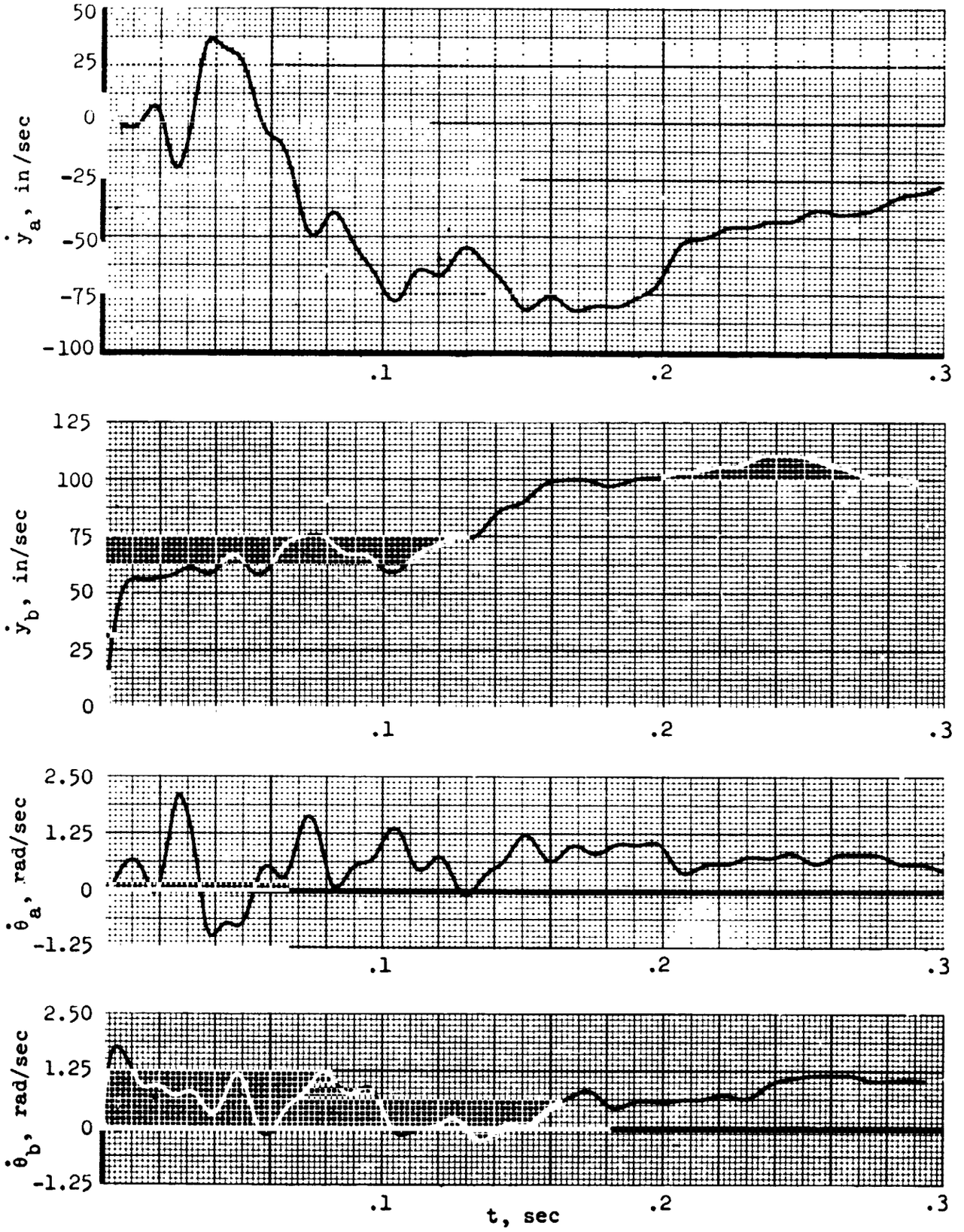

Figure 30.- Response of "$K_{\dot{\theta}} + K_{\dot{y}}$" controller with dual commands ($y_b^* = 100$ in/sec and $\dot{\theta}_b^* = 0.75$ rad/sec)

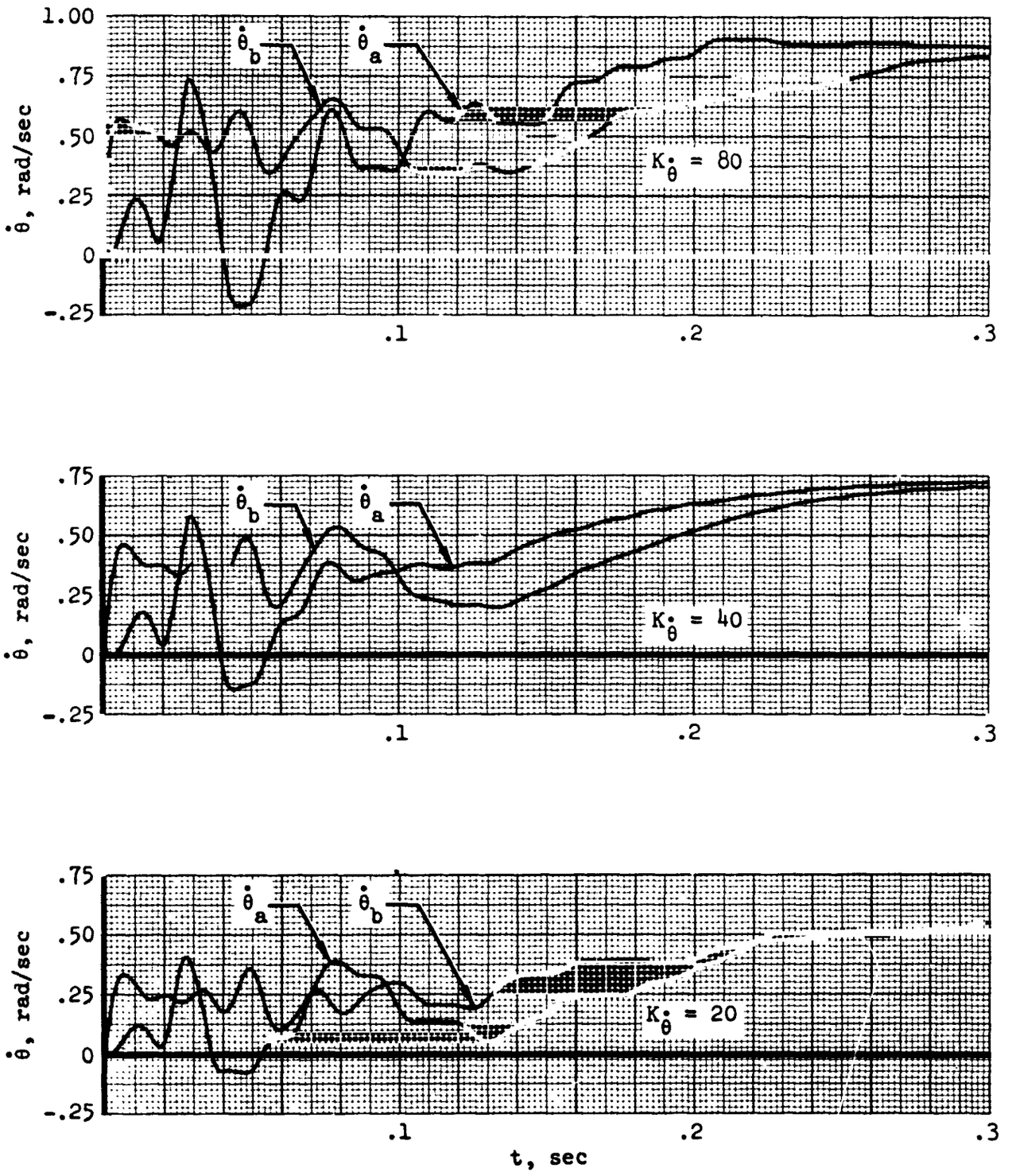

Figure 31.- Sensitivity of "$K_{\dot{\theta}}$" controller response
($\dot{\theta}_b^*$ = 0.75 rad/sec)

When $K_{\dot\theta} = 41.5$, the rigid-body real root is -8.6 rad/sec. This compares with the first bending mode frequency of 32 rad/sec. Why the "Z_o" control is not superior to the "$K_{\dot\theta}$" control is at present unexplained. One source of difficulty may be the way commands are put into the control loop. For the "Z_o" control, simultaneous commands constrained to the ratio $\dot y_b^* = (2\ell/3)\,\dot\theta_b^*$ gave $\dot\theta_b$ response which is superior to that achieved with only a $\dot\theta_b^*$ command (compare figures 28 a and b with 29). A further modification which might be investigated is a prefilter in the command structure. The configuration shown in figure 32 may have merit.

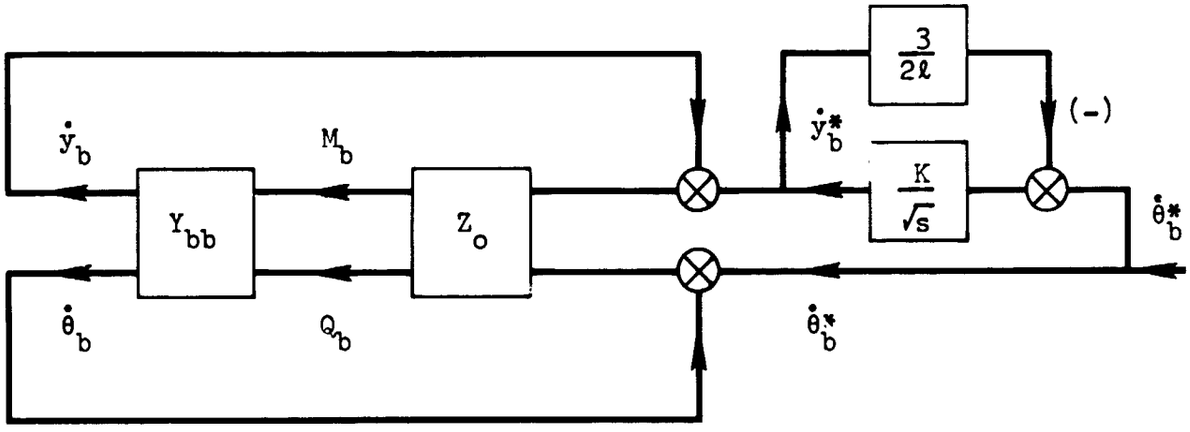

Figure 32. "Z_o" Matrix Control with pre-filter.

It uses $K/\sqrt{s}$ in the $\dot y_b^*$ channel to cancel the $\sqrt{s}$ term in the first matrix of equation (119b); this would eliminate the initial spike in the $\dot\theta_b$ response shown in figure 29. Preliminary studies of this prefilter scheme were made in the frequency domain.

Frequency response: The frequency responses of $\dot\theta_b/\dot\theta_b^*$ were computed for the "$K_{\dot\theta}$", "$K_{\dot\theta} + K_{\dot y}$", and the "$Z_o$" controls, using dual commands with $\dot y_b^* = (2\ell/3)\,\theta_b^*$. The responses, computed from equation (118b), using rational algebraic approximations to Y_{bb} and Z_b, are shown in figure 33. The low-frequency tracking ability of all three systems is good. The "$K_{\dot\theta}$" control is clearly superior through the important range $10 \le \omega \le 100$ rad/sec and, particularly, at the first bending frequency of 32 rad/sec.

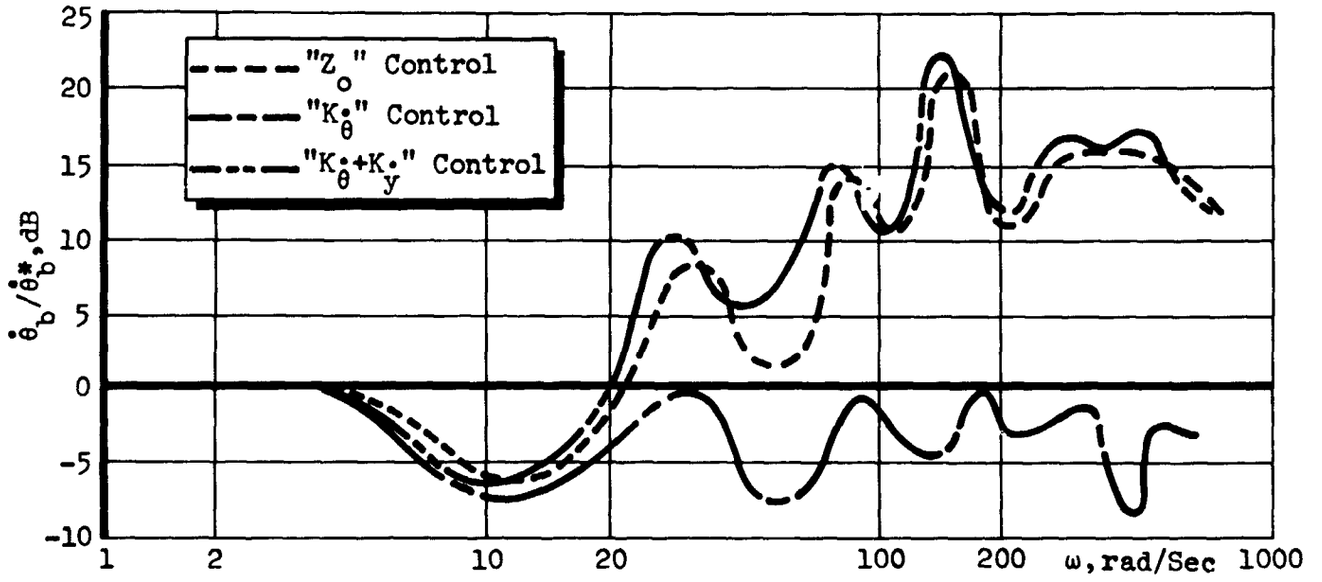

Figure 33. Effect of Z_b on $\dot{\theta}_b(j\omega)/\dot{\theta}_b^*(j\omega)$

The "Z_o" matrix control with the prefilter is shown in figure 32, and its frequency response is compared with that of the "$K_{\dot{\theta}}$" control in figure 34.

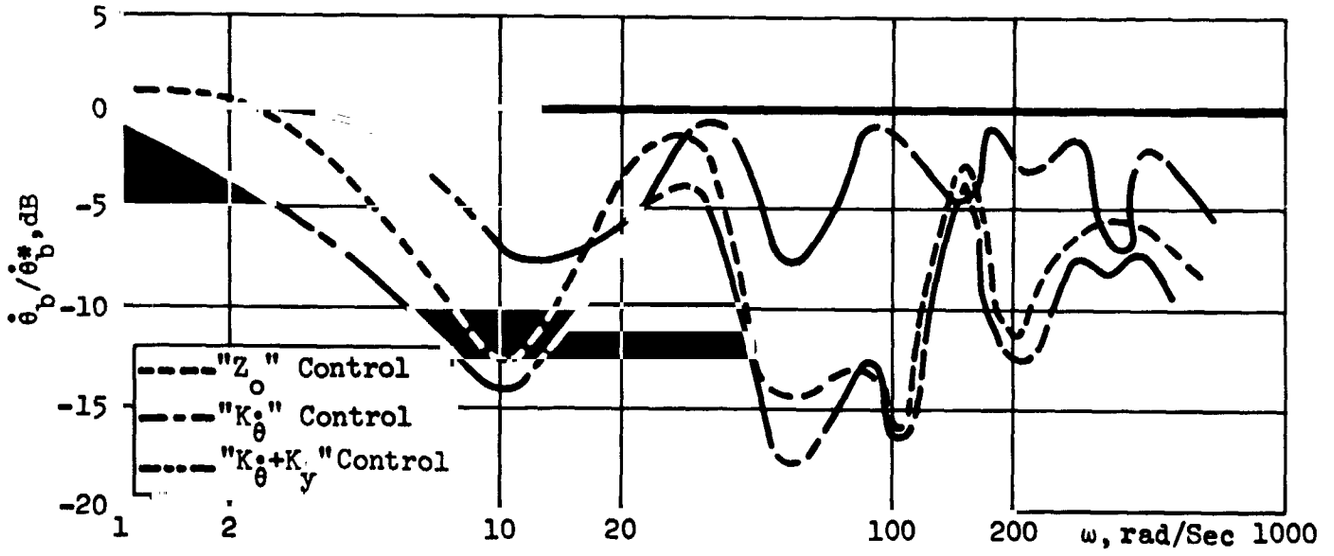

Figure 34. Effect of pre-filter on $\dot{\theta}_b(j\omega)/\dot{\theta}_b^*(j\omega)$ for "Z_o" control.

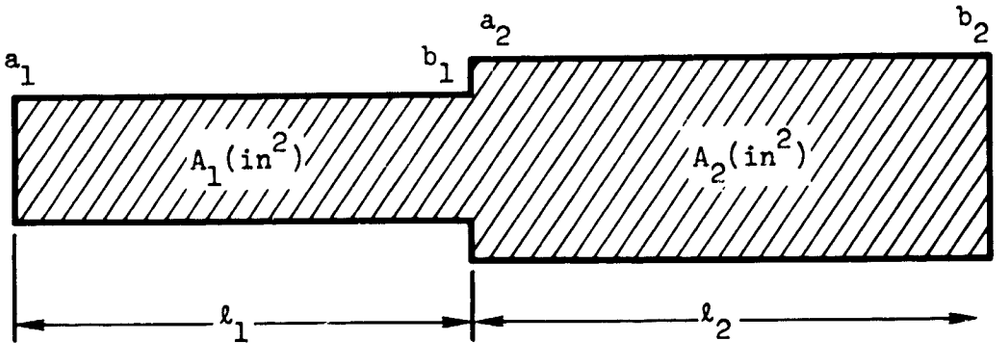

Figure 35. Two uniform beams in cascade

Although the bending resonance previously exhibited by the "Z_o" control is eliminated as predicted, the oscillation of gain is still much greater than that for the "$K_{\dot{\theta}}$" control. The prefilter investigated could not correct these deficiencies. This, of course, does not rule out the possibility that some other prefilter configuration, combined with the "Z_o" matrix control or the "$K_{\dot{\theta}} + K_{\dot{y}}$" control, might respond to commands better than the "$K_{\dot{\theta}}$" control. In fact, this is highly likely in view of the slightly superior performance of these schemes for disturbance alleviation.

Transverse vibration of nonuniform beams.- The application of propagation and reflection concepts to the dynamics and control of uniform beams leaves many questions open. Nevertheless, a composite beam comprised of two uniform beams in cascade was studied to glean an insight into possible applications of these concepts to nonuniform beams. The subscripts 1 and 2 denote the left and right beams shown in figure 35.

The factored transmission relations for the two uniform sections can be mated, as shown in figure 36. Here, end-effects matrices are distinguished as impedance (subscript z) and admittance (subscript y), because the interface must have an admittance on one side to mate with an impedance on the other. Figure 36 clearly shows that the matrix relation must be of the form

$$\begin{bmatrix} v_{2a}^{+} \\ u_{2a}^{+} \\ u_{2a}^{-} \\ v_{2a}^{-} \end{bmatrix} = \overbrace{\begin{bmatrix} J_{21} & J_{22} \\ J_{11} & J_{12} \end{bmatrix}}^{J} \begin{bmatrix} v_{1b}^{+} \\ u_{1b}^{+} \\ u_{1b}^{-} \\ v_{2b}^{-} \end{bmatrix} \tag{124}$$

The J matrix will be called the interface matrix. To determine the elements of the J matrix, note that

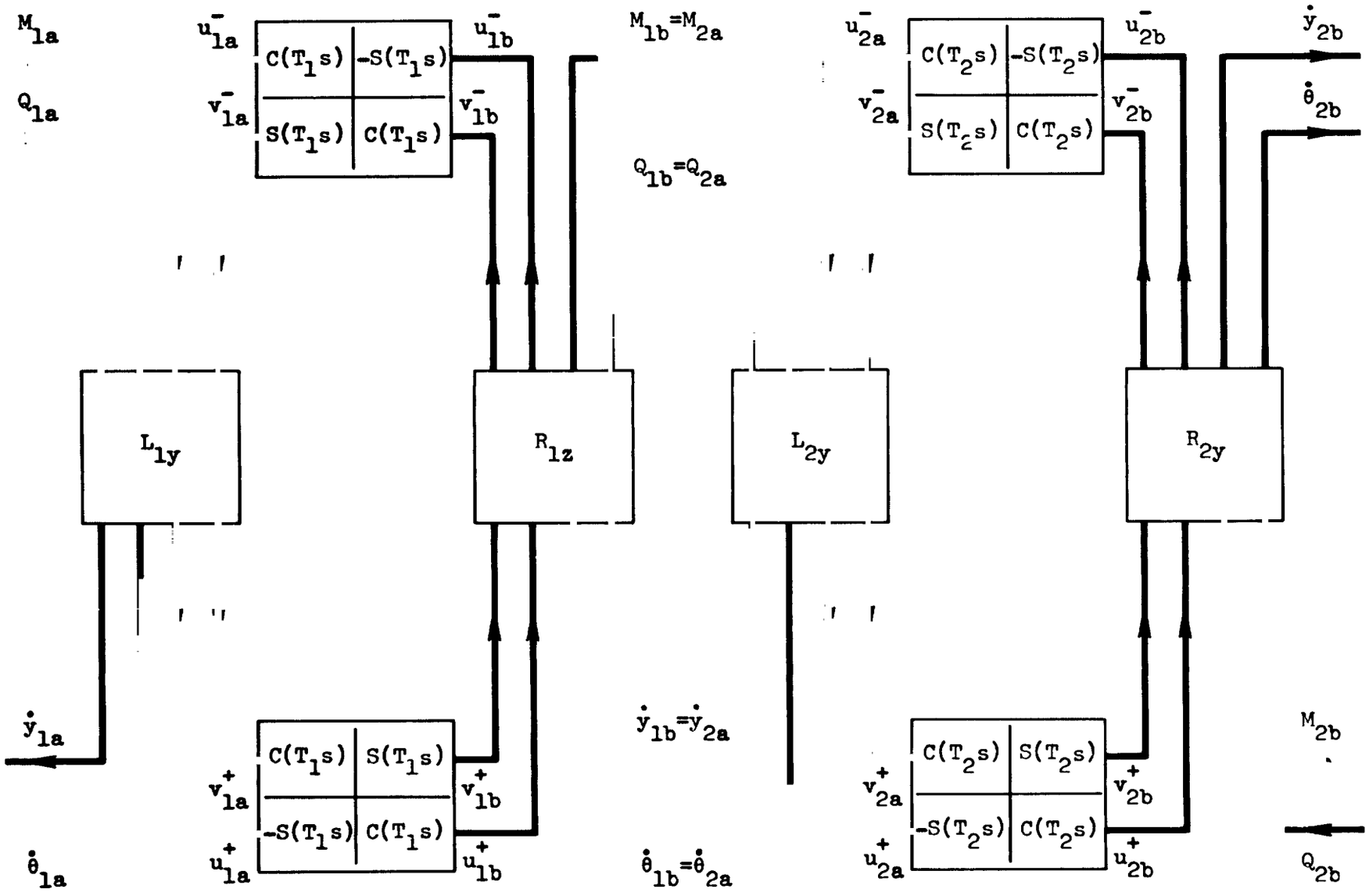

Figure 36. Cascaded beam in terms of propagation and end-effects relations.

$$U_{1b} = W_1^{*-1} Y_{1b} \tag{125a}$$

$$Y_{2a} = W_2^{*} U_{2a} \tag{125b}$$

where W_1^* and W_2^* are the W^* matrices for beams 1 and 2, and Y_{1b} and Y_{2a} are the Y state vectors at stations 1b and 2a, and, where

$$U_{1b} = [u_{1b}^- , v_{1b}^- , v_{1b}^+ , u_{1b}^+]^T \tag{126a}$$

$$U_{2a} = [u_{2a}^- , v_{2a}^- , v_{2a}^+ , u_{2a}^+]^T \tag{126b}$$

Because $Y_{1b} \equiv Y_{1a}$, equations (125a and b) give

$$U_{1b} = [W_1^{*-1} W_2^*] U_{2a} \tag{127}$$

For the trivial case, where the beams are identical, equation (127) is merely $U_{1b} = U_{2a}$; this means that $J_{21} = J_{12} = I$ and $J_{11} = J_{22} = 0$, and the variables are transmitted in both directions without reflection, as they, of course, must be in this case. If the matrix product in equation (127) is formed, the general result is

$$\begin{bmatrix} u_{1b}^- \\ v_{1b}^- \\ v_{1b}^+ \\ u_{1b}^+ \end{bmatrix} = \frac{1}{4} \left[\begin{array}{c|c|c|c} 2+k_{21}+k_{21}^3 & k_{21}-k_{21}^3 & 2-k_{21}-k_{21}^3 & k_{21}-k_{21}^3 \\ \hline k_{21}k_{21}^3 & k_{21}+2k_{21}^2+k_{21}^3 & k_{21}-k_{21}^3 & k_{21}-2k_{21}+k_{21}^3 \\ \hline 2-k_{21}-k_{21}^3 & k_{21}-k_{21}^3 & 2+k_{21}+k_{21}^3 & k_{21}-k_{21}^3 \\ \hline k_{21}-k_{21}^3 & k_{21}-2k_{21}^2+k_{21}^3 & k_{21}-k_{21}^3 & k_{21}+2k_{21}^2+k_{21}^3 \end{array}\right] \begin{bmatrix} u_{2a}^- \\ v_{2a}^- \\ v_{2a}^+ \\ u_{2a}^+ \end{bmatrix} \tag{128}$$

where

$$K_{21} \equiv \sqrt{\frac{E_1 I_1 \rho_2 A_2}{E_2 I_2 \rho_1 A_1}} \tag{129}$$

The trivial case, where beams 1 and 2 are identical, checks in equation (128) also. The elements of the matrix in equation (128) are independent of s, even in the general case. For any particular (numerical) case, converting equation (127) into the interface matrix form of equation (124) is simple.

A treatment of the enormous number of ways to generalize the uniform-beam relations with these concepts is beyond the scope of this report. The fact that the interface matrix is composed of real numbers is considered promising for future work in nonuniform beams.

BLANK PAGE

CONCLUDING REMARKS

Specific Conclusions

The following specific conclusions can be drawn from the investigations of Distributed System Concepts in Dynamic Analysis and Control of Bending Vibrations:

1. The solution of the Bernoulli-Euler equation for transverse bending vibration of a thin semi-infinite beam shows that $e^{-\sqrt{Ts}} \cos \sqrt{Ts}$ and $e^{-\sqrt{Ts}} \sin \sqrt{Ts}$ are propagation operators, and the matrix of input admittances of a semi-infinite beam (characteristic-admittance matrix) contains the fractional derivative and integral operators $\sqrt{s}$ and $1/\sqrt{s}$.

2. A matrix transformation ($U = W^{-1} Y$), carrying the local state vector Y to a vector of characteristic variables (U), permits factorization of the solution to the Bernoulli-Euler equation for uniform-thin-beam bending into three constituent matrices that represent (1) the left-side end-effects; (2) left-to-right and right-to-left propagation, which is diagonalized in the partitioned sense; and (3) right-side end-effects. The end-effects matrices depend only upon the boundary conditions, cross-section geometry, and local properties of the beam. They contain only the operations found in the characteristic-impedance matrix. The propagation matrices contain only the propagation operators. This matrix factorization has the same structure as that for the solution to the wave equation, which is factored into end-effects matrices and scalar-delay operators that describe the wave propagation.

3. For terminal dampers and controls, which can be represented as impedance matrices, the end-effects matrices can be derived from those for the free-free beam and the terminating-impedance matrices, by simple matrix algebra. The propagation matrices are not involved in this computation.

4. The matrix relation (reflection matrix) between the incident and reflected U variables is identically zero, when the terminal-impedance and characteristic-impedance matrices are equal. If the elements of the terminal-impedance and the characteristic-impedance matrices, have the same functional form, then the reflection matrix contains only real numbers. Some elements of the reflection matrix are nulled by terminal-impedance matrices, which are simpler and more practical to implement than characteristic-impedance matrices.

5. The response of the controlled system to load disturbances or commands can be expanded in powers of the reflection and propagation matrices. This is a generalization of the sucessive-wave expansion in powers of the reflection coefficient and the wave delay.

6. Conventional angular rate damping or control (in which lateral restoring force is proportional to angular-rate error) is optimized when the gain equals the (lateral force)/(angular rate) term of the characteristic-impedance matrix. For this value of gain, the reflection matrix is reduced to the identity matrix.

7. The matrices describing reflection and refraction of the U variables at the interface between two cascaded uniform beams have only real elements.

Remarks

No specific conclusions are drawn concerning use of fractional-derivative and fractional-integral operators in the impedance matrix for damping or control. Although such terms can change the reflection matrix and, in fact, make it zero, the results of analog simulation and frequency-response calculations both for load disturbances and command inputs are inconclusive and emphasize the need for a more comprehensive understanding of the Bernoulli-Euler reflection matrix.

APPENDIX A

THE FRACTIONAL-DERIVATIVE OPERATOR $\sqrt{s}$ AND THE FRACTIONAL-INTEGRAL OPERATOR $1/\sqrt{s}$

Analog Simulation

Approximate analog simulation of the operators $\sqrt{s}$ and $1/\sqrt{s}$ has been treated by Carlson and Halijak (ref 37); they show that good approximations can be achieved by an operational amplifier with a lattice-network feedback having a driving-point impedance which approximates $1/\sqrt{s}$. The configurations for $1/\sqrt{s}$ and $\sqrt{s}$ are shown in figures 37a and b, respectively.

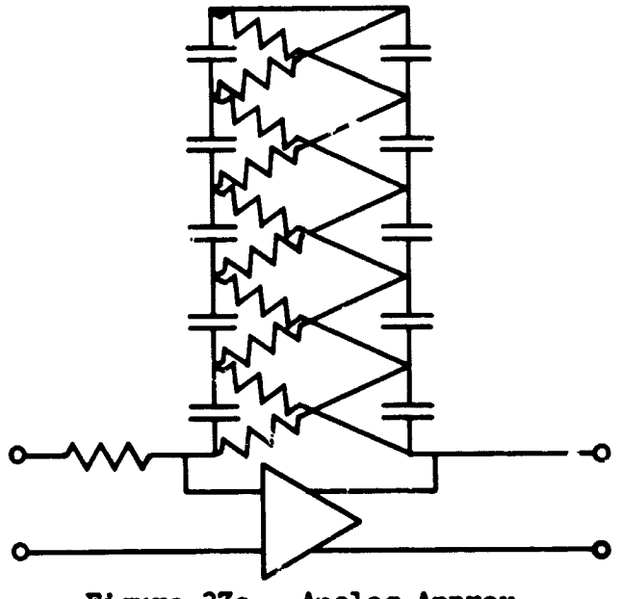

Figure 37a. Analog Approx. for fractional integral $1/\sqrt{s}$

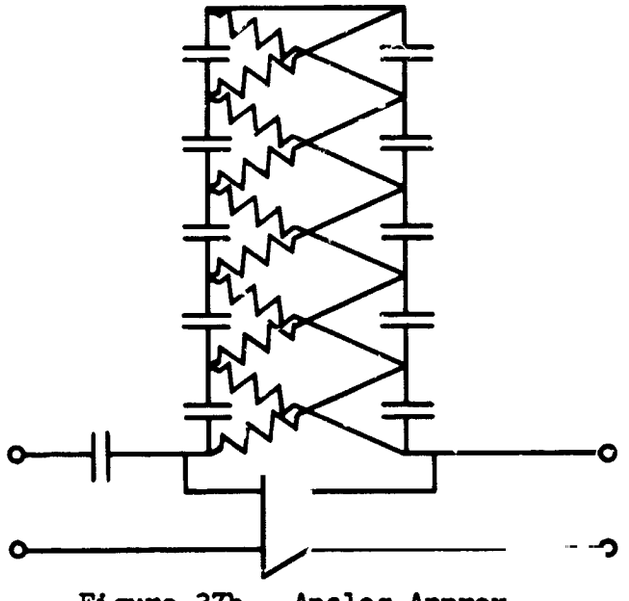

Figure 37b. Analog Approx. for fractional derivative $\sqrt{s}$

These networks approximate the required function quite well over a broad range of frequency with R, C, short-circuit, or open-circuit termination of the feedback lattice. The asymptotic form for low frequencies does depend upon the termination, however. For example, if the approximation for $1/\sqrt{s}$ is terminated in a capacitor, as shown in figure 38, then the low-frequency approximation is a gain.

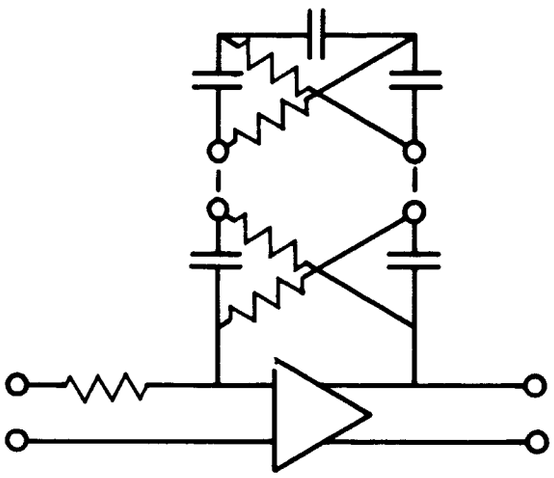

Figure 38. Lattice for $1/\sqrt{s}$ terminated with a capacitor.

The circuits originally set up in the analog simulation of the "Z_o" control had the low-frequency, asymptotic forms shown in the block diagram of figure 39.

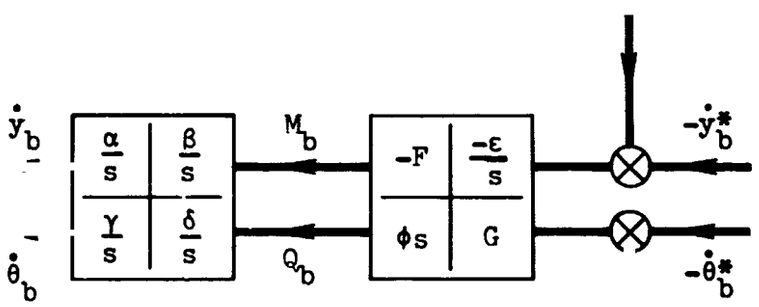

Figure 39. Low frequency approx. for original "Z_o" control simulation.

Here, the symbols F, G, α, β, γ, ϵ, and ϕ are assumed to be arbitrary positive constants, and the rigid-body approximation to Y_{bb} is used. The

steady-state errors in $\dot{y}_b$ and $\dot{\theta}_b$ did not go to zero as predicted by the exact relations for the "Z_o" control (eq 120b). The transfer function for the system in figure 39 is

$$\begin{bmatrix} \dot{y}_b^* - \dot{y}_b \\ \dot{\theta}_b^* - \dot{\theta}_b \end{bmatrix} = \frac{\left[\begin{array}{c|c} (s^2 + \delta G s + \gamma\varepsilon) & (\delta\phi s^2 + \gamma F s) \\ \hline (\beta G s + \alpha\varepsilon) & (1 + \beta\phi)s^2 + rFs) \end{array}\right]}{[s^2(1 + a) + bs + c]} \begin{bmatrix} \dot{y}_b^* \\ \dot{\theta}_b^* \end{bmatrix} \tag{A1}$$

where

$$a = \beta\phi \; ; \; b = (\alpha F + \delta G)$$

$$c = (\gamma\varepsilon + \beta\phi\gamma\varepsilon + \alpha F\delta G - \gamma F\beta G - \delta\phi\alpha\varepsilon) \tag{A2}$$

The first-row numerator elements contain constant terms that cause steady-state errors in $\dot{y}_b$ for step inputs in $\dot{y}_b^*$ and $\dot{\theta}_b^*$. Analysis also showed that an algebraic loop results from multiplying ϕs by β/s. If the approximation for $\sqrt{s}$ is changed so that its low-frequency asymptotic form is a gain ϕ, rather than a derivative ϕs, the transfer function becomes

$$\begin{bmatrix} \dot{y}_b^* - \dot{y}_b \\ \dot{\theta}_b^* - \dot{\theta}_b \end{bmatrix} = \frac{\left[\begin{array}{c|c} s^2(s + \alpha F + \beta\phi) & -s(\alpha\varepsilon + \beta G s) \\ \hline -s^2(\gamma F + \delta\phi) & s(s^2 + \delta G s + \gamma\varepsilon) \end{array}\right]}{[s^3 + as^2 + bs + c]} \begin{bmatrix} \dot{y}_b^* \\ \dot{\theta}_b^* \end{bmatrix} \tag{A3}$$

where

$$\begin{aligned} a &= (\alpha F + \beta\phi + \delta G) \\ b &= (\gamma\varepsilon + \alpha F\delta G - \gamma F\beta G) \\ c &= (\gamma\varepsilon\beta\phi - \delta\phi\alpha\varepsilon) \end{aligned} \tag{A4}$$

Now, none of the numerator elements contains a constant term. Thus, the steady-state errors have the correct behavior. One way to make the approximation for $\sqrt{s}$ behave as a gain for low frequency is to connect a resistor across the input capacitor, as shown in figure 40. The RC time constant chosen for operational-amplifier input impedance was 0.4 sec. Thus, break frequency for this network is less than 10% of the first-mode frequency.

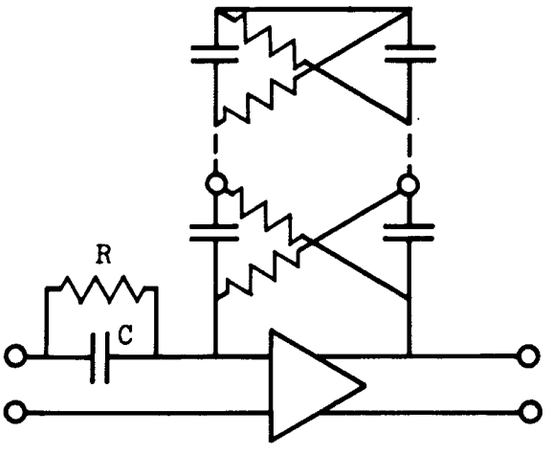

Figure 40.- Input resistor used to correct low frequency behavior of $\sqrt{s}$ approx.

The analog model was changed, and the errors in $\dot{y}_b$ and $\dot{\theta}_b$ properly returned to zero in response to the steps of $\dot{y}_b^*$ and $\dot{\theta}_b^*$.

Rational Algebraic Approximations

For the lattice network shown in figure 41a, the driving point impedance can be shown to be

$$Z_{40} = \frac{(\tau s)^4 + 28\,(\tau s)^3 + (70)(\tau s)^2 + 28\,\tau s + 1}{Cs\,[8\,(\tau s)^3 + 56\,(\tau s)^2 + 56\,\tau s + 1]} \qquad (A5)$$

For the special case $R = 1$ ohm, and $C = 1$ farad, the frequency response is shown in figure 41b. The exact frequency response of $1/\sqrt{s}$ has a phase of 45°, and the gain is a straight line passing through 0 dB at $\omega = 1$ with a slope of -10 dB/decade. The figure clearly shows that the function $Z_{40}(s)$ fits within $\pm$ 0.5 dB and $\pm$ 2° over the range $0.1 \leq \omega \leq 10$ rad/sec. For $\tau \neq 1$, it fits $1/\sqrt{s}$ to the same accuracy over a frequency range centered at $\omega\tau = 1$.

The analog-simulation networks finally used are shown in figures 42a and c. The driving-point impedances are

$$Z_{5s} = \frac{R\,[10\,(\tau s)^4 + 120\,(\tau s)^3 + 25\,(\tau s)^2 + 120\,\tau s + 10]}{[(\tau s)^5 + 45\,(\tau s)^4 + 210\,(\tau s)^3 + 210\,(\tau s)^2 + 45\,\tau s + 1]} \qquad (A6)$$

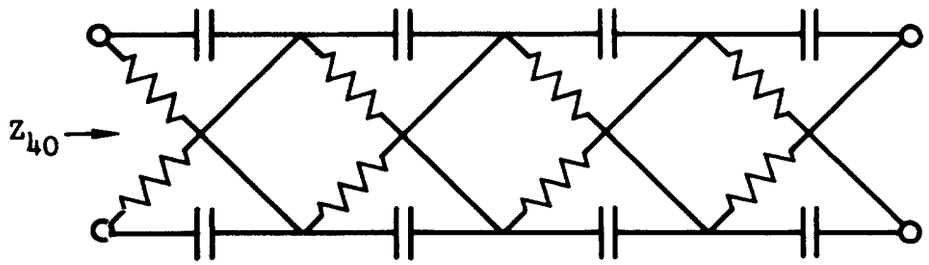

Figure 41a.- Four stage lattice with open circuit termination.

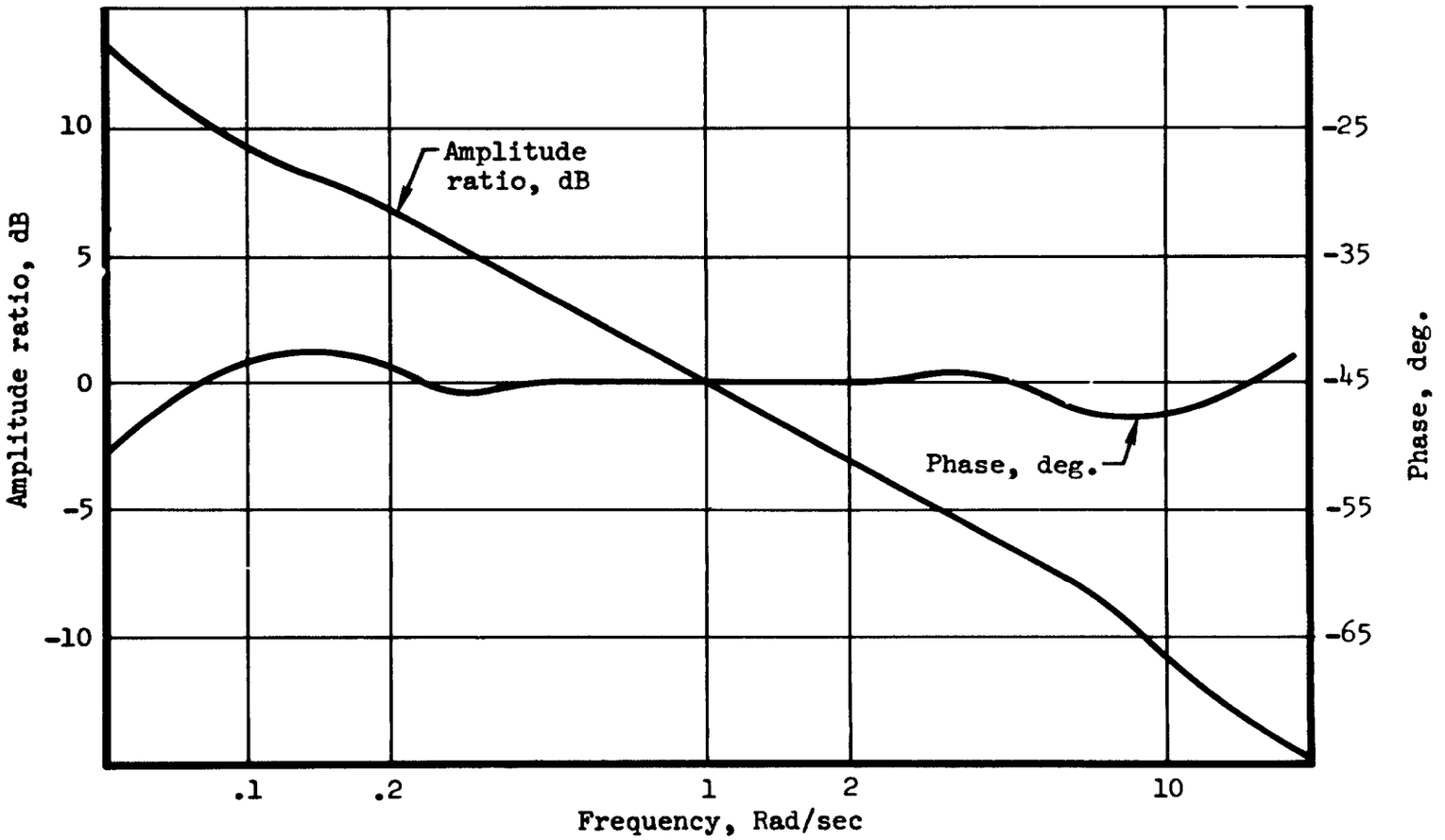

Figure 41b.- Frequency response of Z_{40} with $\tau = 1$ sec.

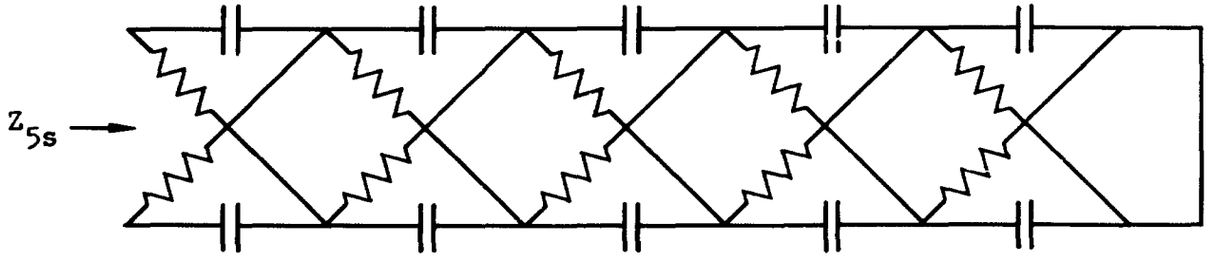

Figure 42a.- Five stage lattice with shortcircuit termination.

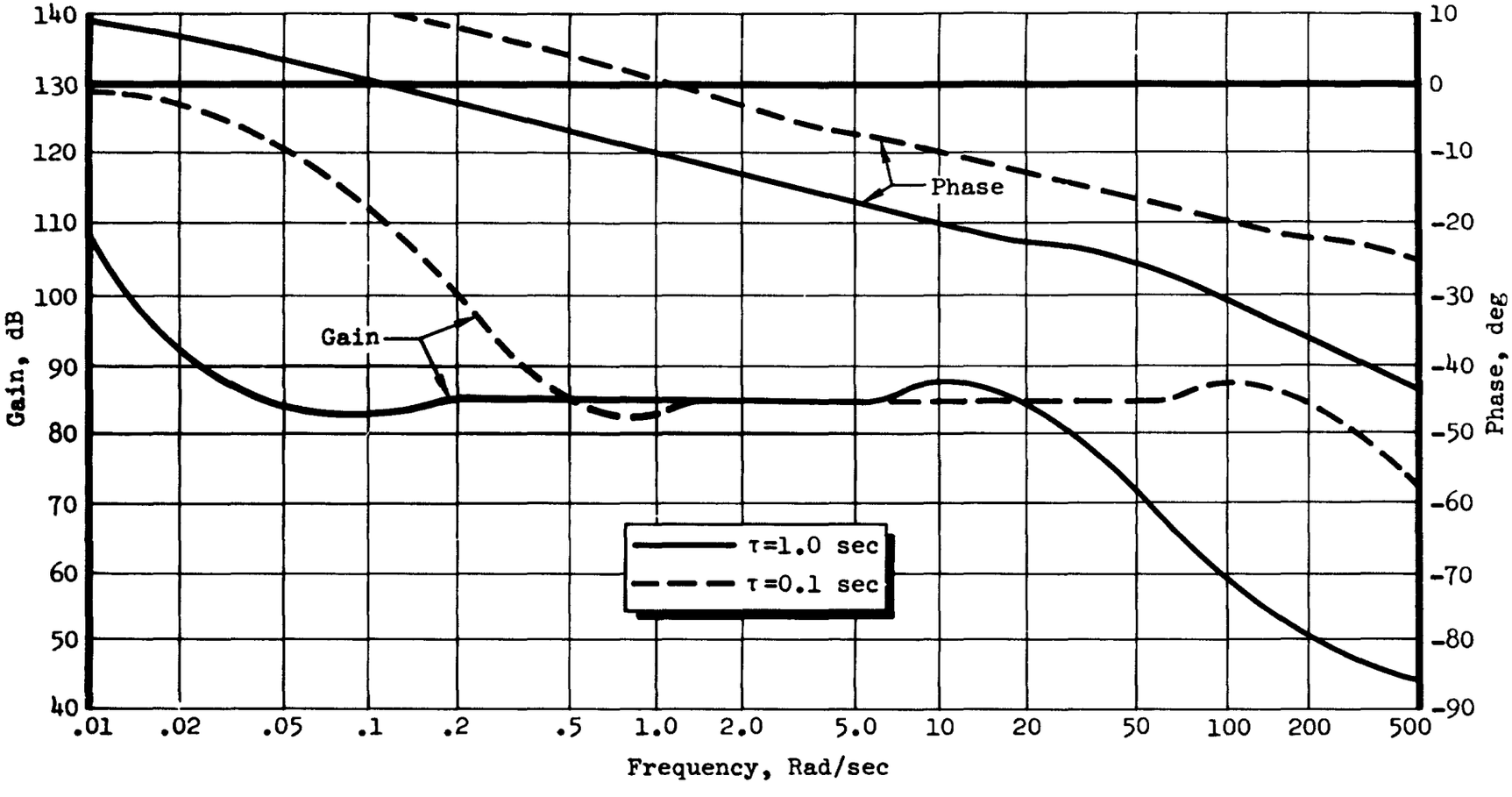

Figure 42b.- Frequency response of $Z_{5s}(s)$ with $R=10^6$ ohms.

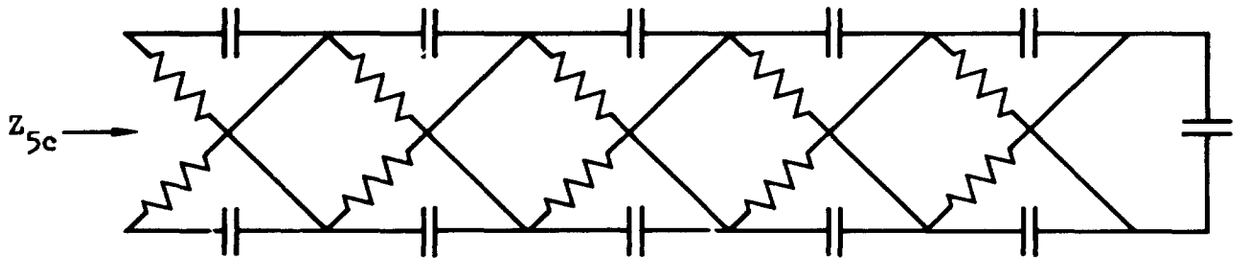

Figure 42c.- Five stage lattice with capacitor termination.

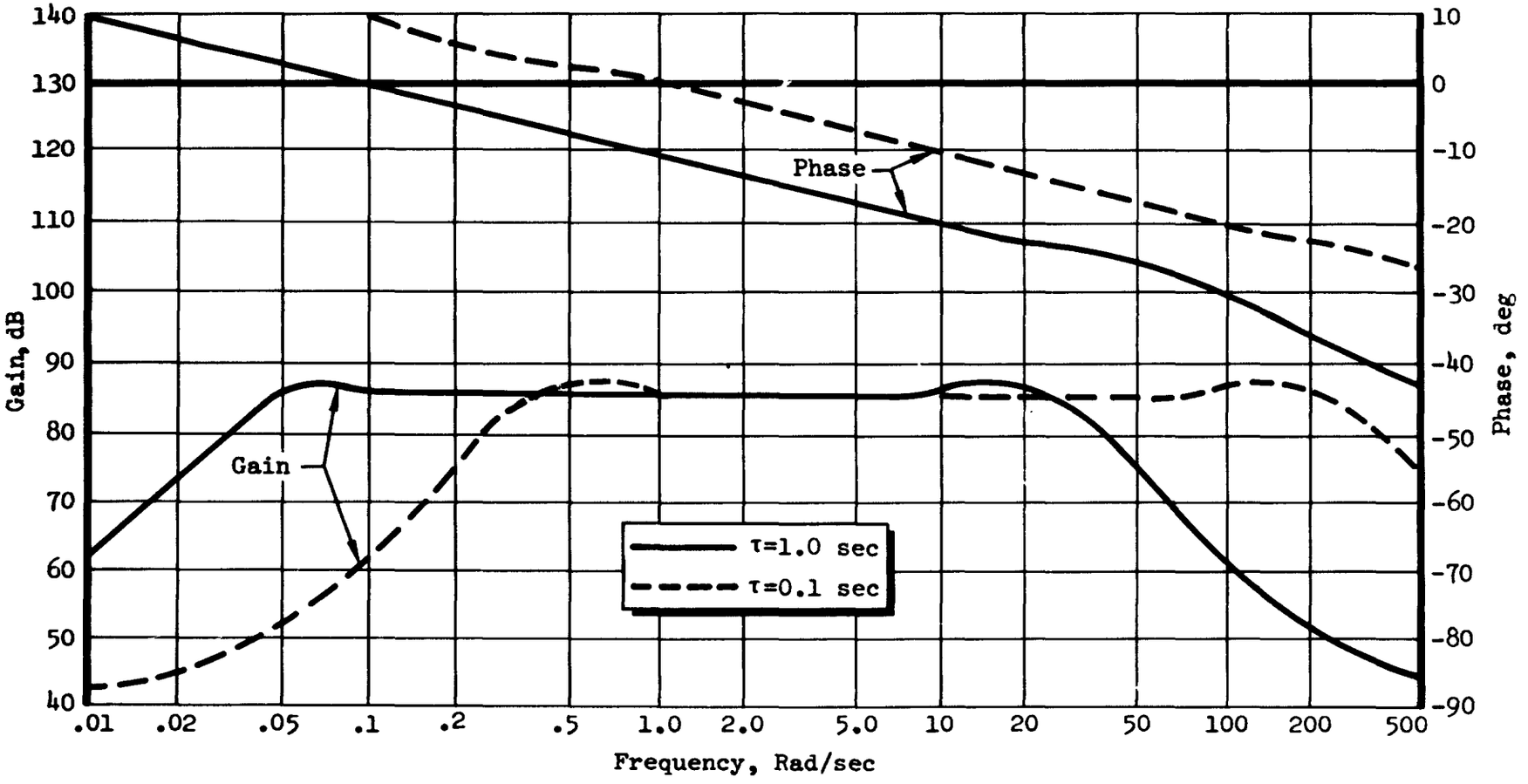

Figure 42d.- Frequency response of $Z_{5c}(s)$ with $R=10^6$ ohms.

$$Z_{5c} = \frac{[11\,(\tau s)^5 + 165\,(\tau s)^4 + 462\,(\tau s)^3 + 330\,(\tau s)^2 + 55\,\tau s + 1]}{Cs\,[(\tau s)^5 + 55\,(\tau s)^4 + 330\,(\tau s)^3 + 462\,(\tau s)^2 + 165\,\tau s + 11]} \qquad (A7)$$

The frequency responses of Z_{5s} and Z_{5c} are shown in figures 42b and d for the cases $R = 10^6$ ohms, $\tau = 1.0$ and $R = 10^6$ ohms, $\tau = 0.1$; they clearly show how τ shifts the range of fit, and how the termination affects the behavior outside the range of fit.

REFERENCES

1. Bisplinghoff, Raymond L.; Ashley, Holt; and Halfman, Robert L.: Aeroelasticity. Addison-Wesley Publishing Co., Inc., 1955.

2. Andeen, Richard E.: Stabilizing Flexible Vehicles. Astronaut. Aeron., vol. 2, no. 8, August 1964.

3. Vigness, Irwin: Propagation of Transverse Waves in Beams. Naval Research Laboratory Report NRL F-3476, June 1949.

4. Boussinesq, J.: Applications des Potentiels. Paris, 1885.

5. Leonard, Robert W.; and Budiansky, Bernard: On Traveling Waves in Beams. NACA TN 2874, 1953.

6. Dengler, M.A.; and Goland, M.: Transverse Impact of Long Beams, Including Rotary Inertia and Shear Effects. Proceedings of the First U.S. National Congress of Applied Mechanics, 1951, pp. 179-186.

7. Henny, Alex; and Raney, P.J.: The Optimization of Damping of Four Configurations of a Vibrating Uniform Beam. J.Engineering Industry, Trans-ASME. Aug. 1963, pp. 259-264.

8. Young, Dana: Theory of Dynamic Vibration Absorbers for Beams. Proceedings of the First U.S. National Congress of Applied Mechanics, 1951, pp. 91-96.

9. Rockwell, T.H.; and Lawther, J.M.: Theoretical and Experimental Results on Active Vibration Dampers. J. Acoust. Soc. Am., vol. 36, no. 8, Aug. 1964, pp. 1507-1515.

10. Klyukin, I.I.: Attenuation of Flexural Waves in Rods and Plates by Means of Resonance Vibrational Systems. Soviet Physics-Acoustics, vol. 6, 1960, p. 209.

11. Klyukin, I.I.; and Sergeev, Yu. D.: Scattering of Flexural Waves by Antivibrators on a Plate. Soviet Physics-Acoustics, vol. 10, no. 1, 19[illegible], pp. 49-53.

12. Jakobsen, L.S.; and Ayre, R.S.: Engineering Vibrations. McGraw-Hill Book Co., Inc., 1958.

13. Shearer, J. Lowen; Beethof, Gerhard; Blackburn, John F.: Fluid Power Control. John Wiley & Sons, Inc., 1960.

14. Weber, Ernst: Linear Transient Analysis, vol. II. John Wiley & Sons, Inc. 1954.

15. Pipes, L.A.: Matrix Methods for Engineering. Prentice-Hall, Inc., 1963.

16. Paynter, Henry M.: Analysis and Design of Engineering Systems. The M.I.T. Press, 1960.

17. Zadeh, Lotfi A.; and Desoer, Charles A.: Linear System Theory - The State Space Approach. McGraw-Hill Book Co., Inc., 1963.

18. Bellman, Richard: Introduction of Matrix Analysis. McGraw-Hill Book Co., Inc., 1960.

19. Johnson, Walter C.: Transmission Lines and Networks. McGraw-Hill Book Co., Inc., 1950.

20. Buckley, Page S.: Techniques of Process Control. John Wiley & Sons, Inc., 1964.

21. Paynter, Henry M.; and Ezekiel, F.D.: Water Hammer in Nonuniform Pipes as an Example of Wave Propagation in Gradually Varying Media. Transactions of the ASME, Oct. 1958, pp. 1581-1595.

22. Brown, Forbes T.: On the Dynamics of Distributed Systems. Applied Mechanics Reviews, vol. 17, no. 5, May 1964, pp. 353-359.

23. Flügge, W.; and Zajaoc, E.E.: Bending Impact Waves in Beams. Sonderabdruk Aus Ingenier-Archiv, Bd. 28, 1959.

24. Lamb, H.: On Waves in an Elastic Plate. Proc. Roy. Soc. (London), Ser. A, vol. 93, 1916-1917, p. 114.

25. Flügge, W.: Du Ausbreitung von Biegungswellen in Staben. Zeitschrift für angewandte Mathematic und Mechanik, Bd. 22, Nr. 6, Dec. 1942, pp. 312-318.

26. Schneider, P.J.: Conduction Heat Transfer. Addison-Wesley Publishing Co., Inc., 1955.

27. Bishop, R.E.D.; and Johnson, D.C.: The Mechanics of Vibration. Cambridge University Press, 1960.

28. Bishop, R.E.D.; and Johnson, D.C.: Vibration Analysis Tables. Cambridge University Press, 1956.

29. Carslaw, H.S.; and Jaeger, J.C.: Operational Methods in Applied Mathematics. Oxford University Press, 1941.

30. Janke, E.; and Emde, F.: Tables of Functions with Formulae and Curves. Dover Publications, 1945.

31. Mason, W.P.: Electromechanical Transducers and Wave Filters. D. Van Nostrand Co., Inc., 1942.

32. Thomas, Dan A.: Characteristic Impedances for Flexure Waves in Thin Plates. J. Acoust. Soc. Am., vol. 30, no. 3, March 1958.

33. Thomas, Dan A.: Mechanical Impedances for Thin Plates. J. Acoust. Soc. Am., vol. 32, no. 10, Oct. 1960.

34. Dyer, Ira: Moment Impedance of Plates. J. Acoust. Soc. Am., vol. 32, no. 10, Oct. 1960.

35. Gibson, John, E.: Nonlinear Automatic Control. McGraw-Hill Book Co., Inc., 1964.

36. Pestel, Edward C.; and Leckie, Frederick A.: Matrix Methods in Elastomechanics. McGraw-Hill Book Co., Inc., 1963.

37. Carlson, G. E.; and Halijak, C. A.: Simulation of the Fractional Derivative Operator $\sqrt{s}$ and the Fractional Integral Operator $1/\sqrt{s}$. Kansas State Engineering Experiment Station, Kansas State University.